

# THERMAL PERFORMANCE ANALYSIS OF PHASE CHANGE MATERIAL BASED SYSTEMS WITH VOLUMETRIC EXPANSION AND SHRINKAGE

MS (R) Thesis

By

JAYANTA SUTRADHAR



(Roll No. : 1904103003)

DEPARTMENT OF MECHANICAL ENGINEERING  
INDIAN INSTITUTE OF TECHNOLOGY INDORE

JUNE 2021



# **THERMAL PERFORMANCE ANALYSIS OF PHASE CHANGE MATERIAL BASED SYSTEMS WITH VOLUMETRIC EXPANSION AND SHRINKAGE**

**A THESIS**

*Submitted in partial fulfillment of the  
requirements for the award of the degree*

*of*

**Master of Science (Research)**

*by*

**JAYANTA SUTRADHAR**



**(Roll No. : 1904103003)**

**DEPARTMENT OF MECHANICAL ENGINEERING  
INDIAN INSTITUTE OF TECHNOLOGY INDORE**

**JUNE 2021**





# INDIAN INSTITUTE OF TECHNOLOGY INDORE

## CANDIDATE'S DECLARATION

I hereby certify that the work which is being presented in the thesis entitled **Thermal performance analysis of phase change material based systems with volumetric expansion and shrinkage** in the partial fulfillment of the requirements for the award of the degree of **MASTER OF SCIENCE (RESEARCH)** and submitted in the **Department of Mechanical Engineering, Indian Institute of Technology Indore**, is an authentic record of my own work carried out during the time period from June 2019 to June 2021 under the supervision of **Dr. Santosh Kumar Sahu, Associate Professor, Indian Institute of Technology Indore**.

The matter presented in this thesis has not been submitted by me for the award of any other degree of this or any other institute.

Jayanta Sutradhar  
07/06/2021

Signature of the student with date  
(Jayanta Sutradhar)

-----  
This is to certify that the above statement made by the candidate is correct to the best of my/our knowledge.



06.09.2021

Signature of the Supervisor of

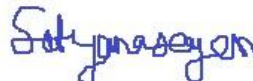
MS (Research) thesis #1 (with date)

(Dr. Santosh K Sahu)

-----  
**Jayanta Sutradhar** has successfully given his/her MS (Research) Oral Examination held on **Date of MS (Research) Oral Examination**

  
06/09/2021

Signature of Chairperson (OEB) with date

  
08/09/2021

Signature of Convener, DPGC with date



06.09.2021

Signature(s) of Thesis Supervisor(s) with date



08.09.2021

Signature of Head of Discipline with date



## ACKNOWLEDGEMENTS

I want to express my sincere gratitude to my supervisor, **Dr. Santosh Kumar Sahu**, Department of Mechanical Engineering, Indian Institute of Technology Indore, for the patient guidance, support, encouragement, and advice he has provided throughout my research work. I have been fortunate to have a supervisor who cared so much about my work and responded to my questions and queries so promptly. At many stages in the course of this research project, I benefited from his advice, particularly so when exploring new ideas. His careful editing contributed enormously to the production of this thesis.

I wish to express my gratitude to my Ph.D. progress committee members, **Dr. Shanmugam Dhinakaran**, Associate Professor, Department of Mechanical Engineering, Indian Institute of Technology Indore, **Dr. Sumanta Samal**, Assistant Professor, Department of Metallurgy Engineering and Materials Science, Indian Institute of Technology Indore, and **Dr. Prabhat Kumar Upadhyay**, Associate Professor, Department of Electrical engineering, Indian Institute of Technology Indore for their valuable suggestions and comments during this work. I am also thankful to Head, DPGC convener, all faculty members, and staff of the Discipline of Mechanical Engineering for their timely help and support throughout.

My sincere acknowledgement and respect to Professor **Neelesh Kumar Jain**, Director, **Indian Institute of Technology Indore** for providing me the opportunity to explore my research capabilities at IIT Indore. I am grateful to him for providing me financial support to present my research work in International conferences within and outside India.

I am thankful to all the staff members of **Mechanical Workshop** for their extended effort during development of test facility at IIT Indore. Many thanks to **Mr. Arun Kumar Bhagwaniya**, Fluid Mechanics and Machinery Lab and **Mr. Satish Bisen**, Central Library, Indian Institute of Technology Indore for extending their help during my MS work.

I am indebted to my seniors, lab mates and colleague researchers especially **Mr. Rohit Kothari**, **Mr. Anuj Kumar**, **Mr. Akhilesh Sharma**, **Mr. Vivek Saxena**, **Dr. Avadhesh Kumar Sharma**, **Dr. Saurabh Yadav**, **Dr. Vishal Nirgude**, **Mr. Pushpanjay K Singh**, **Mr. Jay Joshi**, **Mr. Pradeep Singh**, **Mr. Pawan Sharma**, **Mr. Deepak Kag** for their cooperation and stay so as to make my MS (R) journey happy and joyful.

I would like to express my sincere respect to **my late grandparents, and my parents** for their love, care, and support they have provided to me throughout my life. Special thanks to **my brother, my sister, and my sisters-in-law** for their support and encouragements.

I would like to give special thanks to my parents who supports me in every step of my life from my childhood. Their constant support and encouragement in my academic career from my school to master's degree help me a lot to achieve my goals.

Finally, I am thankful to all who directly or indirectly contributed, helped, and supported me.

*-Jayanta Sutradhar*

*Dedicated to my family for their love, care, and blessings*







## Abstract

Present thesis reports the theoretical investigations pertaining to the heat transfer characteristics of phase change materials (PCMs) during melting/solidification incorporating volumetric expansion and shrinkage void in the thermal energy system. The objective of the present study is to investigate the thermal performance of PCM based systems for numerous applications including thermal management of electronic devices and thermal energy storage systems.

Initially, a one dimensional analytical model is proposed to analyze the solidification/melting of phase change materials (PCMs) incorporating the shrinkage/expansion void in an annulus. An air-PCM system is considered in the analysis; paraffin wax is considered as PCM and filled inside the annulus, while air is considered inside the void. Separation of variable method involving Bessel's function is employed to obtain temperature distribution for air, solid and liquid domains and to locate interface positions. Stefan condition and mass conservation equation are used at the interfaces. Effect of various parameters such as density ratio, end wall temperature, and radius ratio on the solidification/melting of PCM have been investigated. Results obtained from the analytical model are found to be in good agreement with the existing test results.

Next, the analysis is extended to investigate the thermal performance of PCM/PCM-metal foam (MF) composite based rectangular energy storage system incorporating the volumetric change and void in PCM with steady and transient heat loads. Separation of variable method with Bessel function has been employed to solve the conduction equation associated with different thermal boundary conditions; Stefan condition and mass balance equation are used to locate the interface position. Paraffin wax and copper is considered as PCM and MF material, respectively. Solutions are obtained for temperature distribution and interface position for different domains namely, air, solid, and liquid. Effect of various parameters such as density ratio, wall heat flux, convective heat transfer coefficient, and porosity on the melting/solidification of PCM are investigated.

Also, the energy stored/extracted in PCM-MF composite is greater compared to pure PCM. The theoretical prediction exhibits good agreement with existing test data.

**Keywords:** *Phase change material (PCM), Shrinkage/expansion, Void, Metal foam (MF), Melting/solidification*

# List of Publications

## International Journal

1. **J. Sutradhar**, R. Kothari, S. K. Sahu, Solidification and melting model of phase change material with volumetric shrinkage/expansion void in an annulus, Applied Thermal Engineering, 2021. (**Accepted, Impact Factor: 5.295**)
2. **J. Sutradhar**, R. Kothari, S. K. Sahu, Melting and solidification analysis of phase change material-metal foam composite with expansion/shrinkage void in rectangular system, Journal of Energy Storage, Manuscript No: EST-D-21-01239, 2021. (**Under Revision, Impact Factor: 6.583**)

## International Conferences

1. **J. Sutradhar**, R. Kothari, A. Kumar, and S. K. Sahu, Study of solidification process of PCM with shrinkage void effect in an annulus, *Proceedings of the 8th International and 47th National Conference on Fluid Mechanics and Fluid Power (FMFP2020-164)*, December 09-11, 2020, IIT Guwahati, India.
2. **J. Sutradhar**, R. Kothari, V. Saxena, and S. K. Sahu, Investigation of solidification of nano-enhanced phase change material considering volumetric shrinkage: an analytical approach, *Proceedings of the 15th International Conference on Heat Transfer, Fluid Mechanics and Thermodynamics (Submission ID:254)*, July 25-28, 2021, Amsterdam, Netherlands (ATE). (**Accepted**)



# TABLE OF CONTENTS

<b>ABSTRACT</b>	<b>i</b>
<b>LIST OF PUBLICATIONS</b>	<b>iii</b>
<b>LIST OF FIGURES</b>	<b>ix</b>
<b>LIST OF TABLES</b>	<b>xiii</b>
<b>NOMENCLATURE</b>	<b>xv</b>
<b>1. Introduction and Literature Survey</b>	<b>1</b>
1.1 General background	1
1.2 Thermal Energy Storage (TES) System	2
1.2.1 Sensible heat thermal energy storage system	2
1.2.2 Latent heat thermal energy storage system	2
1.2.3 Thermochemical heat thermal energy storage system	3
1.3 Thermal management system	3
1.4 Phase change material	4
1.5 Various techniques for thermal conductivity enhancement of PCM	7
1.6 Review of literature	9
1.6.1 Steady heat load	9
1.6.2 Transient heat load	16
1.7 Scope of the present investigation	17
<b>2. Melting and solidification model of phase change material with volumetric shrinkage/expansion void in an annulus</b>	<b>21</b>
2.1 General background	21
2.2 Description of the physical problem	22

2.3 Mathematical formulation	24
2.3.1 Air domain	26
2.3.2 Solid PCM domain	28
2.3.3 Liquid domain	29
2.3.4 Calculation of energy extracted/stored during solidification/melting of PCM	33
2.4 Validation of Present Model	37
2.5 Result and Discussions	39
2.5.1 Solidification analysis	39
2.5.2 Melting analysis	46
2.6 Concluding remarks	52
<b>3. Melting and solidification analysis of phase change material- metal foam composite with expansion/shrinkage void in rectangular system</b>	<b>55</b>
3.1 General background	55
3.2 Physical model	56
3.3 Mathematical formulation	59
3.3.1 Air domain	61
3.3.2 Solid domain	63
3.3.3 Liquid domain	64
3.4 Validation of the present analytical model	68
3.5 Result and Discussions	70
3.5.1 Melting and solidification analysis of pure PCM for steady heat load with air gap	70
3.5.2 Melting/solidification analysis in PCM-MF composite	77

with void for steady heat load	
3.5.3 Melting analysis of pure PCM with void for transient heat load	80
3.5.4 Total melting time and solidification time for steady and transient heat loads	82
3.5.5 Energy stored/extracted during melting and solidification for steady and transient heat load.	85
3.6 Concluding remarks	87
<b>4. Conclusions and Scope of Future Work</b>	<b>89</b>
4.1 Solidification and melting model of phase change material with volumetric shrinkage/expansion void in an annulus	89
4.2 Solidification and melting analysis of phase change material metal foam composite with expansion/shrinkage void in rectangular system	90
4.3 Scope of future work	92
<b><i>References</i></b>	<b>93</b>
<b>Resume</b>	<b>107</b>



## LIST OF FIGURES

<b>Fig. 1.1</b>	Energy storage in PCM	5
<b>Fig. 1.2</b>	Types of PCM	5
<b>Fig. 2.1</b>	(a) Schematic diagram of the physical domain with PCM in an annulus, (b) One dimensional formulation for solidification process with void near cold wall (c) One dimensional formulation for melting process with void near hot wall	23
<b>Fig. 2.2</b>	Comparison of present predication with the test data of Sari et al. [116] and Akgun et al. [117] for (a) Different time instant at $r = 28$ mm during solidification process, (b) Different radial distance at $t = 20$ min during solidification process, and (c) Different time instant at $r = 21.25$ mm during melting process	38
<b>Fig. 2.3</b>	Spatial variation of non-dimensional temperature at different time duration, (b) Non-dimensional air-solid ( $R_{as}$ ) and solid-liquid ( $R_{sl}$ ) interface positions with $F_0$ for density ratio of 1 and 1.1	41
<b>Fig. 2.4</b>	(a) Temperature variation with radial distance for different cold wall temperatures at $t = 800$ s ( $F_0 = 1.49$ ) and density ratio of 1.16, (b) Temperature history during solidification at $r = 5$ mm ( $r' = 0.625$ ) at density ratio of 1.16	42
<b>Fig. 2.5</b>	(a) Temperature variation with radial distance for different density ratio values (b) Energy extracted from liquid PCM for density ratio of 1, 1.16 (c) Fraction of total energy extracted at density ratio 1 and 1.16	45
<b>Fig. 2.6</b>	Temperature variation with radial distance for radius ratio values of 0.2 and 0.3	45

<b>Fig. 2.7</b>	(a) Spatial variation of temperature with radial distance at different time duration, (b) Air-solid (Ras) and solid-liquid (Rsl) interface positions at different time duration for density ratio of 1 and 1.16	47
<b>Fig. 2.8</b>	(a) Temperature variation with radial distance for different hot wall temperatures at $t = 1000$ s ( $F_0 = 3.33$ ) and density ratio of 1.16, (b) Temperature history during melting at $r = 5$ mm ( $r' = 0.625$ ) at density ratio of 1.16	49
<b>Fig. 2.9</b>	(a) Temperature variation with radial distance for different density ratio values (b) Energy stored from liquid PCM for density ratio of 1, 1.16 (c) Fraction of total energy stored at density ratio 1.16 and 1	51
<b>Fig. 2.10</b>	Temperature variation with radial distance for radius ratio values of 0.2 and 0.3	52
<b>Fig. 3.1</b>	Schematic of rectangular PCM system with void near left wall for (a) melting, (b) solidification process	57
<b>Fig. 3.2</b>	Comparison of temperature of pure PCM obtained from present predictions with the test data of Zhou et al. [121] at $x=10$ mm ( $x' = 0.33$ ) for (a) melting, (b) solidification process	69
<b>Fig. 3.3</b>	Comparison of temperature of PCM-MF composite obtained from present predictions with the test data of Zhou et al. [121] at $x=10$ mm ( $x' = 0.33$ ) for (a) melting, (b) solidification process	70
<b>Fig. 3.4</b>	Spatial variation of non-dimensional temperature at different time duration (a) melting, (b) solidification process	72
<b>Fig. 3.5</b>	Temperature variation for different wall heat fluxes at (a) $t = 300$ s ( $F_0 = 0.64$ ) for different axial distance, (b) $x = 2.5$	75

	mm ( $x' = 0.25$ ) for different time duration	
<b>Fig. 3.6</b>	Temperature variation for different convective heat transfer coefficient ( $h$ ) values at (a) $t = 2000$ s ( $F_0 = 2.39$ ) for different axial distance, (b) $x = 1.5$ mm ( $x' = 0.15$ ) for different time duration	75
<b>Fig. 3.7</b>	Temperature variation with axial distance for different density ratio values, (a) melting, (b) solidification process	76
<b>Fig. 3.8</b>	(a) Comparison of interface movement in TES system with pure PCM and PCM-MF composite (97% porosity) for 2400 s ( $F_0 = 5.12$ ) duration, and (b) Spatial variation of temperature with different axial distance at $t = 1400$ s ( $F_0 = 2.99$ ) for different porosity, during melting process	78
<b>Fig. 3.9</b>	(a) Comparison of interface movement in TES system with pure PCM and PCM-MF composite (97% porosity) for 2400 s ( $F_0 = 2.87$ ) duration, and (b) Spatial variation of temperature with different axial distance at $t = 2000$ s ( $F_0 = 2.39$ ) for different porosity, during solidification process	80
<b>Fig. 3.10</b>	Movement of air-liquid and solid-liquid interface (a) Initiation of various pulse heat load 200 W/m <sup>2</sup> ( $\gamma = 1$ ), 300 W/m <sup>2</sup> ( $\gamma = 2$ ), and 400 W/m <sup>2</sup> ( $\gamma = 3$ ) during $500$ s $< t < 1400$ s ( $1.07 < F_0 < 2.99$ ) (b) Initiation of various pulse heat load 400 W/m <sup>2</sup> ( $\gamma = 1$ ), 600 W/m <sup>2</sup> ( $\gamma = 2$ ), and 800 W/m <sup>2</sup> , ( $\gamma = 3$ ) during $100$ s $< t < 800$ s ( $0.213 < F_0 < 1.7$ ) and shut-off for 1800 s ( $F_0 = 3.84$ )	81
<b>Fig. 3.11</b>	Comparison of total melting time for (a) different density ratio of pure PCM (b) pure PCM with and without air void and PCM-MF with air void	83
<b>Fig. 3.12</b>	Comparison of total solidification time for (a) Different density ratio of pure PCM (b) Pure PCM with and without	84

air gap and PCM-MF with air gap

- Fig. 3.13** Comparison of total energy stored (a) pure PCM 86  
considering with and without air gap (b) pure PCM and  
PCM-MF composite considering void for (c) transient heat  
load condition for different value
- Fig. 3.14** Comparison of total energy extracted (a) pure PCM 87  
considering with and without air gap, (b) pure PCM and  
PCM-MF composite considering void

## LIST OF TABLES

<b>Table 1.1</b>	Comparison of properties of different PCMs	6
<b>Table 1.2</b>	Various studies without consideration volumetric change	10
<b>Table 1.3</b>	Various studies with consideration volumetric change	13
<b>Table 1.4</b>	Various studies related to effect of nano-particle	14
<b>Table 1.5</b>	Various studies related to effect of Porous matrix	16
<b>Table 2.1</b>	Thermo-physical properties of paraffin wax	22
<b>Table 2.2</b>	Comparison of mathematical expressions for temperature distribution of three domains	35
<b>Table 2.3</b>	Thermo-physical properties of Lauric acid [116] and Paraffin wax [117]	37
<b>Table 3.1</b>	Thermo physical properties of paraffin wax RT27 and Copper	58



## Nomenclature

<b>English Symbols</b>	
A	Constants used in Eq. 2.11
B	Constants used in Eq. 2.15a
C	Constants used in Eq. 2.15b
$C_p$	Specific heat capacity, $\text{Jkg}^{-1}\text{K}^{-1}$
$F_0$	Fourier Number
h	Convective heat transfer coefficient, $\text{Wm}^{-2}\text{K}^{-1}$
$J_0$	Bessel function of Zero order of first kind
$L$	Latent heat of PCM, $\text{Jkg}^{-1}$
m	Mass, kg
$q_w''$	Heat flux, $\text{Wm}^{-2}$
$R_{as}$	Air-Solid, m
$R_{al}$	Air-Liquid, m
$R_{sl}$	Solid-Liquid interface position, m
$R_{in}$	Inner radius of annulus, m
$R_{out}$	Outer radius of annulus, m
t	Time, s
$T$	Temperature, $^{\circ}\text{C}$
$T_p$	Air-Solid and air liquid interface temperature for solidification and melting processes, respectively, $^{\circ}\text{C}$
$T_{\infty}$	Ambient Temperature, $^{\circ}\text{C}$
$T_m$	Melting point, $^{\circ}\text{C}$
x	Coordinate, m
$Y_0$	Bessel function of zero order of second kind
<b>Greek Symbols</b>	

$\alpha_s, \alpha_l$	Thermal diffusivity of Solid and liquid, respectively, $m^2s^{-1}$
$\alpha_a$	Thermal diffusivity of air, $m^2s^{-1}$
$\beta_m$	$m^{\text{th}}$ Eigen value
$\mathcal{D}$	Function definition expressed in Eq. 2.32
$\rho$	Density of PCM, $kgm^{-3}$
$\rho_n$	Density ratio defined in Eq. 2.33b
$\psi$	Dimensionless number defined in Eq. 3.6a
$\eta$	Dimensionless number defined in Eq. 3.6b
$\lambda$	Dimensionless number defined in Eq. 3.9
$\gamma$	Dimensionless number defined in Eq. 2.28c
$\xi$	Porosity
$N(\beta_m)$	Norm
<b>Subscripts</b>	
$a$	Air
$c$	Cold wall
$e$	Extracted
$h$	Hot wall
$l$	Liquid
$\mathcal{O}$	Initial value
$P$	Air-solid and Air-liquid interface
$s$	Solid
$s$	Stored
<b>Superscript</b>	
$k$	Time step

# Chapter 1

## Introduction and Literature Review

### 1.1 General background

Global annual energy consumption has increased by more than 350% since 1965, which is equivalent to the energy consumption of 14186.6 million tons of oil by 2016 [1]. During 2016, nearly 86% of the total global primary energy consumption was obtained from fossil fuels (oil, natural gas, and coal), 10% from renewable sources and 4% from nuclear energy. Excessive use of fossil fuels result in the increase in greenhouse gases and leads to global warming and environmental pollution. As per the US energy information administration report [2], the use of global energy, in various sectors, will increase from  $1.7 \times 10^{11}$  MWh to  $2.2 \times 10^{11}$  MWh between 2015 and 2040. This has motivated various researchers to design thermal energy storage (TES) system for storing and later utilizing the energy from renewable sources.

In addition to this, the use of electronic devices such as tablet, laptop, computers (PCs), and mobiles have been significantly increased because of advance in technology [3]. Because of higher power density, the heat generation increases significantly and affects the reliability and performance. Also, it has been observed that holding a tablet PC with surface temperature exceeding 42 to 45 °C (in the back side) can lead to severe user discomfort [4-8]. With the rise in operating temperature of 1°C, device life can be reduced by 4%. Also, device failure can happen with 10°C to 20°C rise in operating temperature [9-10]. In such a case, suitable passive cooling technique needs to be developed for the thermal management and safe operation of electronic components. In view of this, efforts have been made to develop passive cooling techniques for thermal management of portable electronic devices. PCM based thermal management technique can play an important role as the passive cooling technique for the portable devices.

The TES systems are classified as sensible heat thermal energy storage (SHTES) system and latent heat thermal energy storage (LHTES) system. Later

option is the more promising candidate compared to the former one due to constant temperature phase transition and high energy storage in a small volume. Phase change material (PCM) based LHTES system is the most effective thermal energy storage and thermal management technique due to higher energy storage density and constant phase transition. Also, PCM plays an important role to balance the supply and demand in various sectors such as industrial, domestic, and commercial applications. In addition, PCM based LHTES systems finds application in building, waste heat recovery, aerospace, photovoltaic (PV) system, automobiles, solar water heating, electronic cooling, and thermal comfort [11-23].

## 1.2 Thermal energy storage (TES) system

Thermal energy storage system is the promising candidate to smoothen the temporal variation of energy supply and demand. It can be used to recover the excess amount of heat produced in various industries, commercial and domestic sectors. TES systems are classified as follows:

- Sensible heat thermal energy storage (SHTES) system
- Latent heat thermal energy storage (LHTES) system
- Thermochemical heat thermal energy storage (THTES) system

### 1.2.1 Sensible heat thermal energy storage system (SHTES)

In SHTES, the, heat is stored in the material due to the rise in temperature. Either liquid or solid can be used as the sensible heat storage material; while, the liquid based SHTES are bulkier compared to solid based systems. Sensible heat storage depends on the mass and its specific heat of the material. Expression for sensible energy stored in a TES system is as follows.

$$Q_s = m \int_{T_i}^{T_f} C_p dt \quad (1.1)$$

### 1.2.2 Latent heat thermal energy storage system (LHTES)

In case of LHTES, the energy is stored/released during change of phase of the material, which occurs at a constant temperature. The energy, in PCMs, is

stored in three different forms such as solid to solid, solid to liquid, and liquid to vapor. In case of solid to solid transition, heat is stored or released when material change its lattice structure. In such a case, the volume change is less and there is no leakage problem. While, during solid to liquid transition, the phase change occurs, with latent heat interaction, nearly at constant temperature with volumetric changes. On the contrary, during liquid to vapor transition, large amount of volumetric change occurs at faster rate, which may lead the failure of storage system. Latent heat stored can be expresses as:

$$Q_l = mh \quad (1.2)$$

Here, h is the latent heat fusion and m is the mass of the system.

### **1.2.3 Thermochemical heat thermal energy storage system (THTES)**

In THTES, the energy stored/ released with the breaking/forming of new molecular bonds in a reversible chemical reaction. In general, higher amount of heat energy is required to provide the binding energy to break the bond/form a new bond. The THTES depends on the mass, enthalpy of the system and fraction of the reaction; expressed as:

$$Q_{Th} = m\Delta h_e \alpha \quad (1.3)$$

## **1.3 Thermal management system**

Currently, the usage of electronic devices has increased due to increase in technology. In addition to this, the multi features and compact device generates more amount of heat. The removal of excess heat is important as the failure of devices increases beyond a certain temperature. Moreover, in most of the PCs or electronic devices the heat generation fluctuates with time. One needs to propose the novel thermal management techniques to dissipate the generated heat and prevent the failure of electronic components. Thermal management techniques

are broadly classified as active and passive cooling techniques. The active thermal cooling techniques, that employ liquid and air, are not preferred for certain applications due to various reasons such as large space requirement, higher maintenance, higher power requirement and higher noise level which in turn result in higher operating cost. On the contrary, passive thermal management techniques are found to be cost effective and efficient. The active cooling techniques can be achieved by forced air cooling, forced liquid cooling and thermoelectric heat pump. While, the passive cooling techniques include heat sinks, heat pipes, heat spreaders and Phase change materials. Phase change material (PCM) based thermal energy storage can absorb the excessive heat generated during spikes and able to dissipate during the rest period. This arrangement can significantly reduce the temperature related failure of electronic components.

#### **1.4 Phase change material**

Phase change material can release/ absorb sufficient amount of heat during its phase change process. The PCM change its phase at a constant temperature and during this process it can store or release large amount of energy with a small volume change. During melting process, PCM takes energy from the hot fluid and stores energy nearly at constant temperature in the form of latent heat, while, during solidification process, PCM releases energy. The energy storage process in PCM is shown in Fig. 1.1.

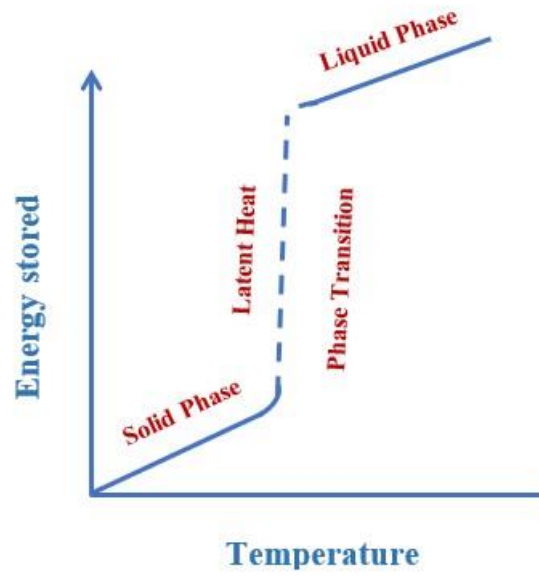


Fig 1.1 Energy storage in PCM

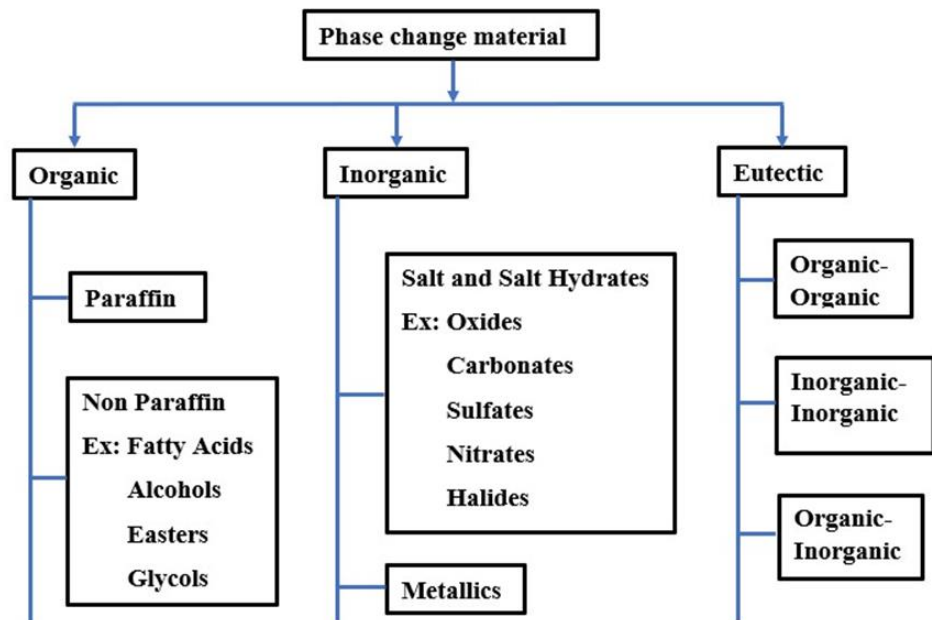


Fig 1.2 Types of PCM

**Table 1.1** Comparison of different PCMs property [28-37]

Property	Organic	Inorganic	Metallics
Latent heat	Fatty acids: 100–250 J/g Methyl esters: 205-260 J/g Sugar Alcohols: 200-310J/g Paraffins: 173-270 J/g	90 – 495 J/g	15-570 J/g
Conductivity	0.14 - 0.4 W/m.K	0.5-1.3 W/m.K	8-238 W/m.K
Specific heat	1.5 – 2.9 J/g.K	2.5 – 5 J/g.K	0.2-1.5 J/g.K
Density	0.7-0.98 kg/m <sup>3</sup>	1.3-2.5 kg/m <sup>3</sup>	1730-7040 kg/m <sup>3</sup>
Supercooling	Minimal to Self-nucleating	High	Minimal
Melting	Very sharp	Wide sharp	Very sharp
Phase separation	No phase separation	Phase separation	No separation
Thermal stability	Mostly stable	Mostly unstable	Stable
Flammability	Some are Flammable	Non-flammable	Non-flammable
Corrosiveness	Mostly Non-corrosive	Corrosive	Non-corrosive
Cost	Moderate	Low	Low to High
Availability	Widely available	Widely available	Varies

Phase change materials are categorized as organic, inorganic, and eutectic salt mixture (Fig. 1.2). Organic PCMs such as fatty acids are widely used in various thermal energy storage systems. Most of the organic PCMs have sharp melting, good thermal stability, non-corrosive, and non-toxicity [24-25]. The main disadvantage is their poor thermal conductivity and limited range of phase transition temperature. The organic PCMs include stearic acid, palmitic acid, and oleic acid. The inorganic PCMs have high thermal conductivity compared to organic compounds, wide range of melting temperature, higher density, and low cost [26, 27]. The inorganic PCMs include potassium fluoride tetra hydrate ( $\text{KF}\cdot 4\text{H}_2\text{O}$ ), manganese nitrate hexahydrate ( $\text{Mn}(\text{NO}_3)_2\cdot 6\text{H}_2\text{O}$ ), and calcium chloride hexahydrate ( $\text{CaCl}_2\cdot 6\text{H}_2\text{O}$ ). The salt hydrates have poor thermal stability and phase separation upon cyclic heating and cooling, which is the major drawback of this kind of PCMs [26]. The eutectic mixtures, are the promising candidate for many heat storage applications, exhibit high thermal conductivity, high latent heat, high specific heat, and high density. However, further investigation is required to analyze their thermo-physical properties. Detailed thermo-physical properties of various PCMs can be seen in Table 1.1.

## **1.5 Various thermal conductivity enhancement techniques**

Although, PCMs exhibit various advantages, because of lower value of thermal conductivity the thermal performance of the system decreases. The thermal conductivity of most of the PCMs vary between 0.1 to 0.6 W/m-K. Various thermal conductivity enhancement techniques are employed to increase the thermal conductivity of PCM. These include incorporation of various thermal conductivity enhancers (TCEs) such as extended surfaces, multiple PCMs, nano particles and porous matrix in the PCM. The details are elaborated below.

### **Extended surfaces**

Extended surface, provide extra surface area, are used for the heat transfer enhancement in the PCM based TES system. This method is widely used due to

its various advantages such as simplicity, ease in fabrication and low cost of construction. Extended surfaces are usually fins involving various shapes such as circular, square, rectangular and triangular. The efficiency of the system is found to depend on the fin geometry, size, orientation, and number. It is observed that fins increase the natural convection heat transfer in the molten PCM while in solid phase heat transfer increased by conduction.

### **Multiple PCMs**

Multiple PCMs are used to enhance the heat transfer process as it maintains nearly constant temperature difference between HTF and molten PCM. In case of single PCM system the temperature drops significantly which deteriorate the heat transfer process. During charging process, the multiple PCMs are arranged in decreasing order of their melting point in the flow direction of the heat transfer fluid (HTF) to maintain constant temperature difference. While, during discharge process, the flow direction of the HTF is reversed, i.e, in the increasing orders of the melting point of PCMs. This method is found to be more efficient during homogeneous phase change process.

### **Nano particle**

Nanomaterials/ nanoparticles are nanometer sized particles usually composed of metals, oxides, non-metals and carbides. When these nanoparticles are dispersed in PCM, they are termed as nano enhanced PCM (NePCM). The use of NePCM exhibits superior performance compared to pure PCM based systems for certain quantity of nanoparticle concentration. The thermal performance PES is found to depend on nanoparticle type, size, and concentration in the PCM.

### **Porous matrix**

The porous matrix made of aluminum, carbon, and copper is infiltrated in PCM and termed PCM-Foam composite. The PCM-Foam matrix is found to significantly increase the thermal conductivity of and results in the increase in the

heat transfer. The heat transfer performance is found to depend on the porosity of the material, and pore size of the structure.

## **1.6 Review of literature**

Various studies have been made to analyze the thermal performance of TESs involving rectangular, annulus and spherical configuration. These studies mostly consider analytical methods, numerical techniques and experimental investigation to analyze the performance. Most of the studies predict the temperature distribution in different domains and obtain the solid liquid interface position with time. Various analytical methods such as the perturbation method, the Megerlin method, the quasi-stationary approximation, Kantorovich method, and the heat balance integral method (HBIM) have been used to obtain the solution [42-43]. Phase change process in PCMs is complex non-linear problem that involves moving solid-liquid interface; termed as Stefan problem [43]. However, most of the analytical and numerical studies usually neglect the volumetric change in PCM during phase transition. During the phase transition of PCM in TES, small amount of air can be trapped inside the TES which may alter the heat transfer process. Alternatively, due to the difference in the density, small void/shrinkage may be generated during phase transition, which may alter the performance of the system. Therefore, the effect of void should be considered during analysis of thermal performance of TES with PCM. Some of the important studies relevant to the present work are mentioned in the following sections.

### **1.6.1 Steady heat load**

#### *Studies without consideration of volumetric change*

Over the years, various analytical [42-53] and numerical studies [54-59] have been made to analyze the melting and solidification process of PCM. Efforts have been made to propose the analytical solution by assuming semi-infinite domain in the liquid phase [44-45]. The authors neglected the solidification shrinkage effects on heat transfer during solidification of PCMs. Mazzeo et al. [46] developed an analytical model for the solidification and melting of PCM in a finite TES.

**Table 1.2** Various studies without consideration volumetric change

Author	Process	Geometry	Nature of study	Boundary condition	Parameter investigated
Mosaffa et al. [52]	Solidification	Rectangle	Analytical and Numerical	Convective air	Cell aspect ratio, HTF temperature, Convective heat transfer coefficient.
Kothari et al. [53]	Solidification	Rectangle	Analytical	Constant wall temperature, Constant heat flux, and Convective air	Aspect ratio, Heat flux, End wall temperature, Convective heat transfer coefficient.
Talati et al. [54]	Solidification	Rectangle	Analytical and Numerical	Constant heat flux	Cell aspect ratio, Solid fraction of PCM.
Lamberg [55]	Solidification	Rectangle	Analytical and Numerical	Constant wall temperature	Fin temperature, Fin length, Width to height ratio ( $\lambda$ ) of the storage.
Saha et al. [56]	Melting and Solidification	Rectangle	Analytical and Numerical	Constant heat flux and convective air	Heat flux, Effective heat transfer coefficient ( $h_{eff}$ ), PCM height, Thermal conductivity enhancer (TCE).
Bechiri et al. [57]	Melting and Solidification	Cylindrical	Analytical	Convective wall	Heat transfer fluid temperature, cylinder size, Biot number, and heat generation value.

In their study, the two-phase Stefan problem is solved by considering the periodic boundary conditions of temperature and heat flux. In another study, the same authors [47] developed an analytical model for sinusoidal boundary condition. Singh et al. [48] analyzed the 1-D phase change Stefan problem in a semi-infinite domain with convective boundary condition. The authors considered the temperature dependent thermal coefficients and the movement of phase change material in the system. Mosaffa et al. [49] proposed an analytical model for solidification of PCM in a shell and tube configuration. The authors employed Separation of Variable method and Bessel's function to obtain temperature distribution and position of solid-liquid interface. Bansal et al. [50] analyzed the thermal behavior of PCM during charging and discharging in cylindrical configuration using Bessel's function. Kothari et al. [51] analyzed melting and solidification in an annulus with constant heat flux and convective air boundary conditions. The authors employed Kantorovich method for the analysis. In another study, the authors employed Heat Balance Integral Method (HBIM) to solve the conduction equation in the PCM and fin for a PCM based finite TES involving fins [53]. They reported the solution for temperature distribution, and interface location of solid-liquid. Voller et al. [59] proposed a numerical model with enthalpy formulation technique to study the convection/diffusion phase change problem valid for either isothermal phase change or over a range of temperature. In another analysis, the same authors [60] studied solidification of a binary alloy through numerical investigation without considering volumetric effects. Bennon et al. [63] numerically studied the binary solid-liquid phase change system. Table 1.2 shows various studies without considering volumetric change during melting and solidification of PCM.

#### *Studies with consideration volumetric change*

It may be noted that studies, discussed in the previous section, neglect the effect of shrinkage/expansion during solidification/melting of PCM. This may be due to the fact that the authors consider same value of density for solid and liquid

phases. However, PCM density varies with temperature and it possess different value of densities in solid and liquid phases. Expansion or shrinkage of PCM may occur during the solidification and melting process depending on the density variation and therefore the void is created in the TES system. Additionally, some amount of air is trapped between different PCM layers during filling of PCM in the TES system and results in the formation of void during melting and solidification process. Air in the void act as an insulator during heat transfer in PCM based LHTESS and thus affects the thermal performance of the TES system. Some of the studies [42, 64-79, 80-81] consider the void in the model during solidification and melting of PCM in their investigations. Alexiades and Solomon [42] proposed an analytical model incorporating void near cold wall for a semi-infinite domain; the authors proposed solution for constant air-solid interface. Monde and Chakraborty [74] studied volumetric expansion and shrinkage due to the difference in solid and liquid densities of PCM. Santiago et al. [75] carried out analytical investigation to predict the behavior of a one dimensional liquid-solid phase transition in the asymptotic time regime by considering volumetric effects through mass conservation. They employed Heat Balance Integral Method (HBIM) to obtain the solution. Solomon et al. [76] analyzed the effect of void during solidification of an encapsulated PCM in spherical configuration. They considered void near the cold wall. Hassab et al. [77] carried out numerical investigation and compared melting process of wax with and without volumetric expansion. The authors reported that significant difference in the melting time is obtained at low Biot number. Chiew et al. [78] investigated the effect of void considering two cases; one with 100% PCM and other with 80% PCM and 20% air gap in the TES system. The authors concluded that air acts as an insulator and effect the heat transfer performance. Janghel et al. [79] developed a one-dimensional semi-analytical model for the finite domain of air-PCM systems in order to analyze the formation of void during the solidification shrinkage. The authors employed Separation of Variable Method and observed that the effect of void growth due to shrinkage is more significant when density ratio is 1.1. Yang et al. [82] reported the numerical solution of PCM

embedded in MF considering volumetric changes during melting process. Melting rate of PCM was found to be affected by shrinkage/expansion of PCM. Table 1.3 shows various studies with consideration of volumetric change during melting and solidification of PCM

**Table 1.3** Various studies with consideration volumetric change

Author	Process	Geometry	Nature of study	Boundary condition	Parameter investigated
Monde et al. [74]	Solidification	Rectangle	Analytical	Isothermal and adiabatic wall.	Density ratio.
Santiago et al. [75]	Melting and solidification	Rectangle	Analytical and Numerical	Constant wall temperature	Length and mass of the system.
Janghel et al. [79]	Solidification	Rectangle	Analytical and Numerical	Constant wall temperature and adiabatic wall	Density ratio, Cold wall temperature, Initial temperature of PCM, Thermal conductivity with macro porosity.

#### *Effect of Nano-particle*

Studies have been carried out to analyze the effect of nanoparticle embedded phase change materials on the thermal performance [83-101]. It was argued that inclusion of nanoparticles with PCM may either enhance or deteriorate the thermal performance of PCM based system, which depends on the geometrical design, PCM type, type of nanoparticles and volume fraction of nanoparticles. Bechiri et al. [57] proposed an analytical model to study the melting and solidification of PCM embedded with nano particles.

**Table 1.4** Various studies related to effect of addition of nano-particle in the PCM

Author	Process	Geometry	Nature of study	Boundary condition	Parameter investigated
Bondareva et al. [86]	Melting	Rectangle	Numerical	Convective and insulated wall.	Nano-particle concentration, inclination angle,
Bondareva et al. [87]	Melting	Rectangle	Numerical	Constant heat flux	Volume fraction of nano-particles, finning length and intensity of heat generation inside the heat source
Ghalambaz et al. [88]	Melting	Rectangle	Numerical	Constant wall temperature	Nano-particle volume fraction, various types of nano-particle
Sheikholeslami et al. [90]	Solidification	Wavy shape cylinder	Numerical	Constant wall temperature	Nano-particle volume fraction, particle diameter, Length, and angle of fin.
Alizadeh et al. [93]	Solidification	Cylinder	Numerical	Constant wall temperature	Geometric parameters of Y-shaped fins including the bifurcation angle and fin length
Alizadeh et al. [95]	Solidification	Cylinder	Numerical	Constant wall temperature	Nanoparticles shape factor, radiation parameter and fractal pattern iteration

Volumetric heat generation has been considered in their model. Solutions are obtained by employing separation of variable method and exponential integration function. The efficiency of the TES system is found to be greater and lower than unity with positive and negative heat generation, respectively [57]. Kalaiselvam et al. [101] analyzed the heat transfer through PCM dispersed with nano particles in a spherical container by employing quasi steady approximation method. The authors reported the solution for temperature variation, interface positions, rate of solidification and melting; the melting and solidification rate is found to be enhanced by addition of nanoparticles. Table 1.4 shows various studies related to effect of addition of nano-particle in the PCM.

#### *Effect of porous matrix*

Apart from fins and nanoparticles, porous matrix structure is widely used to enhance the thermal performance of PCM based systems [82, 102-110]. Hossain et al. [107] proposed a numerical model to investigate the free convection melting process in a rectangle enclosure with PCM-metal foam (MF) composite involving constant temperature boundary condition at the top and adiabatic condition at the bottom. The melting time of PCM is found to be reduced with the inclusion of MF in PCM. Based on the natural convection study of PCM in a cavity filled with porous medium, it was argued that with the increase of Rayleigh number or Darcy number the heat transfer rate improves in PCM [109]. Table 1.5 shows various studies related to effect of addition of porous matrix in the PCM.

**Table 1.5** Various studies related to effect of porous matrix

Author	Process	Geometry	Nature of study	Boundary condition	Parameter investigated
Sivasankaran et al. [102]	Melting	Rectangle	Numerical	Constant wall temperature	Nano-particle volume fraction, porosity, Rayleigh number, Nusselt number.
Sardari et al. [103]	Charging and discharging	Rectangle	Numerical	Constant wall temperature	Metal foam porosity
Paknezhad et al. [104]	Melting	Rectangle	Experimental	Constant heat flux	Incline angle. Foam porosity, heat flux
Zheng et al. [106]	Melting	Rectangle	Experimental	Constant heat flux	Effect of copper foam and heater position
Jethelah et al. [109]	Melting	Cylinder	Numerical	Constant wall temperature	Geometric parameters of Y-shaped fins including the bifurcation angle and fin length
Zhu et al. [110]	Melting	Rectangle	Experimental	Constant heat flux	Pore size of copper foam, heating power

### 1.6.2 Studies considered transient boundary condition

Most of the above studies consider steady heat load for the analysis, while in real situation the heat load can be cyclic or transient in nature. Many a times, the electronic devices undergo sudden periodic or pulse heat generation, load transition, irregular switching, irregular change of operation. In such a case, because of fluctuating/transient loads thermal shocks may develop and may deteriorate the thermal performance. Also, because of mismatch between the

availability and demand of energy, the heat load on thermal energy resources vary with time. In view of this, numerous studies have been made to address the effect of transient/cyclic heat load on the thermal performance of PCM based systems. Analytical models are proposed to analyze the solidification and melting behavior of PCM in a finite TES with periodic temperature/heat flux [46] and sinusoidal [47] boundary conditions. The position of interface was obtained as the sum of steady component and a fluctuating component with mean value equal to zero. Chakraborty et al. [110] proposed an analytical model to study the melting/solidification behavior of PCM for constant heat flux and convection boundary conditions at the walls by employing variational formulation method coupled with the Kantorovich method. The transient cooling behavior of paraffin-nickel foam composite thermal systems in an annulus was studied through numerical investigation [112]. In their study, pulse heat load is applied at inner surface and outer surface is maintained at convective cooling. The cooling power was found to increase by four times using PCM-MF composite compared to pure PCM.

## **1.7 Scope of the present investigation**

The literature review reports various available analytical models on the heat transfer performance of thermal energy storage and thermal management systems. These studies consider the effect of various parameters such as voids, TCEs, input heat load condition on the thermal performance. Also, studies have been made that consider various parameters such as length of the fin, dimension of the container, inclination angle, volume concentration of the nano-particles, porosity and pore size of the metal foam, on the thermal performance. Nevertheless, following issues are identified that need further investigations and are detailed below:

- Limited analytical studies are available that consider the effect of air voids during melting/solidification process of PCM. It is observed that voids present in TES affects the thermal performance and therefore, the effect of

air voids need to be incorporated in the model while designing TES system.

- The effect of various parameters such as density ratio, radius ratio, and cold wall temperature on the heat transfer performance for cylindrical TES involving air voids during solidification/melting has not been reported extensively in the literature.
- Limited studies have been made that consider effect of expansion/shrinkage and air void on thermal performance during design of PCM based thermal management systems involving different geometries.
- Many a times, electronic devices undergo sudden periodic or pulse heat generation during its operation; therefore, studies need to be made to analyze the effect of transient/cyclic heat load on the thermal performance of PCM based systems. Very often, these models neglect the effect of volumetric changes (shrinkage and expansion) in the analysis.
- Analytical studies incorporating the effect of voids on PCM-metal foam (MF) composite based heat sinks for transient heat loads has not been reported in the literature. Efforts should be made to study the effect of transient heat load/pulse heat load on the thermal performance.

The present study is aimed to obviate some of the issues highlighted above. The aim of the present thesis is to analyze the effect of volumetric change and air void in PCM on the thermal performance of PCM based systems considering two geometries mainly annular and rectangular. Here, expansion is considered during melting while shrinkage during solidification. Also, efforts have been made to analyze the heat transfer performance with incorporation of metal foam along with PCM in heat sinks involving steady and transient heat loads. The separation of variable method using Bessel function has been employed to solve the conduction equation associated with different thermal boundary conditions. Effect of various parameters such as density ratio, wall temperature, wall heat flux condition, convective heat transfer coefficient, radius ratio, and porosity of MF on the thermal performance is investigated.

The organization of the thesis is as follows:

Chapter 1: This chapter introduces a brief description of the phase change material along with various types of thermal energy storage systems. A brief literature review is reported; the scope and objectives are highlighted in this chapter.

Chapter 2: Chapter two presents the analytical investigation pertaining to the solidification and melting of phase change material involving shrinkage/expansion void in an annulus. Here, efforts have been made to study the effect of various parameters such as air void, density ratio, radius ratio, and wall temperature on the thermal performance.

Chapter 3: This chapter reports the thermal performance of PCM-MF composite inside rectangular domain with volumetric expansion/shrinkage during melting/solidification process. The effect of various parameters such as density ratio, wall heat flux, convective heat transfer coefficient, and porosity of MF on thermal performance is analyzed. The energy efficiency of storage systems with pure PCM and PCM-MF matrix is reported.

Chapter 4: Conclusions obtained from the present analytical investigations are presented in this chapter. Scope for further investigation is also discussed.



## **Chapter 2**

# **Melting and solidification model of phase change material with volumetric shrinkage/expansion void in an annulus**

### **2.1 General background**

It may be noted that many a times air voids are present in the thermal energy storage (TES) system. This may be due to various reasons such as entrapment of air bubbles between the PCM layer while filling the TES container and the air voids are provided to accommodate the possible volume expansion/shrinkage of PCM due to melting/solidification process. This occurs because of the large density difference of solid and liquid phases of PCM. The air voids act as an insulating layer and lowers the heat transfer performance. Therefore, the effect of air voids needs to be taken into account while designing TES system. Limited analytical studies are available [74, 79] that consider the effect of air voids during solidification process of PCM. Both the studies consider rectangular TES system for the analysis. It may be noted that TES involving cylindrical geometries are widely used in variety of applications because of higher efficiency and lesser volume [113]. These includes space and green house heating [114, 115], solar heating and cooling [113], and domestic hot water system [113]. The effect of various parameters such as density ratio, radius ratio, and cold wall temperature on the heat transfer performance for cylindrical TES involving air voids during solidification/melting has not been reported in the literature. Also, the movement of solid-liquid interface changes during solidification and melting process due to different melting and solidification temperature and varying thermal conductivity of PCM. It is expected that the air void may hinder the melting process of PCM.

In this chapter, efforts have been made to propose an analytical model to analyze the solidification/melting behavior of PCM in cylindrical TES considering voids to incorporate volume shrinkage/ expansion of PCM due to solidification/melting process. Separation of variable method using Bessel

function has been employed for all domains, namely, air, solid and liquid to obtain the solution. Effect of various parameters, namely density ratio, radius ratio and cold wall temperature on the heat transfer performance have been analyzed for cylindrical TES.

## 2.2 Description of the physical problem

Here, pure paraffin wax having solid to liquid density ratio  $\sim 1.16$  has been chosen as a PCM and the thermo-physical properties of solid and liquid phases are presented in Table 2.1 [79]. Due to the density difference, shrinkage and expansion takes place during solidification/melting of PCM, respectively in an annulus and leads to formation of void either near the cold or hot walls.

**Table 2.1** Thermo-physical properties of paraffin wax

Properties	Solid phase (20 <sup>0</sup> C)	Liquid phase (70 <sup>0</sup> C)
Density (kg/m <sup>3</sup> )	916	790
Thermal conductivity (W/m-K)	0.346	0.167
Specific heat (J/kg-K)	1770	1770
Melting temperature (K)	337	-
Latent heat (J/kg)	173500	-

Fig. 2.1(a) shows the schematic diagram of the annular cavity with inner and outer radius of 2 mm ( $R'_{in} = 0.25$ ) and 10 mm ( $R'_{out} = 1.25$ ), respectively. The height (H) of the annulus is taken as 15 mm ( $h' = 1.875$ ). Here, two cases are analyzed, viz. (i) evolution of void near the cold wall while other walls are maintained at adiabatic condition during solidification of PCM, and (ii) evolution of void near the hot wall while other walls are maintained at adiabatic condition during melting of PCM.



as 4.0 mm ( $R'_{al} = 0.5$ ) and 4.01 mm ( $R'_{sl} = 0.501$ ) from the center of annulus, respectively. During initial phase of solidification, temperature drops in the air domain and air-solid/solid-liquid interface moves towards the adiabatic wall and the thickness of void tends to increase in the annulus. While during melting analysis, PCM expands, and thickness of void starts to decrease, and temperature increases in the air domain.

Following assumptions are made for the analysis for solidification and melting analysis of PCM with consideration of void [79].

- (i) Constant thermo-physical properties of air, solid and liquid are considered in the respective phases.
- (ii) Conduction is considered as dominant mode of heat transfer; the effect of buoyancy and gravity are considered to be negligible.
- (iii) PCM is considered as pure material with isothermal melting and solidification.
- (iv) Initially, the difference in the values of  $R_{as}(t)$  or  $R_{al}(t)$  and  $R_{sl}(t)$  is assumed to be very small.

### 2.3 Mathematical formulation

The one dimensional governing equation for three domains, namely, air, solid and liquid for solidification and melting of PCM in an annulus (Fig 1a) is given by

$$\frac{1}{r} \frac{\partial}{\partial r} \left( r \frac{\partial T_\phi}{\partial r} \right) = \frac{1}{\alpha_\phi} \frac{\partial T_\phi}{\partial t} \quad R_{in} < r < R_{out} \quad (2.1)$$

And  $\alpha$  is the thermal diffusivity of the domain.

The above equation can be converted into non-dimensional form with the use of following non-dimensional parameters.

$$\theta_\phi = \frac{T_\phi - T_\phi}{T_o - T_\phi} \begin{cases} \varphi = c, & \text{for solidification} \\ \varphi = h, & \text{for melting} \end{cases} \quad (2.2a)$$

$$r' = \frac{r}{R_{out} - R_{in}} \quad (2.2b)$$

$$F_0 = \frac{\alpha_f t}{(R_{out} - R_{in})^2} \begin{cases} f = l, & \text{for solidification} \\ f = s, & \text{for melting} \end{cases} \quad (2.2c)$$

And the non-dimensional form of air-solid, air-liquid and solid-liquid interface position can be expressed as follows.

$$R'_{as} = \frac{R_{as}}{R_{out} - R_{in}} \quad (2.2d)$$

$$R'_{al} = \frac{R_{al}}{R_{out} - R_{in}} \quad (2.2e)$$

$$R'_{sl} = \frac{R_{sl}}{R_{out} - R_{in}} \quad (2.2f)$$

$$h' = \frac{H}{R_{out} - R_{in}} \quad (2.2g)$$

Therefore, Eq. (1.1) can be converted into non-dimensional form for the three domains as follows:

*For solidification*

$$\text{air domain, } \frac{1}{r'} \frac{\partial}{\partial r'} \left( r' \frac{\partial \theta_a}{\partial r'} \right) = \frac{1}{\alpha'_a} \frac{\partial \theta_a}{\partial F_0} \quad R'_{in} < r' < R'_{as}(F_0) \quad (2.3a)$$

$$\text{solid domain, } \frac{1}{r'} \frac{\partial}{\partial r'} \left( r' \frac{\partial \theta_s}{\partial r'} \right) = \frac{1}{\alpha'_s} \frac{\partial \theta_s}{\partial F_0} \quad R'_{as}(F_0) < r' < R'_{sl}(F_0) \quad (2.3b)$$

$$\text{liquid domain, } \frac{1}{r'} \frac{\partial}{\partial r'} \left( r' \frac{\partial \theta_l}{\partial r'} \right) = \frac{\partial \theta_l}{\partial F_0} \quad R'_{sl}(F_0) < r' < R'_{out} \quad (2.3c)$$

*For melting*

$$\text{air domain, } \frac{1}{r'} \frac{\partial}{\partial r'} \left( r' \frac{\partial \theta_a}{\partial r'} \right) = \frac{1}{\alpha'_a} \frac{\partial \theta_a}{\partial F_0} \quad R'_{in} < r' < R'_{al}(F_0) \quad (2.4a)$$

$$\text{liquid domain, } \frac{1}{r'} \frac{\partial}{\partial r'} \left( r' \frac{\partial \theta_l}{\partial r'} \right) = \frac{1}{\alpha'_l} \frac{\partial \theta_l}{\partial F_0} \quad R'_{al}(F_0) < r' < R'_{sl}(F_0) \quad (2.4b)$$

$$\text{solid domain, } \frac{1}{r'} \frac{\partial}{\partial r'} \left( r' \frac{\partial \theta_s}{\partial r'} \right) = \frac{\partial \theta_s}{\partial F_0} \quad R'_{sl}(F_0) < r' < R'_{out} \quad (2.4c)$$

Subjected to following initial and boundary conditions

$$r' = R'_{in}, \theta_a = 0 \quad \text{For solidification and melting} \quad (2.5)$$

$$F_0 = 0, \theta_o = 1 \quad \text{For solidification and melting} \quad (2.6)$$

$$\theta_\phi = \theta_z \begin{cases} \phi = a \left\{ \begin{array}{l} z = p, \text{ at } r' = R'_{as}, R'_{sl}, \text{ for solidification and melting} \end{array} \right. & (2.7) \\ \phi = s \left\{ \begin{array}{l} z = p, \text{ at } r' = R'_{as}, \text{ for solidification} \\ z = m, \text{ at } r' = R'_{sl}, \text{ for solidification and melting} \end{array} \right. & (2.8a) \\ \phi = l \left\{ \begin{array}{l} z = p, \text{ at } r' = R'_{al}, \text{ for melting} \\ z = m, \text{ at } r' = R'_{sl}, \text{ for solidification and melting} \end{array} \right. & (2.8b) \\ & (2.9a) \\ & (2.9b) \end{cases}$$

And,

$$r' = R'_{out}, \theta_\phi = \frac{\partial \theta_\phi}{\partial r'} = 0 \quad \left\{ \begin{array}{l} \phi = l, \text{ for solidification} \\ \phi = s, \text{ for melting} \end{array} \right. \quad (2.10a)$$

$$(2.10b)$$

$$\alpha' = \frac{\alpha_\chi}{\alpha_\phi}$$

$$\phi = \begin{cases} l, \text{ for solidification} \\ s, \text{ for melting} \end{cases} \quad \text{and } \chi = \begin{cases} a, \text{ for air domain} \\ s, \text{ for solid domain} \\ l, \text{ for liquid domain} \end{cases} \quad (2.11)$$

Here,  $\theta_p$  is air-solid interface temperature in case of solidification and air-liquid interface temperature in case of melting of PCM.

The governing equations (Eqs. 2.3-2.4) along with the initial condition (Eq. 2.6) and boundary conditions (Eqs. 2.5, 2.6-2.10) are solved by employing Separation of Variable method. Initially the solution for temperature distribution is obtained for each region (air, solid and liquid). Subsequently, the energy balance and mass balance are used at the interface of air-solid, air-liquid, and solid-liquid interface. The solutions are obtained to estimate the solidification and melting rate of PCM inside the annulus. The solutions for each domain are elaborated below.

### 2.3.1 Air domain

Utilizing the governing Eqs. (2.3a and 2.4a), initial condition (Eq. 2.6), boundary conditions (Eqs. 2.5, 2.7) and employing the method of Separation of Variable, the temperature distribution of air domain is expressed as:

$$\theta_a^k = \frac{\theta_p^k \ln\left(\frac{R'_{in}}{r'}\right)}{\ln\left(\frac{R'_{in}}{R'_y}\right)} + \sum_{m=1}^{\infty} A_m^{k-1} \left( J_0(\beta'_m r') Y_0(\beta'_m R'_y) - Y_0(\beta'_m r') J_0(\beta'_m R'_y) \right) e^{(-\alpha'_m \beta_m'^2 F_0^k)} \quad (2.11)$$

Here, k denotes the present time step,  $A_m^{k-1}$  is the constant which is used from Eq. (2.11) by using initial condition (Eq. 2.6) and is given by

$$A_m^{k-1} = \frac{1}{N(\beta'_m)} \int_{R_m}^{R_m^{k-1}} r' M_1 \left( J_0(\beta'_m r') Y_0(\beta'_m R_y^{k-1}) - Y_0(\beta'_m r') J_0(\beta'_m R_y^{k-1}) \right) dr \quad (2.12a)$$

where

$$M_1 = \left( \frac{\theta_p^{k-1} \ln \frac{r'}{R'_{in}} + \theta_a^{k-1} \ln \left( \frac{R'_{in}}{R'_y} \right)}{\ln \left( \frac{R'_{in}}{R'_y} \right)} \right), \quad y = \begin{cases} as, \text{Solidification} \\ al, \text{Melting} \end{cases} \quad (2.12b)$$

Here,  $\theta_c$  is cold wall temperature,  $\theta_h$  is hot wall temperature  $\beta'_m$  is Eigen value,  $\theta_p$  is air-solid interface temperature in case of solidification and air-liquid interface temperature in case of melting of PCM,  $J_0$  and  $Y_0$  are the Bessel function of zero order of the first and second kind.  $\beta'_m$  is calculated using the following equation.

$$J_0(\beta'_m R'_{in}) Y_0(\beta'_m R'_y) - Y_0(\beta'_m R'_{in}) J_0(\beta'_m R'_y) = 0 \quad (2.13)$$

The Norm  $N(\beta'_m)$  used in the Eq. (12a) can be expressed as

$$N(\beta'_m) = \frac{2}{\pi^2} \frac{J_0^2(\beta'_m R'_{in}) - J_0^2(\beta'_m R_y^{k-1})}{\beta_m'^2 J_0^2(\beta'_m R'_{in})} \quad (2.14)$$

Eqs. (2.12a), (2.13), and (2.14) can be solved by considering  $R_{as}^{k-1} = 2.299 \text{ mm}$  ( $R'_{as} = 0.29$ ) for solidification and  $R_{al}^{k-1} = 4.0 \text{ mm}$  ( $R'_{al} = 0.5$ ) for melting.

### 2.3.2 Solid PCM domain

This section reports the estimation of temperature distribution in the solid PCM. Utilizing the governing Eqs. (2.3b and 2.4c), initial condition (Eq. 2.6), boundary conditions (Eqs. 2.8a-2.8b) and employing the Separation of Variable method, the temperature distribution of solid domain is expressed as:

$$\theta_s^k = \frac{\theta_p^k \ln\left(\frac{r'}{R_{sl}^k}\right) + \theta_m \ln\left(\frac{R_{as}^k}{r'}\right)}{\ln\left(\frac{R_{as}^k}{R_{sl}^k}\right)} + \sum_{m=1}^{\infty} B_m^{k-1} \left( J_0(\beta'_m r') Y_0(\beta'_m R_{sl}^k) - Y_0(\beta'_m r') J_0(\beta'_m R_{sl}^k) \right) e^{(-\alpha'_m \beta_m'^2 F_0^k)}$$

for solidification (2.15a)

$$\theta_s^k = \theta_m + \sum_{m=1}^{\infty} C_m^{k-1} \left( J_0(\beta'_m r') Y_0'(\beta'_m R_{out}^k) - Y_0(\beta'_m r') J_0'(\beta'_m R_{out}^k) \right) e^{(-\beta_m'^2 F_0^k)}$$

for melting (2.15b)

Here, k denotes the present time step,  $B_m^{k-1}$  and  $C_m^{k-1}$  are the constants which is used from Eqs. (2.15a) and (2.15b), respectively by using initial condition (Eq. 2.3c) and are given by

$$B_m^{k-1} = \frac{1}{N(\beta'_m)} \int_{R_{as}^{k-1}}^{R_{sl}^{k-1}} Q_2 r' \left( J_0(\beta'_m r') Y_0(\beta'_m R_{sl}^{k-1}) - Y_0(\beta'_m r') J_0(\beta'_m R_{sl}^{k-1}) \right) dr$$

(2.16a)

where

$$Q_2 = \left( \frac{\theta_m^{k-1} \ln\left(\frac{r'}{R_{as}^{k-1}}\right) + \theta_s^{k-1} \ln\left(\frac{R_{as}^{k-1}}{R_{sl}^{k-1}}\right) - \theta_p^{k-1} \ln\left(\frac{r'}{R_{sl}^{k-1}}\right)}{\ln\left(\frac{R_{as}^{k-1}}{R_{sl}^{k-1}}\right)} \right)$$

(2.16b)

And,

$$C_m^{k-1} = \frac{1}{N(\beta'_m)} \int_{R_{sl}^{k-1}}^{R_{out}^k} \left[ r' \left( J_0(\beta'_m r') Y_0'(\beta'_m R_{out}^k) - Y_0(\beta'_m r') J_0'(\beta'_m R_{out}^k) \right) (\theta_s^{k-1} - \theta_m) \right] dr$$

(2.17)

Here,  $\theta_m$  is the melting temperature,  $\beta'_m$  is Eigen value,  $\theta_p$  is the air-solid interface temperature,  $J_0$  is the Bessel functions of zero order of the first kind, while  $Y_0$  is the Bessel functions of zero order of second kind.  $\beta'_m$  is calculated using the following equation.

$$J_0(\beta'_m R_{as}^{k-1})Y_0(\beta'_m R_{sl}^{k-1}) - Y_0(\beta'_m R_{as}^{k-1})J_0(\beta'_m R_{sl}^{k-1}) = 0 \quad \text{for solidification} \quad (2.18a)$$

$$J_0(\beta'_m R_{sl}^{k-1})Y'_0(\beta'_m R'_{out}) - Y_0(\beta'_m R_{sl}^{k-1})J'_0(\beta'_m R'_{out}) = 0 \quad \text{for melting} \quad (2.18b)$$

The Norm  $N(\beta'_m)$  used in the Eqs. (2.16a) and (2.17) can be expressed as

$$N(\beta'_m) = \frac{2}{\pi^2} \frac{J_0^2(\beta'_m R_{as}^{k-1}) - J_0^2(\beta'_m R_{sl}^{k-1})}{\beta_m'^2 J_0^2(\beta'_m R_{as}^{k-1})} \quad \text{for solidification} \quad (2.19a)$$

$$N(\beta'_m) = \frac{2}{\pi^2} \frac{J_0^2(\beta'_m R_{sl}^{k-1}) - J_0^2(\beta'_m R'_{out})}{\beta_m'^2 J_0^2(\beta'_m R_{sl}^{k-1})} \quad \text{for melting} \quad (2.19b)$$

Eqs. (2.16a), (2.18a) and (2.19a) can be solved by considering  $R_{as}^{k-1} = 2.299$  ( $R'_{as} = 0.29$ ) mm and  $R_{sl}^{k-1} = 2.3$  mm ( $R'_{sl} = 0.288$ ) at the initial stage ( $F_0 = 0$ ). While Eqs. (2.17), (2.18b) and (2.19b) are solved by considering  $R_{sl}^{k-1} = 4.01$  mm ( $R'_{sl} = 0.501$ ) at the initial stage ( $F_0 = 0$ ).

### 2.3.3 Liquid domain

By using initial and boundary condition Eqs. (2.6, 2.9a-2.9b) and applying the Separation of Variable Method in the governing Eqs. (2.3c and 2.4b), final temperature distribution of liquid domain is expressed as:

$$\theta_l^k = \theta_m + \sum_{m=1}^{\infty} C_m^{k-1} \left( J_0(\beta'_m r') Y'_0(\beta'_m R'_{out}) - Y_0(\beta'_m r') J'_0(\beta'_m R'_{out}) \right) e^{(-\beta_m'^2 F_0^k)} \quad \text{for solidification} \quad (2.20a)$$

$$\theta_l^k = \frac{\theta_p \ln\left(\frac{r'}{R_{sl}^k}\right) + \theta_m \ln\left(\frac{R_{al}^k}{r'}\right)}{\ln\left(\frac{R_{al}^k}{R_{sl}^k}\right)} + \sum_{m=1}^{\infty} B_m^{k-1} \left( J_0(\beta'_m r') Y_0(\beta'_m R_{sl}^k) - Y_0(\beta'_m r') J_0(\beta'_m R_{sl}^k) \right) e^{(-\alpha'_m \beta_m'^2 F_0^k)} \quad \text{for melting} \quad (2.20b)$$

Here,  $k$  denotes the present time step,  $C_m^{k-1}$  and  $B_m^{k-1}$  are the constants which is used from Eqs. (2.20a) and (2.20b), respectively by using initial condition (Eq. 2.6) and are given by

$$C_m^{k-1} = \frac{1}{N(\beta'_m)} \int_{R_{sl}^{k-1}}^{R'_{out}} r' \left( J_0(\beta'_m r') Y_0'(\beta'_m R'_{out}) - Y_0(\beta'_m r') J_0'(\beta'_m R'_{out}) \right) (\theta_l^{k-1} - \theta_m) dr \quad (2.21)$$

And,

$$B_m^{k-1} = \frac{1}{N(\beta'_m)} \int_{R_{al}^{k-1}}^{R_{sl}^{k-1}} Q_2 r' \left( J_0(\beta'_m r') Y_0(\beta'_m R_{sl}^{k-1}) - Y_0(\beta'_m r') J_0(\beta'_m R_{sl}^{k-1}) \right) dr \quad (2.22a)$$

where

$$Q_2 = \left( \frac{\theta_m \ln\left(\frac{r'}{R_{al}^{k-1}}\right) + \theta_l^{k-1} \ln\left(\frac{R_{al}^{k-1}}{R_{sl}^{k-1}}\right) - \theta_p^{k-1} \ln\left(\frac{r'}{R_{sl}^{k-1}}\right)}{\ln\left(\frac{R_{al}^{k-1}}{R_{sl}^{k-1}}\right)} \right) \quad (2.22b)$$

Here,  $\theta_m$  is the melting temperature,  $\beta'_m$  is Eigen value,  $\theta_p$  is the air-liquid interface temperature,  $J_0$  are the Bessel functions of zero order of the first kind, while  $Y_0$  are the Bessel functions of zero order of second kind.  $\beta'_m$  is calculated using the following equation.

$$J_0(\beta'_m R_{sl}^{k-1}) Y_0'(\beta'_m R_{out}) - Y_0(\beta'_m R_{sl}^{k-1}) J_0'(\beta'_m R_{out}) = 0 \quad \text{for solidification} \quad (2.23a)$$

$$J_0(\beta'_m R_{al}^{k-1}) Y_0(\beta'_m R_{sl}^{k-1}) - Y_0(\beta'_m R_{al}^{k-1}) J_0(\beta'_m R_{sl}^{k-1}) = 0 \quad \text{for melting} \quad (2.23b)$$

The Norm  $N(\beta'_m)$  used in the Eqs. (21) and (22a) can be expressed as

$$N(\beta'_m) = \frac{2}{\pi^2} \frac{J_0^2(\beta'_m R_{sl}^{k-1}) - J_0'^2(\beta'_m R_{out})}{\beta_m^2 J_0^2(\beta'_m R_{sl}^{k-1})} \quad \text{for solidification} \quad (2.24a)$$

$$N(\beta'_m) = \frac{2}{\pi^2} \frac{J_0^2(\beta'_m R_{al}^{k-1}) - J_0^2(\beta'_m R_{sl}^{k-1})}{\beta_m^2 J_0^2(\beta'_m R_{al}^{k-1})} \quad \text{for melting} \quad (2.24b)$$

Eqs. (2.21), (2.23a) and (2.24a) can be solved by considering  $R_{sl}^{k-1} = 2.3$  mm ( $R'_{sl} = 0.29$ ) at the initial stage ( $F_0 = 0$ ). While Eqs. (2.22a), (2.23b) and (2.24b) are solved by considering  $R_{al}^{k-1} = 4.0$  mm ( $R'_{al} = 0.5$ ) and  $R_{sl}^{k-1} = 4.01$  mm ( $R'_{sl} = 0.501$ ) at the initial stage ( $F_0 = 0$ ).

It may be noted that in case of solidification analysis of PCM,  $\theta_p^k$  is unknown in Eqs. (2.11), (2.15a), and (2.20b) In order to find the value of  $\theta_p^k$  heat balance is considered at an air-solid interface. Air-solid interface condition is given by

$$\left. \frac{d\theta_u}{dr'} \right|_{r'=R'_y} = K_{ua} \left. \frac{d\theta_u}{dr'} \right|_{r'=R'_y} \quad (2.25)$$

By using Eqs. (2.11), (2.15a) and (2.20b) expression of  $\theta_p^k$  can be written as

$$\theta_p^k = \frac{\frac{K_{ua}\theta_m}{\ln\left(\frac{R'_y}{R'_{sl}}\right)} + R'_y{}^{k-1} \left( P'_a(R'_y{}^k) - K_{ua}P'_u(R'_y{}^k) \right)}{\frac{K_{ua}}{\ln\left(\frac{R'_y}{R'_{sl}}\right)} + \frac{1}{\ln\left(\frac{R'_{in}}{R'_y}\right)}} \quad (2.26a)$$

where  $P'_a$  and  $P'_u$  can be written as

$$P'_a = \sum_{m=1}^{\infty} A_m^{k-1} \left( J_0(\beta'_m r') Y_0(\beta'_m R'_{as}{}^k) - Y_0(\beta'_m r') J_0(\beta'_m R'_y{}^k) \right) e^{(-\alpha'_a \beta_m'^2 F_0^k)} \quad (2.26b)$$

$$P'_u = \sum_{m=1}^{\infty} B_m^{k-1} \left( J_0(\beta'_m r') Y_0(\beta'_m R'_{sl}{}^k) - Y_0(\beta'_m r') J_0(\beta'_m R'_{sl}{}^k) \right) e^{(-\alpha'_u \beta_m'^2 F_0^k)} \quad (2.26c)$$

$$K_{ua} = \frac{K_u}{K_a} \quad (2.26d)$$

and,

$$u = \begin{cases} s, \text{Solidification} \\ l, \text{Melting} \end{cases} \quad (2.26e)$$

Stefan condition is used to find out the position of solid-liquid interface position and expressed as follows:

$$\rho_s L \frac{dR'_{sl}}{dt} = K_s \left. \frac{dT_s}{dr} \right|_{r=R'_{sl}} - K_l \left. \frac{dT_l}{dr} \right|_{r=R'_{sl}} \quad (2.27)$$

Equation can be expressed in non-dimensional form as follows.

$$\frac{dR'_{sl}}{dF_0} = \gamma_s \alpha'_s \frac{d\theta_s}{dr'} - \gamma_l \frac{d\theta_l}{dr'} \quad \text{for solidification} \quad (2.28a)$$

$$\frac{dR'_{sl}}{dF_0} = \gamma_s \frac{d\theta_s}{dr'} - \gamma_l \alpha'_l \frac{d\theta_l}{dr'} \quad \text{for melting} \quad (2.28b)$$

where

$$\gamma_\phi = \frac{\rho_\phi c_{p\phi} \left( \frac{St_s}{c_{p_s}} + \frac{St_l}{c_{p_l}} \right)}{\rho_s} \quad (2.28c)$$

By using Eqs. (2.15a), (2.20a) during solidification and (2.15b), (2.20b) during melting, expression of solid-liquid interface position can be written as

$$\frac{dR'_{sl}}{dF_0} = \gamma_s \alpha'_s \left( \frac{\left( \frac{\theta_p^{k-1} - \theta_m}{R'_{sl}{}^{k-1}} \right) + P'_s (R'_{sl}{}^{k-1})}{\ln \left( \frac{R'_{as}{}^{k-1}}{R'_{sl}{}^{k-1}} \right)} \right) - \gamma_l M'_l (R'_{sl}{}^{k-1}) \quad \text{for solidification} \quad (2.29)$$

$$\frac{dR'_{sl}}{dF_0} = \gamma_s M'_s (R'_{sl}{}^{k-1}) - \gamma_l \alpha'_l \left( \frac{\left( \frac{\theta_p^{k-1} - \theta_m}{R'_{sl}{}^{k-1}} \right) + P'_l (R'_{sl}{}^{k-1})}{\ln \left( \frac{R'_{al}{}^{k-1}}{R'_{sl}{}^{k-1}} \right)} \right) \quad \text{for melting} \quad (2.30)$$

$P_s$  for solidification and  $P_l$  for melting is given by Eq. (2.26c), while  $M_l$  for solidification and  $M_s$  for melting is given by

$$M_w = \sum_{m=1}^{\infty} C_m^{k-1} \left( J_0(\beta'_m r') Y'_0(\beta'_m R'_{out}) - Y_0(\beta'_m r') J'_0(\beta'_m R'_{out}) \right) e^{(-\beta_m^2 F_0^k)} \quad (2.31a)$$

and,

$$w = \begin{cases} l, & \text{Solidification} \\ s, & \text{Melting} \end{cases} \quad (2.31b)$$

Value of solid-liquid interface at any time instant during solidification and melting of PCM can be calculated by using Euler method as follows

$$R'_{sl}{}^k = R'_{sl}{}^{k-1} + \Delta F_0 (\delta^{k-1}) \quad (2.32)$$

Where,  $\delta^{k-1}$  is given by right hand sides of Eqs. (2.29) and (2.30) for solidification and melting, respectively. Initial values of  $R'_{sl}{}^{k-1}$  and  $R'_{as}{}^{k-1}$  is taken as 2.3 mm ( $R'_{sl} = 0.29$ ) and 2.299 mm ( $R'_{as} = 0.29$ ), respectively for solidification and

initial values of  $R_{sl}^{k-1}$  and  $R_{al}^{k-1}$  is taken as 4.01 mm ( $R'_{sl} = 0.501$ ) and 4.0 mm ( $R'_{al} = 0.5$ ) for melting of PCM.

In order to find air-solid interface position, a mass balance equation is used through the air-solid interface and the position of air-solid interface is expressed below.

$$R_y^k = \sqrt{(R_y^{k-1})^2 + (1 - \rho_n) \left( (R_{sl}^k)^2 - (R_{sl}^{k-1})^2 \right)} \quad (2.33a)$$

where

$$\rho_n = \begin{cases} \frac{\rho_l}{\rho_s}, & \text{Solidification} \\ \frac{\rho_s}{\rho_l}, & \text{Melting} \end{cases} \quad (2.33b)$$

After solving all the equations, the values of  $\theta_a^k$ ,  $\theta_s^k$ ,  $\theta_l^k$ ,  $\theta_p^k$ ,  $R_{as}^k$ ,  $R_{al}^k$  and  $R_{sl}^k$  at the present time step is obtained.

Present prediction for the annulus, obtained through separation of variable method, is compared with results of Janghel et al. [79] for rectangular thermal energy storage system (Table 2.2). Present model yields closed form expression for temperature distribution in different domains such as (air, solid and liquid) and interface position as a function of various parameters (Eqs 2.11, 2.15a, 2.15b, 2.22a, 2.22b, 2.26a, 2.32, 2.33a ). Based on the known values of thermo-physical properties and geometrical parameters one can estimate the temperature distribution and the interface location.

#### 2.3.4 Calculation of energy extracted/stored during solidification/melting of PCM.

To analyze the effect of shrinkage/expansion on the TES system efficiency, fraction of energy extracted and stored during solidification and melting at any time instant need to be calculated. The fraction of energy extracted/stored during solidification/melting is expressed as the ratio of total energy extracted to total energy stored during solidification. Also, it is defined as

the ratio of the total energy stored to the total energy provided during melting of PCM [79].

*Fraction of total energy extracted/stored [79]*

$$Q'_{e/s} = \frac{\int_0^t Q_{\text{extracted/stored}} dt}{m(c_{p_s}(T_m - T_c) + c_{p_l}(T_o - T_m) + L)} \quad (2.34)$$

Where energy extracted and energy stored during solidification and melting of PCM, respectively are calculated by the following equation.

$$Q_{\text{extracted/stored}} = -K_a \left. \frac{dT_a}{dr} \right|_{\substack{\text{cold wall, for solidification} \\ \text{hot wall, for melting}}} \quad (2.35)$$

**Table 2.2** Comparison of mathematical expressions for temperature distribution of three domains

Source	Process	Expression for Temperature Distribution		
		Air domain	Solid domain	Liquid domain
Janghel et al. [79]	Solidification	$\theta_a^k = \frac{(\theta_p^k)x}{x_{as}^k} + \sum_{n=1}^{\infty} A_n^{k-1} \sin\left(\frac{n\pi x'}{x_{as}^k}\right) \exp(-\alpha_a' \lambda_n^2 F_0^k)$	$\theta_s^k = \frac{(\theta_p^k - \theta_m)(x' - x_{ls}^k)}{x_{as}^k - x_{sl}^k} + \theta_m + \sum_{n=1}^{\infty} B_n^{k-1} \sin\left(\frac{n\pi(x' - x_{ls}^k)}{x_{as}^k - x_{sl}^k}\right) \exp(-\alpha_s' \lambda_n^2 F_0^k)$	$\theta_l^k = \theta_m + \sum_{n=1}^{\infty} C_n^{k-1} \sin\left(\frac{(2n-1)\pi(x' - x_{sl}^k)}{2(1-x_{sl}^k)}\right) \exp(-\lambda_n^2 F_0^k)$
Present analysis	Solidification	$T_a^k = \frac{T_c \ln\left(\frac{r}{R_{as}^k}\right) + T_p \ln\left(\frac{R_{in}}{r}\right)}{\ln\left(\frac{R_{in}}{R_{as}^k}\right)} + \sum_{m=1}^{\infty} A_m^{k-1} \left( J_0(\beta_m r) Y_0(\beta_m R_{as}^k) - Y_0(\beta_m r) J_0(\beta_m R_{as}^k) \right) e^{(-\alpha_a \beta_m^2 t^k)}$	$T_s^k = \frac{T_p \ln\left(\frac{r}{R_{sl}^k}\right) + T_m \ln\left(\frac{R_{as}^k}{r}\right)}{\ln\left(\frac{R_{as}^k}{R_{sl}^k}\right)} + \sum_{m=1}^{\infty} B_m^{k-1} \left( J_0(\beta_m r) Y_0(\beta_m R_{sl}^k) - Y_0(\beta_m r) J_0(\beta_m R_{sl}^k) \right) e^{(-\alpha_s \beta_m^2 t^k)}$	$T_l^k = T_m + \sum_{m=1}^{\infty} C_m^{k-1} \left( J_0(\beta_m r) Y_0'(\beta_m R_{out}) - Y_0(\beta_m r) J_0'(\beta_m R_{out}) \right) e^{(-\alpha_l \beta_m^2 t^k)}$

	Melting	$T_a^k = \frac{T_h \ln\left(\frac{r}{R_{al}^k}\right) + T_p^k \ln\left(\frac{R_{in}}{r}\right)}{\ln\left(\frac{R_{in}}{R_{al}^k}\right)} +$ $\sum_{m=1}^{\infty} A_m^{k-1} \left( J_0(\beta_m r) Y_0(\beta_m R_{as}^k) - Y_0(\beta_m r) J_0(\beta_m R_{as}^k) \right) e^{(-\alpha_m \beta_m^2 t^k)}$	$T_s^k = T_m +$ $\sum_{m=1}^{\infty} C_m^{k-1} \left( J_0(\beta_m r) Y_0'(\beta_m R_{out}) - Y_0(\beta_m r) J_0'(\beta_m R_{out}) \right) e^{(-\alpha_m \beta_m^2 t^k)}$	$T_l^k = \frac{T_p^k \ln\left(\frac{r}{R_{sl}^k}\right) + T_m \ln\left(\frac{R_{al}^k}{r}\right)}{\ln\left(\frac{R_{al}^k}{R_{sl}^k}\right)} +$ $\sum_{m=1}^{\infty} B_m^{k-1} \left( J_0(\beta_m r) Y_0(\beta_m R_{sl}^k) - Y_0(\beta_m r) J_0(\beta_m R_{sl}^k) \right) e^{(-\alpha_m \beta_m^2 t^k)}$
--	---------	--	--	--

## 2.4 Validation of Present Model

Efforts have been made to compare present results with the test results of Akgun et al. [117] during solidification process and Sari et al. [116] during melting process. Akgun et al. [117] carried out tests to study the solidification of PCM in an annulus. The test set up includes an annulus with inner radius and outer radius of 14 mm ( $R'_m = 0.4242$ ) and 47 mm ( $R'_{out} = 1.4242$ ), respectively. In their study, paraffin wax is considered as a PCM with melting temperature 44.23°C ( $\theta_m = 0.55$ ). Thermo-physical properties of paraffin, considered in their study, are shown in Table 2.3. The HTF with temperature 293 K ( $\theta_c = 0$ ) was allowed to flow at three different flow rates (4, 6, and 8 kg/min) through the inner cylinder during solidification process. Fig. 2.2a shows the comparison of temperature distribution with time at  $r = 28$  mm ( $r' = 0.8484$ ) during solidification process. Present model exhibits good agreement with the test data of Akgun et al. [117] and the maximum error was found to be 2.051%. In addition to this, the temperature variation at different radial distance ( $r' = 0.4242$ , 0.8484, and 1.4242) at  $t = 20$  min ( $Fo = 0.002401$ ) during solidification process obtained from present model are compared with the test data of Akgun et al. [117] and is shown in Fig. 2.2b. The results obtained from the present analytical model is in good agreement with the test data of Akgun et al. [117] with the maximum deviation of ~1%.

**Table 2.3** Thermo-physical properties of Lauric acid [116] and Paraffin wax [117]

PCM	Melting point (°C)	Density (kg/ m <sup>3</sup> )	Latent heat (J/kg)	Thermal conductivity (W/m-K)	Specific heat capacity (J/kg-K)
Paraffin wax	44.23	794	249000	0.21	2100
Lauric acid	41-43	1007(s), 862(l)	211600	0.147	1760 (s), 2270 (l)

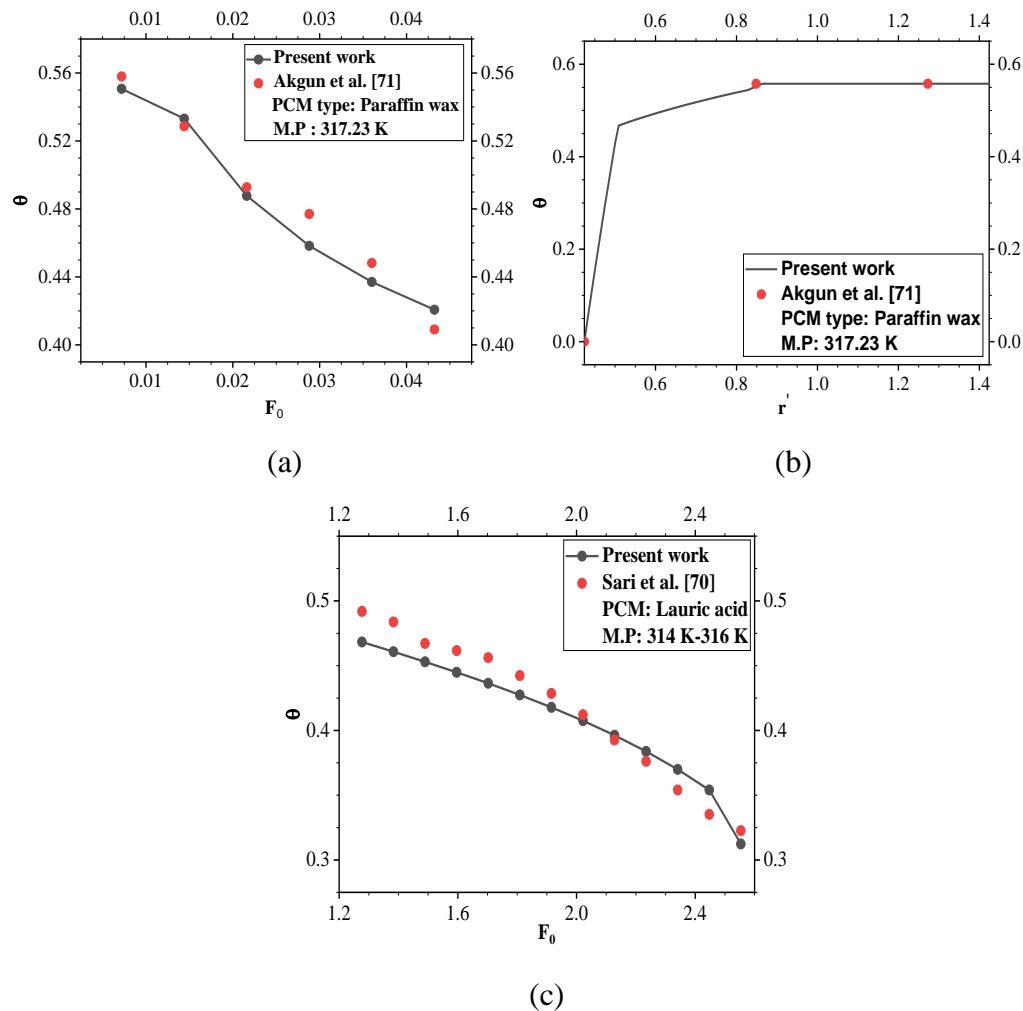


Fig. 2.2 Comparison of present prediction with the test data of Sari et al. [116] and Akgun et al. [117] for (a) Different time instant at  $r = 28$  mm during solidification process, (b) Different radial distance at  $t = 20$  min during solidification process, and (c) Different time instant at  $r = 21.25$  mm during melting process

Also, an effort has been made to compare the present results obtained during melting process with the test result of Sari et al. [116]. The authors [116] carried out tests to study the melting of PCM in a cylindrical annulus. The test set up includes an annulus with inner radius and outer radius of 13.75 mm ( $R'_{in} =$

0.37) and 51.25 mm ( $R'_{out} = 1.37$ ), respectively. In their study, Lauric acid ( $C_{11}H_{23}COOH$ ) is considered as a PCM with the melting temperature range varying between 41°C-43°C ( $\theta_m = 0.5-0.45$ ). The thermo-physical properties of Lauric acid, considered in their study, are shown in Table 2.3. The HTF with temperature 335 K was allowed to flow at Stefan number = 0.283 and Reynolds number = 31.12 through the inner cylinder during melting process. The outside surface of the PCM container was well insulated by a glass wool of 30 mm thickness in order to prevent heat losses to the surroundings. Fig. 2.2c shows the comparison of temperature distribution with time at  $r = 21.25$  mm ( $r' = 0.57$ ) during melting process. Present prediction exhibits good agreement with the test data of Sari et al. [116] with the maximum deviation of ~4.3%.

## 2.5 Result and Discussions

Here, pure paraffin wax having solid to liquid density ratio ~1.16 and ~1 has been chosen as a PCM and the thermo-physical properties of paraffin wax in solid and liquid phases are presented in Table 2.1. An effort has been made to investigate the effect of void during solidification and melting of PCM in an annulus. The model considers shrinkage and expansion during solidification and melting, respectively for the analysis. Constant temperature boundary condition has been imposed on one end wall, while the other walls are kept at adiabatic boundary condition for this analysis. A one dimensional analytical model involving three domains namely, air, solid and liquid is considered for solidification and melting of PCM. Separation of Variable method with Bessel function is used to obtain solution. Conservation of mass is applied at the interface to obtain the amount of shrinkage or expansion. While Stefan condition is used to obtain solid-liquid interface position. Effect of various parameters such as density ratio, wall temperature, and radius ratio during solidification and melting process of PCM are analyzed and detailed in this section.

### 2.5.1 Solidification analysis

### *Effect of shrinkage of PCM during solidification*

Fig. 2.3(a) shows temperature distribution of PCM in the three different domains at different radial distance. Initially, an air gap of 0.299 mm is considered near the cold wall. Cold wall temperature is maintained at 307 K ( $\theta_c = 0$ ). Initial temperature of PCM is taken as 338 K ( $\theta_o = 1$ ), this indicates the entire paraffin wax is in liquid phase during start of solidification. Spatial variation of temperature is measured at different time duration such as 200 s ( $F_o = 0.37$ ), 800 s ( $F_o = 1.49$ ), and 1400 s ( $F_o = 2.61$ ). One can notice the interface of air-solid and solid-liquid by identifying the variation in slope of the curve (Fig. 2.3a). The initial position of air-solid and solid-liquid interfaces is assumed to be 2.299 mm and 2.3 mm, respectively in this study. Air-solid interface at 200 s ( $F_o = 0.37$ ), 800 s ( $F_o = 1.49$ ), and 1400 s ( $F_o = 2.61$ ) are found to be 3.3 mm ( $R'_{as} = 0.4125$ ), 3.5 mm ( $R'_{as} = 0.4375$ ), and 3.6 mm ( $R'_{as} = 0.45$ ), respectively from the center of the annulus. Solid-liquid interface at 200 s ( $F_o = 0.37$ ), 800 s ( $F_o = 1.49$ ), and 1400 s ( $F_o = 2.61$ ) are found to be 6.9 mm ( $R'_{sl} = 0.8625$ ), 7.4 mm ( $R'_{sl} = 0.925$ ), and 7.9 mm ( $R'_{sl} = 0.9875$ ), respectively from the center of the annulus. It is observed that the air-solid interface moves towards the outer wall. This indicates that PCM shrinks during conversion of its phase from liquid to solid. This occurs because of difference in the density of solid and liquid phases of PCM. Therefore, it can be concluded that volume of void increases with the progress of solidification process.

Fig. 2.3(b) shows the position of air-solid and solid-liquid interfaces at different time instant for two different PCMs having density ratio  $\sim 1$  and  $\sim 1.16$ . For density ratio of 1, the position of air-solid interface remains constant with progress of solidification. While the solid-liquid interface propagates from 2.3 mm ( $R'_{sl} = 0.2875$ ) to 9.8 mm ( $R'_{sl} = 1.225$ ) with the time duration of 1400 s. This indicates that the volume of void remains constant in the TES system during solidification. In case of PCM with density ratio  $\sim 1.16$ , air-solid interface moves

from 2.299 at  $t = 0$  s ( $F_0 = 0$ ) to 3.6 mm ( $R'_{as} = 0.45$ ) at  $t = 1400$  s ( $F_0 = 2.61$ ). While solid-liquid interface moves from 2.3 mm ( $R'_{sl} = 0.2875$ ) to 7.9 mm ( $R'_{sl} = 0.9875$ ) with the time duration of 1400 s ( $F_0 = 2.61$ ). Solid-liquid interface moves 76.53% and 70.88% for density ratio of 1 and 1.16, respectively for the time duration of 1400 s ( $F_0 = 2.61$ ). It may be noted that solidification rate is lower in case of density ratio 1.16 compared to density ratio of 1. This indicates that solidification rate decreases because of the shrinkage of PCM.

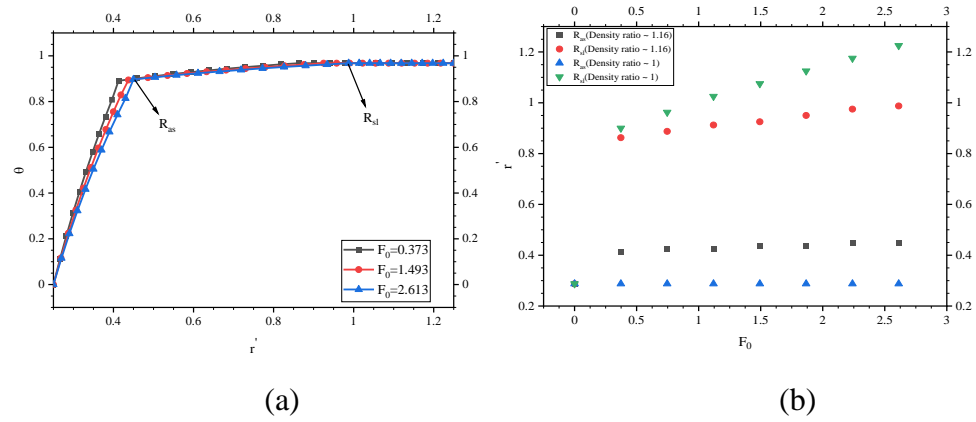


Fig. 2.3(a) Spatial variation of non-dimensional temperature at different time duration, (b) Non-dimensional air-solid ( $R'_{as}$ ) and solid-liquid ( $R'_{sl}$ ) interface positions with  $F_0$  for density ratio of 1 and 1.16

#### *Effect of Cold wall temperature*

Fig. 2.4(a) shows the effect of different cold wall temperatures such as 297 K ( $St_s = 0.408$ ), 307 K ( $St_s = 0.306$ ), and 317 K ( $St_s = 0.204$ ) on temperature distribution, position of air-solid and location of solid-liquid interfaces in an annulus at  $t = 800$  s ( $F_0 = 1.49$ ). The positions of air-solid interface are found to be 3.6 mm ( $R'_{as} = 0.45$ ), 3.5 mm ( $R'_{as} = 0.4375$ ), and 3.4 mm ( $R'_{as} = 0.425$ ) from the center of the annulus at cold wall temperature of 297 K ( $St_s = 0.408$ ), 307 K ( $St_s = 0.306$ ), and 317 K ( $St_s = 0.204$ ), respectively. Also, the positions of solid-liquid interface are found to be 7.7 mm ( $R'_{sl} = 0.9625$ ), 7.4 mm ( $R'_{sl} = 0.925$ ), and

7.2 mm ( $R'_{sl} = 0.9$ ) from the center of the annulus at cold wall temperature of 297 K ( $St_s = 0.408$ ), 307 K ( $St_s = 0.306$ ), and 317 K ( $St_s=0.204$ ), respectively. Also, the temperature transients of PCM at a radial distance of 5 mm ( $r' = 0.625$ ) from the center of the annulus at various cold wall temperatures such as 297 K, 307 K and 317 K is shown in Fig. 2.4(b). It may be noted that non-dimensional temperature increases with the decrease in cold wall temperature at a given location. This indicates that the PCM temperature decreases with the decrease in cold wall temperature at a given location. The maximum increase in non-dimensional temperature (decrease in PCM temperature) is found to be around 0.02 (i.e. 1 K) with the decrease in cold wall temperature from 317 K to 297 K at time duration of 800 s ( $F_0 = 1.49$ ). It may be inferred from the figures that shrinkage as well as solidification rate increases with the decrease in cold wall temperature and increase in Stefan number.

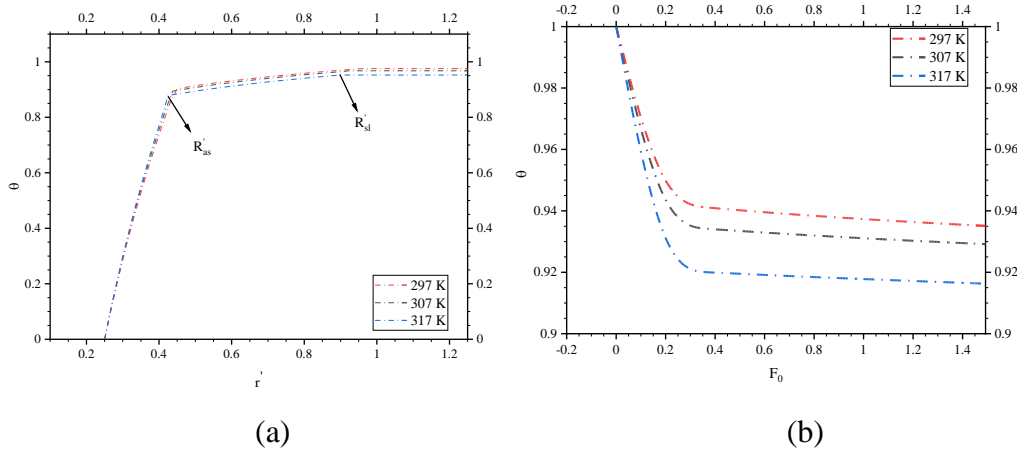


Fig 2.4 (a) Temperature variation with radial distance for different cold wall temperatures at  $t = 800$  s ( $F_0 = 1.49$ ) and density ratio of 1.16, (b) Temperature history during solidification at  $r = 5$  mm ( $r' = 0.625$ ) at density ratio of 1.16

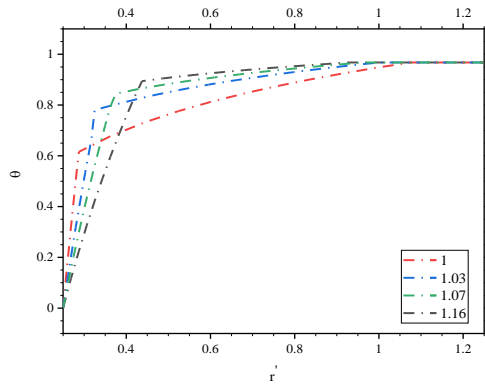
### *Effect of density ratio*

Effect of different density ratio such as 1, 1.03, 1.07, and 1.16 on temperature variation, position of air-solid and location of solid-liquid interfaces in an annulus at different radial distance has been shown in Fig. 2.5(a). The

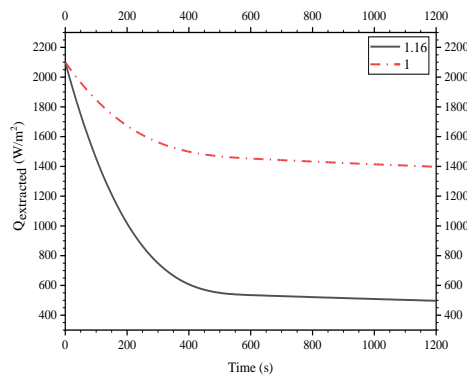
positions of air-solid interface are found to be 2.3 mm ( $R'_{as} = 0.2875$ ), 2.6 mm ( $R'_{as} = 0.325$ ), 3 mm ( $R'_{as} = 0.375$ ), and 3.5 mm ( $R'_{as} = 0.4375$ ) from the center of the annulus for density ratio 1, 1.03, 1.07, and 1.16, respectively at  $t = 800$  s ( $F_0 = 1.49$ ). Also, the positions of solid-liquid interface are found to be 8.6 mm ( $R'_{sl} = 1.075$ ), 8 mm ( $R'_{sl} = 1$ ), 7.7 mm ( $R'_{sl} = 0.9625$ ), and 7.4 mm ( $R'_{sl} = 0.925$ ) from the center of the annulus at for density ratio 1, 1.03, 1.07, and 1.16, respectively at  $t = 800$  s ( $F_0 = 1.49$ ). With the increase in density ratio the solidification shrinkage increases and results in increase in volume of the void. The percentage increase in shrinkage with respect to total PCM volume is found to be from  $\sim 7.35\%$  with the increase in density ratio from 1 to 1.16. Also, as density ratio increases the movement of solid-liquid interface decreases. The percentage decrease in the movement of solid-liquid interface is found to be  $\sim 14\%$  with the increase in density ratio from 1 to 1.16. This indicates that with the increase in density ratio, the solidification rate increases results in the increase in air gap which in turn decreases the heat transfer rate.

Fig. 2.5(b) shows the energy extracted ( $Q_{\text{extracted}}$ ) from the solidified PCM for different values of density ratio (1.16 and 1). For density ratio of 1.16, the energy extracted from TES during solidification decreases with time. The value of  $Q_{\text{extracted}}$  is found to be  $568.3 \text{ W/m}^2$  and  $496.65 \text{ W/m}^2$  for 200 s ( $F_0 = 0.37$ ) and 1200 s ( $F_0 = 2.24$ ), respectively. The value of  $Q_{\text{extracted}}$  is found to be  $1505.1 \text{ W/m}^2$  and  $1397.42 \text{ W/m}^2$  for 200 s ( $F_0 = 0.37$ ) and 1200 s ( $F_0 = 2.24$ ), respectively with density ratio of 1. The energy extraction rate decreases with the progress of time. Here,  $Q_{\text{extracted}}$  is found to decrease by 12.61% and 7.2% for density ratio of 1.16 and 1, respectively. The energy extraction rate is lower for density ratio of 1.16 compared to the unit density ratio. The percentage reduction in the energy extracted with the increase in density ratio of 1 and 1.16 is found to be 62% and 64.24% at 200 s ( $F_0 = 0.37$ ) and 1200 s ( $F_0 = 2.24$ ), respectively. As the density variation occurs in solid to liquid phase, the air gap increases and acts as an insulator subsequently restricts in the path of heat transfer through PCM. It is

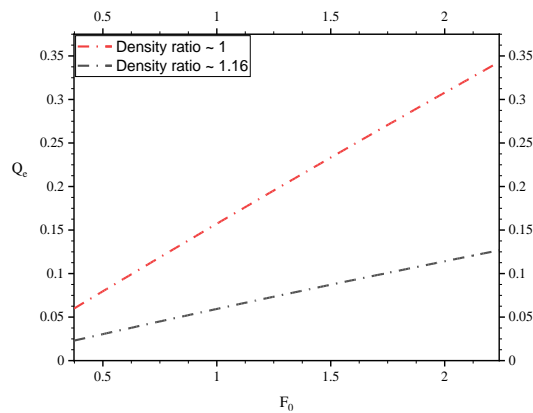
useful to estimate the fraction of total energy extracted and can be estimated by using Eqs. 34-35. From Fig. 2.5(c), the fraction of total energy extracted ( $Q'_e$ ) at density ratios of 1.16 and 1 are found to be 0.02 and 0.06, respectively for the time duration  $t = 0$  s to 200 s ( $F_0 = 0-0.37$ ). While, with the increases in time duration  $t = 0$  s -1200 s ( $F_0 = 0-2.24$ ), the energy extraction rate is found to be 0.13 and 0.34 for the density ratio of 1.16 and 1, respectively. For the density ratio of 1, the fraction of extracted energy is found to increase by 467% with increase in time period from  $t = 200$  s to  $t = 1200$  s ( $F_0 = 0.37$  to  $F_0 = 2.24$ ). While for density ratio of 1.16, the increase in the fraction of extracted energy is found to be 550% with the increase in time period from  $t = 200$  s to  $t = 1200$  s ( $F_0 = 0.37$  to  $F_0 = 2.24$ ). The fraction of total energy extracted is increased by 66.67% and 61.76% for  $t = 200$  s ( $F_0 = 0.37$ ) and  $t = 1200$  s ( $F_0 = 2.24$ ), respectively with the decrease in the density ratio.



(a)



(b)



(c)

Fig. 2.5(a) Temperature variation with radial distance for different density ratio values (b) Energy extracted from liquid PCM for density ratio of 1, 1.16 (c) Fraction of total energy extracted at density ratio 1 and 1.16

### Effect of radius ratio

Radius ratio ( $R_r$ ) is defined as the ratio of inner radius to the outer radius. The effect of radius ratio on temperature variation, and position of air-solid and solid-liquid interfaces in an annulus is analyzed in this study and is shown in Fig. 2.6. For  $R_r = 0.2$ , the air-solid and solid-liquid interfaces are found to be 3.5 mm ( $R'_{as} = 0.4375$ ) and 7.4 mm ( $R'_{sl} = 0.925$ ), respectively at  $t=800$  s ( $F_0 = 1.49$ ). While, for  $R_r = 0.3$ , the air-solid and solid-liquid interface are found to be 4.4 mm ( $R'_{as} = 0.61$ ) and 8.7 mm ( $R'_{sl} = 1.21$ ), respectively at  $t=800$  s ( $F_0 = 1.49$ ) and density ratio  $\sim 1.16$ . For  $t = 800$  s ( $F_0 = 1.49$ ), the solid fraction value is found to be 0.44 and 0.57 for  $R_r = 0.2$  and  $R_r = 0.3$ , respectively. The rate of solidification of PCM is found to increase with the increase in radius ratio. The solidification shrinkage is found to be 328.03 mm<sup>3</sup> and 465.05 mm<sup>3</sup> for  $R_r = 0.2$  and  $R_r = 0.3$ , respectively. Therefore, with increase in radius ratio from 0.2 to 0.3, the solidification shrinkage increases by 41.77%.

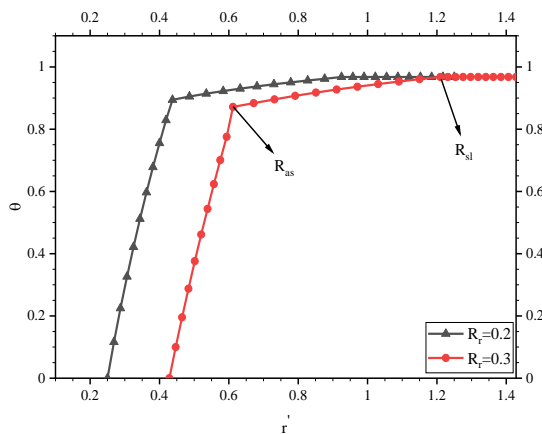


Fig. 2.6 Temperature variation with radial distance for radius ratio values of 0.2 and 0.3

## 2.5.2 Melting analysis

### *Effect of expansion of PCM during melting*

Fig. 2.7(a) shows temperature distribution of PCM in the three different domains at different radial distance. Initially, an air gap of 2.0 mm is considered near the hot wall. Hot wall temperature is maintained at 375 K ( $\theta_h = 0$ ). Initial temperature of PCM is taken as 336 K ( $\theta_o = 1$ ), this indicates that the entire paraffin wax is in solid phase during start of melting. Spatial variation of temperature is calculated at different time duration such as 40 s ( $F_o = 0.13$ ), 800 s ( $F_o = 2.67$ ), and 1400 s ( $F_o = 4.67$ ). One can notice the interface of air-liquid and solid-liquid by identifying the variation in slope of the curve (Fig. 2.7a). The initial position of air-liquid and solid-liquid interface is assumed to be 4.0 mm ( $R'_{al} = 0.5$ ) and 4.01 mm ( $R'_{sl} = 0.501$ ), respectively from the center of the annulus in this study. Air-liquid interface at 40 s ( $F_o = 0.13$ ), 800 s ( $F_o = 2.67$ ), and 1400 s ( $F_o = 4.67$ ) are found to be 4 mm ( $R'_{al} = 0.5$ ), 3.7 mm ( $R'_{al} = 0.4625$ ), and 3.5 mm ( $R'_{al} = 0.4375$ ), respectively from the center of the annulus. Solid-liquid interface at 40 s ( $F_o = 0.13$ ), 800 s ( $F_o = 2.67$ ), and 1400 s ( $F_o = 4.67$ ) are found to be 4.3 mm ( $R'_{sl} = 0.5375$ ), 5.4 mm ( $R'_{sl} = 0.675$ ), and 6.2 mm ( $R'_{sl} = 0.775$ ), respectively from the center of the annulus. It is observed that the air-liquid interface moves towards the center of the annulus. This indicates that PCM expands during conversion of its phase from solid to liquid. This occurs because of difference in the density of solid and liquid phases of PCM. Therefore, it can be concluded that void space must be given for free expansion of liquid PCM during melting of PCM. Also, volume of void reduces with the progress of melting process.

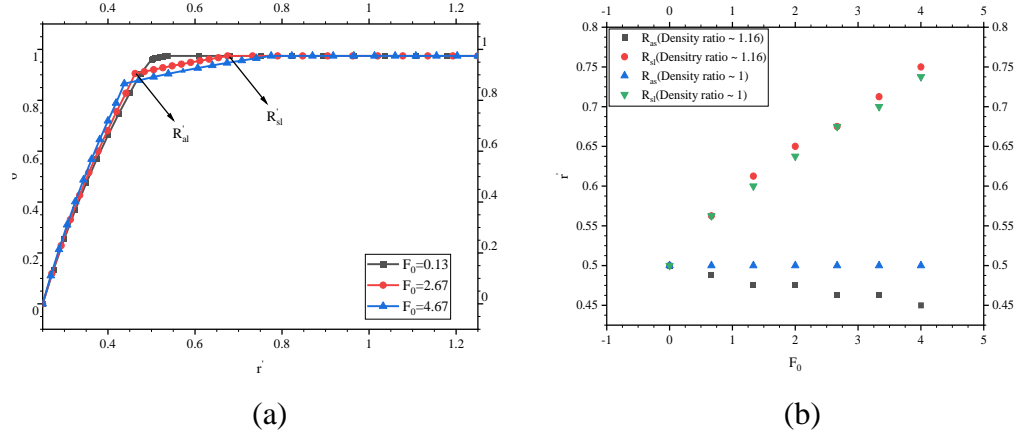


Fig. 2.7 (a) Spatial variation of temperature with radial distance at different time duration, (b) Air-solid ( $R_{as}$ ) and solid-liquid ( $R_{sl}$ ) interface positions at different time duration for density ratio of 1 and 1.16

Fig. 2.7(b) shows the position of air-liquid and solid-liquid interfaces at different time instant for two different PCMs having density ratio  $\sim 1$  and  $\sim 1.16$ . For density ratio 1, the position of air-liquid interface remains constant with progress of melting. The solid-liquid interface propagates from 4.01 mm ( $R'_{sl} = 0.501$ ) to 6.1 mm ( $R'_{sl} = 0.7625$ ) with the time duration of 1400 s ( $F_0 = 2.67$ ). This indicated that the volume of void remains constant in the TES system during melting process. In case of PCM with density ratio  $\sim 1.16$ , air-liquid interface moves from 4.0 ( $R'_{al} = 0.5$ ) at  $t = 0$  ( $F_0 = 0$ ) s to 3.5 mm ( $R'_{al} = 0.4375$ ) at  $t = 1400$  s ( $F_0 = 4.67$ ). While solid-liquid interface moves from 4.01 mm ( $R'_{sl} = 0.501$ ) to 6.2 mm ( $R'_{sl} = 0.775$ ) with the increase in time duration from start of melting to 1400 s ( $F_0 = 4.67$ ). Solid-liquid interface moves 35.32% and 34.26% for density ratio of 1.16 and 1, respectively for the time duration of 1400 s ( $F_0 = 4.67$ ). It may be noted that melting rate is higher in case of density ratio 1.16 compared to density ratio of 1. This indicates that melting rate increases because of the expansion of PCM.

#### *Effect of hot wall temperature*

Fig. 2.8(a) shows the effect of different hot wall temperatures such as 365 K ( $\theta_h = 0$ ), 375 K ( $\theta_h = 0$ ) and 385 K ( $\theta_h = 0$ ) on temperature distribution, position of air-liquid and location of solid-liquid interfaces in an annulus. The positions of air-liquid interface are found to be 3.8 mm ( $R'_{al} = 0.475$ ), 3.7 mm ( $R'_{al} = 0.4625$ ), and 3.6 mm ( $R'_{al} = 0.45$ ) from the center of the annulus at hot wall temperature of 365 K ( $St_1 = 0.2856$ ), 375 K ( $St_1 = 0.3877$ ), and 385 K ( $St_1 = 0.4897$ ), respectively at  $t = 1000$  s ( $F_0 = 3.33$ ). Also, the positions of solid-liquid interface are found to be 5.3 mm ( $R'_{sl} = 0.6625$ ), 5.7 mm ( $R'_{sl} = 0.7125$ ), and 6 mm ( $R'_{sl} = 0.75$ ) from the center of the annulus at hot wall temperature of 365 K ( $St_1 = 0.2856$ ), 375 K ( $St_1 = 0.3877$ ), and 385 K ( $St_1 = 0.4897$ ), respectively at  $t = 1000$  s ( $F_0 = 3.33$ ). Also, the temperature transients of PCM at a radial distance of 5 mm ( $r' = 0.625$ ) from the center of the annulus at various hot wall temperatures such as 365 K ( $\theta_h = 0$ ), 375 K ( $\theta_h = 0$ ) and 385 K ( $\theta_h = 0$ ) is shown in Fig. 2.8(b). It may be noted that non-dimensional temperature decreases with the increase in hot wall temperature at a given location. This indicates that the PCM temperature increases with increase in hot wall temperature at a given location. The maximum decrease in non-dimensional temperature (increase in PCM temperature) is found to be around 1.4 K with the increase in hot wall temperature from 365 K ( $\theta_h = 0$ ) to 385 K ( $\theta_h = 0$ ) at time duration of 1000 s ( $F_0 = 3.33$ ). It may be inferred from the figure that expansion as well as melting rate increases with the increase in hot wall temperature and increase in Stefan number.

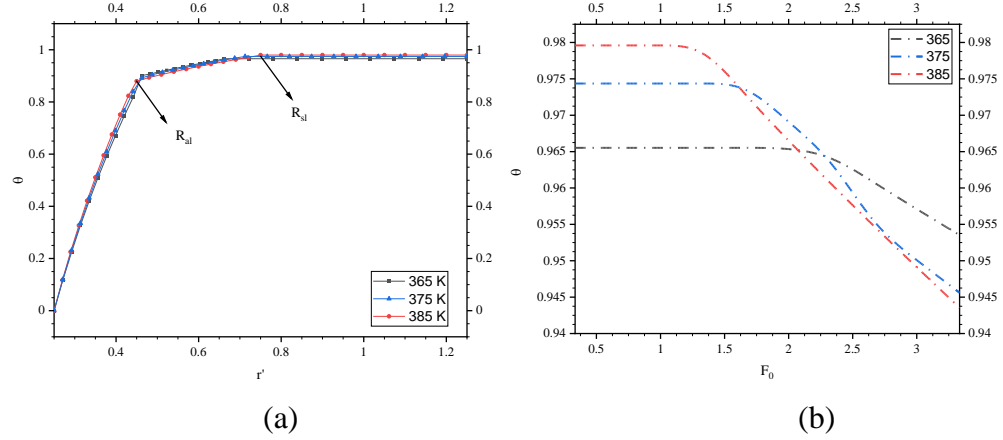


Fig 2.8 (a) Temperature variation with radial distance for different hot wall temperatures at  $t = 1000$  s ( $F_0 = 3.33$ ) and density ratio of 1.16, (b) Temperature history during melting at  $r = 5$  mm ( $r' = 0.625$ ) at density ratio of 1.16

#### *Effect of density ratio*

Effect of different density ratios (1, 1.03, 1.07, and 1.16) on temperature variation, position of air-liquid and location of solid-liquid interfaces in an annulus at different radial distance has been shown in Fig. 2.9(a). The positions of air-liquid interface are found to be 4 mm ( $R'_{al} = 0.5$ ), 3.9 mm ( $R'_{al} = 0.4875$ ), 3.9 mm ( $R'_{al} = 0.4875$ ), and 3.7 mm ( $R'_{al} = 0.4625$ ) from the center of the annulus for density ratio 1, 1.03, 1.07, and 1.16, respectively at  $t = 1000$  s ( $F_0 = 3.33$ ). Also, the positions of solid-liquid interface are found to be 5.6 mm ( $R'_{sl} = 0.7$ ), 5.6 mm ( $R'_{sl} = 0.7$ ), 5.7 mm ( $R'_{sl} = 0.625$ ), and 5.7 mm ( $R'_{sl} = 0.625$ ) from the center of the annulus at for density ratio 1, 1.03, 1.07, and 1.16, respectively at  $t = 1000$  s ( $F_0 = 3.33$ ). With the increase in density ratio the melting expansion increases and results in decreases in the volume of void. The percentage increase in expansion with respect to total PCM volume is found to be from 2.75% with the increase in density ratio from 1 to 1.16. Also, as density ratio increases the movement of solid-liquid interface increases. The percentage increase in the movement of solid-liquid interface is found to be  $\sim 2\%$  with the increase in density ratio from 1 to 1.16. This indicates that with the increase in density ratio, the melting rate

increases results in the decrease in air gap which in turn increases the heat transfer rate.

Fig. 2.9(b) shows the energy stored ( $Q_{\text{stored}}$ ) to the PCM for different values of density ratio (1 and 1.16). For density ratio of 1.16, the energy stored from TES during melting increases with time. The value of  $Q_{\text{stored}}$  is found to be 576.61 W/m<sup>2</sup> and 612.18 W/m<sup>2</sup> for the time instant 200 s ( $F_0 = 0.67$ ) and 1200 s ( $F_0 = 4$ ), respectively. The value of  $Q_{\text{stored}}$  is found to be 560.1 W/m<sup>2</sup> and 535.89 W/m<sup>2</sup> for 200 s ( $F_0 = 0.67$ ) and 1200 s ( $F_0 = 4$ ), respectively with density ratio of 1. The rate of energy storage increases by 6.2% with the progress of time for density ratio 1.16 while for density ratio 1 it is decreased by 4.3%. The energy storage rate is higher for density ratio of 1.16 compared to unit density ratio. The percentage increment in the energy stored with the increase in density ratio of 1 and 1.16 is found to be 3% and 14.24% at 200 s ( $F_0 = 0.67$ ) and 1200 s ( $F_0 = 4$ ), respectively. As the density variation occurs in solid to liquid phase of PCM, the air gap decreases and heat transfer rate increases. It is useful to estimate the fraction of total energy stored and can be estimated by using Eqs. 2.34-2.35. The fraction of total energy stored ( $Q'_s$ ) at density ratio 1 and 1.16 are found to be 0.023 and 0.024, respectively for the time duration  $t = 0$  s ( $F_0 = 0$ ) to  $t = 200$  s ( $F_0 = 0.67$ ) and is shown in Fig. 2.9c. While, with the increase in time duration  $t = 0$  s ( $F_0 = 0$ ) to  $t = 1200$  s ( $F_0 = 4$ ), the energy stored rates are found to be 0.14 and 0.15 for the density ratio of 1 and 1.16, respectively. For density ratio of 1.16, the fraction of total stored energy is found to increase by 525% with increase in time period from  $t = 200$  s ( $F_0 = 0.67$ ) to  $t = 1200$  s ( $F_0 = 4$ ). While for density ratio 1, the increase in fraction of stored energy is found to be 508.7% with increase in time period from  $t = 200$  s ( $F_0 = 0.67$ ) to  $t = 1200$  s ( $F_0 = 4$ ). The fraction of total stored energy is increased by 4.34% and 7.1% for  $t = 200$  s ( $F_0 = 0.67$ ) and  $t = 1200$  s ( $F_0 = 4$ ), respectively with the increase in the density ratio.

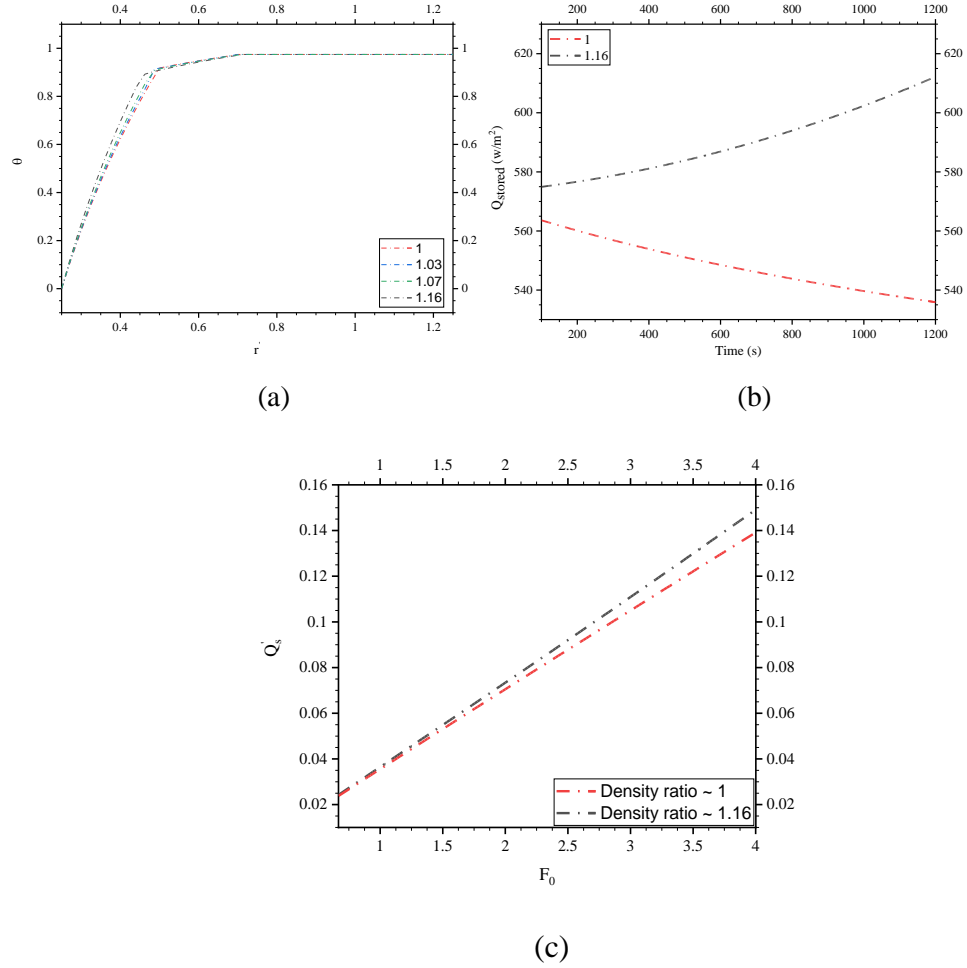


Fig. 2.9 (a) Temperature variation with radial distance for different density ratio values (b) Energy stored from liquid PCM for density ratio of 1, 1.16 (c) Fraction of total energy stored at density ratio 1.16 and 1

### *Effect of radius ratio*

Radius ratio ( $R_r$ ) is defined as the ratio of inner radius to the outer radius. The effect of radius ratio on temperature variation, and position of air-liquid and solid-liquid interfaces in an annulus is analyzed in this study (Fig. 2.10). For  $R_r = 0.2$ , the air-liquid and solid-liquid interfaces are found to be 3.7 mm ( $R'_{al} = 0.4625$ ) and 5.7 mm ( $R'_{sl} = 0.7125$ ), respectively at  $t = 1000$  s ( $F_0 = 3.33$ ) and density ratio  $\sim 1.16$ . While, for  $R_r = 0.3$ , the air-liquid and solid-liquid interface

are found to be 4.1 mm ( $R'_{sl} = 0.501$ ) and 7 mm ( $R'_{sl} = 0.875$ ), respectively at  $t = 1000$  s ( $F_0 = 3.33$ ) and density ratio  $\sim 1.16$ . For  $t = 1000$  s ( $F_0 = 3.33$ ), the liquid fraction value is found to be 0.19 and 0.33 for  $R_r = 0.2$  and  $R_r = 0.3$ , respectively. The rate of melting of PCM is found to increase with the increase in radius ratio. The melting expansion is found to be  $108.801 \text{ mm}^3$  and  $217.93 \text{ mm}^3$  for  $R_r = 0.2$  and  $R_r = 0.3$ , respectively. Therefore, with increase in radius ratio from 0.2 to 0.3, the melting expansion increases by 100.29%.

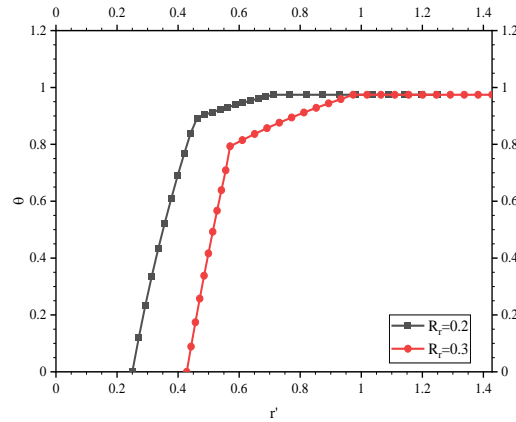


Fig. 2.10 Temperature variation with radial distance for radius ratio values of 0.2 and 0.3

## 2.6 Concluding remarks

A one dimensional analytical model is developed to study the heat transfer process in an annulus with pure PCM incorporating the effect of volumetric change. Here, expansion/ shrinkage is considered during melting/solidification process. Separation of variable method is considered to obtain the solution for temperature distribution and interface position with constant wall temperature and adiabatic boundary condition. Effect of various parameters such as density ratio,

wall temperature, radius ratio on the thermal performance is analyzed. Results obtained from this analysis are found to be in good agreement with the test data. It is summarized that with lower value of cold wall temperature ( $T_c$ ), higher value of hot wall temperature ( $T_h$ ) and higher density ratio, higher value of radius ratio, the effect of shrinkage and expansion is more prominent. This study can be useful in solar heating or cooling, thermal management of electrical vehicle and electronic devices.



## **Chapter 3**

# **Melting and solidification analysis of phase change material-metal foam composite with expansion/shrinkage void in rectangular system**

### **3.1 General background**

Most of the studies consider steady heat load for the analysis, while in real situation the heat load can be cyclic or transient in nature. Many a times, the electronic devices undergo sudden periodic or pulse heat generation, load transition, irregular switching, irregular change of operation. In such a case, because of fluctuating/transient loads thermal shocks may develop and may deteriorate the thermal performance. Also, because of mismatch between the availability and demand of energy, the heat load on thermal energy resources vary with time. It is evident from the literature that limited studies have been made that consider effect of expansion/shrinkage and air void during design of PCM based thermal management systems [79, 120]. These studies either consider pure PCM in the thermal system or consider steady heat load for the analysis. It is argued that PCM possess poor thermal conductivity and very often PCM metal foam (MF) composite are used for better thermal performance [104-106]. Many a times, electronic devices undergo sudden periodic or pulse heat generation during its operation; therefore, studies have been made to analyze the effect of transient/cyclic heat load on the thermal performance of PCM based systems. However, these models neglect the effect of volumetric changes (shrinkage and expansion) in the analysis. Analytical studies incorporating the effect of voids on PCM-MF composite based heat sinks for transient heat loads has not been reported in the literature (can be seen from Table 1.5).

In this study, efforts are made to analyze the effect of volumetric change and void in PCM on the thermal performance of PCM based systems and PCM-MF based heat sinks with steady and transient heat loads. Separation of variable

method using Bessel function has been employed to solve the conduction equation associated with different thermal boundary conditions. Closed form expression for temperature distribution has been proposed for different domains such as air, solid and liquid during melting/solidification process. The effect of steady/transient heat loads on temperature distribution and thermal performance have been analyzed. Also, the effect of inclusion of MF in PCM on the propagation of solid-liquid interface has been analyzed during melting/solidification process. The effect of various parameters such as density ratio, heat flux, convective heat transfer coefficient, and porosity on temperature distribution, interface movement, melting/solidification time have been analyzed.

### **3.2 Physical model**

Fig. 3.1 shows the schematic diagram of present analytical model valid for rectangular system of length 10 mm ( $l' = 1$ ). Present study considers paraffin wax with density ratio  $\sim 1.16$  as a PCM and copper foam as thermal conductivity enhancer (TCE). Thermo-physical properties of the PCM and copper foam are listed in the Table 3.1 [79, 121]. Two cases are considered (i) constant heat flux at one wall and other three walls are maintained at adiabatic condition during melting process (Fig. 3.1a), and (ii) natural convection at one wall and other three boundaries are maintained at adiabatic condition during solidification (Fig. 3.1b). In this study, void space is considered near left boundary where heat flux is provided during melting process, while convection is considered during solidification process (Figs. 3.1a-b).

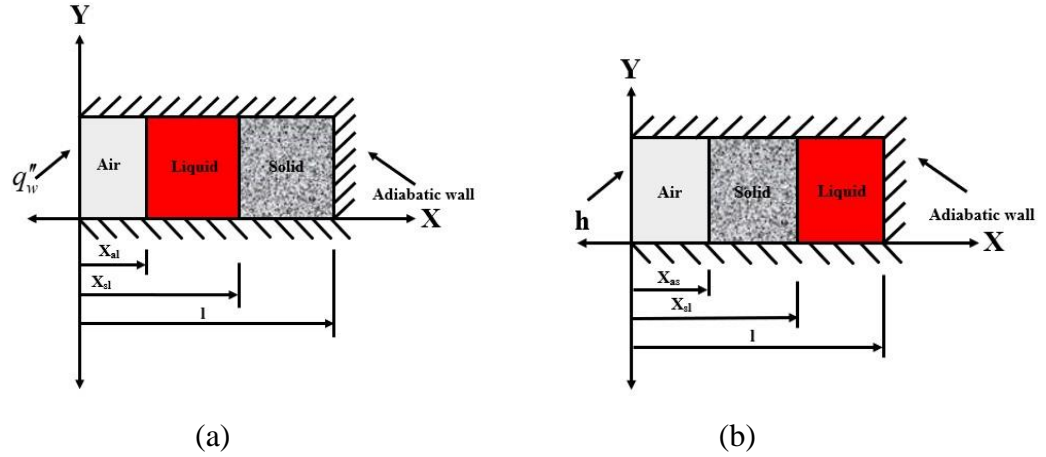


Fig. 3.1 Schematic of rectangular PCM system with void near left wall for (a) melting, (b) solidification process

Here, three domains namely air, liquid and solid are considered for the analysis. At particular time instant ( $t$ ), air-liquid interface (in case of melting), air-solid interface (in case of solidification), and solid-liquid interface are located at  $x_{al}(t)$ ,  $x_{as}(t)$ , and  $x_{sl}(t)$ , respectively. In practical scenario, the initial values of  $x_{al}(t)$  or  $x_{as}(t)$ , and  $x_{sl}(t)$  remain same for melting and solidification. However, one needs to consider different initial values of  $x_{al}(t)$ ,  $x_{as}(t)$ , and  $x_{sl}(t)$  to obtain the solution [60]. The initial values of  $x_{al}(t)$  and  $x_{sl}(t)$  are taken as 2 mm ( $x'_{al} = 0.2$ ) and 2.01 mm ( $x'_{sl} = 0.201$ ) from the left boundary, respectively during melting; the initial positions of  $x_{as}(t)$  and  $x_{sl}(t)$  are chosen as 0.5 mm ( $x'_{as} = 0.05$ ) and 0.501 mm ( $x'_{sl} = 0.501$ ) from the left boundary, respectively during solidification. During initial phase of melting the temperature increases in the air domain. In such a case the solid-liquid interface and air-liquid interface moves toward and away from the adiabatic wall, respectively; the thickness of void decreases in the enclosure due to expansion of PCM. During solidification process, temperature decreases in the air domain and air-solid/solid-liquid interface moves towards the adiabatic wall resulting in the increase in the thickness of void due to shrinkage of PCM.

**Table 3.1** Thermo physical properties of paraffin wax RT27 and Copper

PCM	Melting point (°C)	Density (kgm <sup>-3</sup> )	Latent heat (Jkg <sup>-1</sup> )	Thermal conductivity (Wm <sup>-1</sup> K <sup>-1</sup> )	Specific heat capacity (Jkg <sup>-1</sup> K <sup>-1</sup> )
Paraffin RT27	25-28	840 (s), 750 (l)	184000	0.24 (s), 0.15 (l)	2100
Paraffin wax	64	916 (s), 790 (l)	173500	0.346 (s), 0.167 (l)	1770
Copper	-	8900	-	380	386

Following assumptions are considered for the analysis for PCM based systems [79].

- I. Constant thermo-physical properties of air, solid and liquid are considered in the respective phases.
- II. Conduction is considered as dominant mode of heat transfer; the effect of buoyancy and gravity are considered to be negligible. This is applicable for  $Ra < 1000$  [79].
- III. PCM is considered as pure material with isothermal melting and solidification.
- IV. Initially, the difference in the values of  $x_{as}(t)$  or  $x_{al}(t)$  and  $x_{sl}(t)$  is assumed to be very small.

It may be noted that the physical domain involving boundary and initial conditions such as heat flux and heat transfer coefficient values, initial temperature and initial air-solid, air-liquid, and solid-liquid interfaces considered for the analysis of MF-PCM composite is similar to the pure PCM case. In general, the effective thermo-physical properties are considered to analyze the melting and solidification of PCM-MF composite system [82, 103, 104, 109, 122, 123]. These studies consider linear equations for effective thermal conductivity for the analysis. It may be noted that the correlation of effective thermal

conductivity between pure PCM and MF is complex and linear approximation may not predict the phenomena accurately. Here, the non-linear correlations of thermal conductivity, as considered by Bhattacharya et al. [123], are used to model the effective thermal conductivity of PCM-MF system. While linear variation is considered for the other thermo-physical properties such as specific heat capacity, density, and latent heat and are given as follows.

$$K_{eff} = 0.35(\xi K_{PCM} + (1-\xi) K_{MF}) + \frac{0.65}{\left(\frac{\xi}{K_{PCM}} + \frac{1-\xi}{K_{MF}}\right)} \quad (3.1a)$$

$$(\rho C_p)_{eff} = \xi(\rho C_p)_{PCM} + (1-\xi)(\rho C_p)_{MF} \quad (3.1b)$$

$$(\rho L)_{eff} = \xi(\rho L)_{PCM} \quad (3.1c)$$

### 3.3 Mathematical formulation

Considering the above assumptions, the one dimensional energy equation for the present configuration (Fig.3.1a-b) valid for three different domains, namely, air, liquid and solid for both melting and solidification process is given by:

$$\alpha_\phi \frac{\partial^2 T_\phi}{\partial x^2} = \frac{\partial T_\phi}{\partial t} \quad 0 < x < l \quad (3.2a)$$

Here,  $\alpha$  is the thermal diffusivity of the three different domains.

The above governing equation can be converted into non-dimensional form with the following parameters.

$$\theta_\phi = \frac{T_\phi - T_0}{T_m - T_0} \quad (3.2b)$$

$$x' = \frac{x}{l} \quad (3.2c)$$

$$F_0 = \frac{\alpha_f t}{l^2} \begin{cases} f = s, \text{ for melting} \\ f = l, \text{ for solidification} \end{cases} \quad (3.2d)$$

And non-dimensional air-solid, air-liquid, and solid-liquid interface are expressed as:

$$x'_\phi = \frac{x_\phi}{l} \begin{cases} \phi = al, \text{ for air-liquid interface} \\ \phi = as, \text{ for air-solid interface} \\ \phi = sl, \text{ for solid-liquid interface} \end{cases} \quad (3.2e)$$

Utilizing Eqs. (3.2b-3.2e), Eq. (3.2a) can be expressed in the non-dimensional form for all three domains as follows.

*For melting*

$$\text{Air domain, } \alpha'_a \frac{\partial^2 \theta_a}{\partial x'^2} = \frac{\partial \theta_a}{\partial F_0} \quad 0 < x' < x'_{al} \quad (3.3a)$$

$$\text{Liquid domain, } \alpha'_l \frac{\partial^2 \theta_l}{\partial x'^2} = \frac{\partial \theta_l}{\partial F_0} \quad x'_{al} < x' < x'_{sl} \quad (3.3b)$$

$$\text{Solid domain, } \frac{\partial^2 \theta_s}{\partial x'^2} = \frac{\partial \theta_s}{\partial F_0} \quad x'_{sl} < x' < 1 \quad (3.3c)$$

*For solidification*

Air domain,

$$\alpha'_a \frac{\partial^2 \theta_a}{\partial x'^2} = \frac{\partial \theta_a}{\partial F_0} \quad 0 < x' < x'_{as}(F_0) \quad (3.4a)$$

Solid domain,

$$\alpha'_s \frac{\partial^2 \theta_s}{\partial x'^2} = \frac{\partial \theta_s}{\partial F_0} \quad x'_{as}(F_0) < x' < x'_{sl}(F_0) \quad (3.4b)$$

Liquid domain,

$$\frac{\partial^2 \theta_l}{\partial x'^2} = \frac{\partial \theta_l}{\partial F_0} \quad x'_{sl}(F_0) < x' < 1 \quad (3.4c)$$

Initial and boundary conditions are given as:

$$-\frac{\partial \theta_a(x', F_0)}{\partial x'} = \psi, \text{ at } x' = 0 \text{ for melting} \quad (3.5a)$$

$$-\frac{\partial \theta_a(x', F_0)}{\partial x'} + \eta(\theta_a(x, t) - \theta_\infty) = 0, \text{ at } x' = 0 \text{ for solidification} \quad (3.5b)$$

$$\theta_\phi = \theta_z \begin{cases} \phi = a \left\{ \begin{array}{l} z = p, \text{ at } x' = x'_{as} \text{ \& } x'_{al}, \text{ for solidification and melting} \end{array} \right. & (3.5c) \\ \phi = s \left\{ \begin{array}{l} z = p, \text{ at } x' = x'_{as}, \text{ for solidification} \\ z = m, \text{ at } x' = x'_{sl}, \text{ for solidification and melting} \end{array} \right. & (3.5d) \\ \phi = l \left\{ \begin{array}{l} z = p, \text{ at } x' = x'_{al}, \text{ for melting} \\ z = m, \text{ at } x' = x'_{sl}, \text{ for solidification and melting} \end{array} \right. & (3.5e) \end{cases}$$

$$\frac{\partial \theta_\phi}{\partial x'} = 0, \text{ at } x' = 1 \begin{cases} \phi = s, \text{ for melting} \\ \phi = l, \text{ for solidification} \end{cases} \quad (3.5f)$$

$$\theta_o = 0, \text{ at } F_0 = 0 \text{ for solidification and melting} \quad (3.5g)$$

where

$$\psi = \frac{q_w'' l}{K_a (T_m - T_0)} \quad (3.6a)$$

$$\eta = \frac{hl}{K_a} \quad (3.6b)$$

Here,  $\theta_p$  is the air-liquid/air-solid interface temperature during melting and solidification process.

The governing equations (Eqs. 3.3-3.4) along with boundary conditions (Eqs. 3.5a-3.5f) and initial condition (Eq. 3.5g) are solved by employing separation of variable method. Initially, the solution for temperature distribution is obtained for each region (air, solid and liquid). Subsequently, the energy balance and mass balance are used at the interface of air-solid, air-liquid and solid-liquid interfaces. The solutions are obtained to estimate the solidification and melting rate of PCM inside the rectangular storage. The solutions for each domain are elaborated below.

### 3.3.1 Air domain

Utilizing the governing Eqs. (3.3a and 4a), initial condition (Eq. 3.5g), and boundary conditions (Eqs. 3.5a-3.5c) and employing the method of separation of variable, the temperature distribution of air domain is expressed as:

$$\theta_a^k = \theta_p^k - \psi(x'^k - x'_{al}) + \sum_{m=1}^{\infty} A_m^{k-1} \cos\left(\left(\frac{\pi(2n-1)}{2x'_{al}}\right)x'\right) e^{(-\alpha'_a \beta'_m{}^2 F_0^k)} \quad \text{for melting} \quad (3.7a)$$

$$\theta_a^k = \theta_p^k - \lambda(\theta_p^k - \theta_{\infty}^k)(x'^k - x'_{as}) + \sum_{m=1}^{\infty} B_m^{k-1} \sin \beta'_m(x'_{as} - x'^k) e^{(-\alpha'_a \beta'_m{}^2 F_0^k)} \quad \text{for solidification} \quad (3.7b)$$

Here, k denotes the present time step. The constants  $A_m^{k-1}$  and  $B_m^{k-1}$  are obtained using initial condition (Eq. 3.5g) and are given by:

$$A_m^{k-1} = \frac{2}{x'_{al}{}^{k-1}} \int_0^{x'_{al}{}^{k-1}} (\theta_a^{k-1} - \theta_p^{k-1} + \psi(x'^{k-1} - x'_{al}{}^{k-1})) \cos\left(\left(\frac{\pi(2n-1)}{2x'_{al}{}^{k-1}}\right)x'\right) dx \quad (3.8a)$$

$$B_m^{k-1} = \frac{1}{N(\beta'_m)} \int_0^{x'_{as}{}^{k-1}} (\theta_a^{k-1} - \theta_p^{k-1} - \lambda(\theta_p^{k-1} - \theta_{\infty}^{k-1})(x'^{k-1} - x'_{as}{}^{k-1})) \sin \beta'_m(x'_{as}{}^{k-1} - x'^{k-1}) dx \quad (3.8b)$$

where

$$\lambda = \frac{hl}{K_a + x_{as}h} \quad (3.9)$$

Here,  $\theta_{\infty}$  and  $\beta'_m$  denote the ambient temperature and Eigen value, respectively.

The value of  $\beta'_m$  is estimated by using the following equation.

$$\beta'_m \cos(\beta'_m x'_{as}{}^{k-1}) + \eta = 0 \quad (3.10)$$

$N(\beta'_m)$  used in Eq. (3.8b) can be found using Eq. (3.11)

$$N(\beta'_m) = \frac{x'_{as}{}^k (\beta'_m{}^2 + \eta^2) + \eta}{2(\beta'_m{}^2 + \eta^2)} \quad (3.11)$$

Eqs. (8a-8b) can be solved by considering  $x'_{al}{}^{k-1} = 2$  mm during melting; while for solidification process, one can consider  $x'_{as}{}^{k-1} = 0.5$  mm.

### 3.3.2 Solid domain

This section reports the estimation of temperature distribution in the solid PCM. Utilizing the governing Eqs. (3.3c and 3.4b), initial condition (Eqs. 3.5g), and boundary conditions (Eqs. 3.5d and 3.5f) and employing the separation of variable method, the temperature distribution of solid domain is expressed as:

$$\theta_s^k = \theta_m + \sum_{m=1}^{\infty} C_m^{k-1} \sin\left(\frac{\pi(2n-1)(x' - x_{sl}^{rk})}{2(1-x_{sl}^{rk})}\right) e^{(-\beta_m'^2 F_0^k)} \quad \text{for melting} \quad (3.12a)$$

$$\theta_s^k = \theta_m + \frac{(\theta_p^k - \theta_m)(x' - x_{sl}^{rk})}{(x_{as}^{rk} - x_{sl}^{rk})} + \sum_{m=1}^{\infty} D_m^{k-1} \sin\left(\frac{n\pi(x' - x_{sl}^{rk})}{(x_{sl}^{rk} - x_{as}^{rk})}\right) e^{(-\alpha_s' \beta_m'^2 F_0^k)} \quad \text{for solidification} \quad (3.12b)$$

Here, k denotes the present time step and the constants  $C_m^{k-1}$  and  $D_m^{k-1}$  are estimated by using initial condition (Eq. 5g) as below:

$$C_m^{k-1} = \frac{2}{(1-x_{sl}^{rk-1})} \int_{x_{sl}^{rk-1}}^1 (\theta_s^{k-1} - \theta_m) \sin\left(\frac{\pi(2n-1)(x' - x_{sl}^{rk-1})}{2(1-x_{sl}^{rk-1})}\right) dx \quad (3.13a)$$

$$D_m^{k-1} = \frac{2}{(x_{sl}^{rk-1} - x_{as}^{rk-1})} \int_{x_{as}^{rk-1}}^{x_{sl}^{rk-1}} \left( \theta_s^{k-1} - \theta_m - \frac{(\theta_p^{k-1} - \theta_m)(x' - x_{sl}^{rk-1})}{(x_{as}^{rk-1} - x_{sl}^{rk-1})} \right) \sin\left(\frac{n\pi(x' - x_{sl}^{rk-1})}{(x_{sl}^{rk-1} - x_{as}^{rk-1})}\right) dx \quad (3.13b)$$

Here, the value of  $\beta_m'$ , used in the above Eqs. (3.13a) and (3.13b), are expressed as

$$\frac{\pi(2n-1)}{2(1-x_{sl}^{rk-1})} \quad \text{and} \quad \frac{n\pi}{(x_{sl}^{rk-1} - x_{as}^{rk-1})} \quad \text{for melting and solidification, respectively. The}$$

temperature distribution Eq. (3.13a) can be solved by considering initially at  $t = 0$  ( $F_0 = 0$ ), and  $x_{sl}^{k-1} = 2.01$  mm for the melting process. For solidification process

Eq. (3.13b) can be solved by considering  $x_{as}^{k-1} = 0.5$  mm and  $x_{sl}^{k-1} = 0.501$  mm

### 3.3.3 Liquid domain

The governing Eqs. (3.3b, 3.4c), the initial and boundary conditions Eqs. (3.5g, 3.5e and 3.5f) are solved by employing separation of variable method and the temperature distribution of liquid domain is expressed as:

$$\theta_l^k = \theta_m + \frac{(\theta_p^k - \theta_m)(x' - x_{sl}^{rk})}{(x_{al}^{rk} - x_{sl}^{rk})} + \sum_{m=1}^{\infty} E_m^{k-1} \sin\left(\frac{n\pi(x' - x_{sl}^{rk})}{(x_{sl}^{rk} - x_{al}^{rk})}\right) e^{(-\alpha'_l \beta_m'^2 F_0^k)} \quad \text{for melting} \quad (3.14a)$$

$$\theta_l^k = \theta_m + \sum_{m=1}^{\infty} F_m^{k-1} \sin\left(\frac{\pi(2n-1)(x' - x_{sl}^{rk})}{2(1-x_{sl}^{rk})}\right) e^{(-\beta_m'^2 F_0^k)} \quad \text{for solidification} \quad (3.14b)$$

Here, k denotes the present time step; the constants  $E_m^{k-1}$  and  $F_m^{k-1}$  expressed in Eq. (3.14a-b) can be estimated by using initial condition (Eq. 3.5g) and are given by:

$$E_m^{k-1} = \frac{2}{(x_{sl}^{rk-1} - x_{al}^{rk-1})} \int_{x_{al}^{rk-1}}^{x_{sl}^{rk-1}} \left( \theta_l^{k-1} - \theta_m - \frac{(\theta_p^{k-1} - \theta_m)(x' - x_{sl}^{rk-1})}{(x_{al}^{rk-1} - x_{sl}^{rk-1})} \right) \sin\left(\frac{n\pi(x' - x_{sl}^{rk-1})}{(x_{sl}^{rk-1} - x_{al}^{rk-1})}\right) dx \quad (3.15a)$$

$$F_m^{k-1} = \frac{2}{(1-x_{sl}^{rk-1})} \int_{x_{sl}^{rk-1}}^1 \left( \theta_l^{k-1} - \theta_m \right) \sin\left(\frac{\pi(2n-1)(x' - x_{sl}^{rk-1})}{2(1-x_{sl}^{rk-1})}\right) dx \quad (3.15b)$$

The value of  $\beta_m'$  expressed in Eq. (3.15a) and Eq. (3.15b) are found to be

$\frac{n\pi}{(x_{sl}^{rk-1} - x_{al}^{rk-1})}$  and  $\frac{\pi(2n-1)}{2(1-x_{sl}^{rk-1})}$ , respectively. For t = 0, Eq. (3.15a) can be used to

obtain the temperature distribution by using  $x_{al}^{k-1} = 2$  mm and  $x_{sl}^{k-1} = 2.01$  mm for

melting process; Eq. (3.15b) can be utilized with  $x_{sl}^{k-1} = 0.501$  mm for

solidification process. It may be noted that during melting and solidification

process,  $\theta_p^k$  is unknown in Eqs. (3.7a-3.7b), (3.12b) and (3.14a). In order to find

the value of  $\theta_p^k$ , the heat balance equation is considered at an air-liquid/air-solid interface as below:

$$\frac{d\theta_a}{dx'} \Big|_{x=x'_y} = K_{ua} \frac{d\theta_u}{dx'} \Big|_{x=x'_y} \quad (3.16)$$

For melting process, one can use Eqs (3.7a) and (3.14a) and for solidification process one can Eqs. (3.7b) and (3.12b) to obtain  $\theta_p$ . This is expressed as:

$$\theta_p^k = \left( (K_{au})(P'_{al}(x'_y{}^k)) - (P'_u(x'_y{}^k)) \right) (x'_y{}^k - x'_{sl}{}^k) \quad \text{for melting} \quad (3.17a)$$

$$\theta_p^k = \frac{K_{au} \lambda \theta_\infty + K_{au} (P'_{as}(x'_y{}^k)) + \frac{\theta_m}{(x'_{as}{}^{k-1} - x'_{sl}{}^{k-1})} - (P'_u(x'_y{}^k))}{\frac{1}{(x'_{as}{}^{k-1} - x'_{sl}{}^{k-1})} + K_{au} \lambda} \quad \text{for solidification} \quad (3.17b)$$

where

$$P_{al}(x') = \sum_{m=1}^{\infty} A_m^{k-1} \cos \left( \left( \frac{\pi(2n-1)}{2x'_{al}{}^k} \right) x' \right) e^{(-\alpha'_a \beta'_m{}^2 F_0^k)} \quad (3.18a)$$

$$P_{as}(x') = \sum_{m=1}^{\infty} B_m^{k-1} \sin \beta'_m (x'_{as}{}^k - x'^k) e^{(-\alpha'_a \beta'_m{}^2 F_0^k)} \quad (3.18b)$$

$$P_l(x') = \sum_{m=1}^{\infty} E_m^{k-1} \sin \left( \frac{n\pi(x' - x'_{sl}{}^k)}{(x'_{sl}{}^k - x'_{al}{}^k)} \right) e^{(-\alpha'_l \beta'_m{}^2 F_0^k)} \quad (3.18c)$$

$$P_s(x') = \sum_{m=1}^{\infty} D_m^{k-1} \sin \left( \frac{n\pi(x' - x'_{sl}{}^k)}{(x'_{sl}{}^k - x'_{as}{}^k)} \right) e^{(-\alpha'_s \beta'_m{}^2 F_0^k)} \quad (3.18d)$$

$$K_{ua} = \frac{K_u}{K_a} \quad (3.18e)$$

And,

$$u = \begin{cases} l, & \text{for melting} \\ s, & \text{for solidification} \end{cases} \quad (3.19)$$

In order to estimate the solid-liquid interface position for melting and solidification process, one can use the Stefan condition as below:

$$\rho_s L \frac{dx_{sl}}{dt} = K_s \left. \frac{dT_s}{dx} \right|_{x=x_{sl}} - K_l \left. \frac{dT_l}{dx} \right|_{x=x_{sl}} \quad (3.20)$$

Non-dimensional form of Eq. 3.20 is given as follows.

$$\frac{dx'_{sl}}{dF_0} = \gamma_s \frac{d\theta_s}{dx'} - \gamma_l \alpha'_l \frac{d\theta_l}{dx'} \quad \text{for melting} \quad (3.21a)$$

$$\frac{dx'_{sl}}{dF_0} = \gamma_s \alpha'_s \frac{d\theta_s}{dx'} - \gamma_l \frac{d\theta_l}{dx'} \quad \text{for solidification} \quad (3.21b)$$

where

$$\gamma_\phi = \frac{\rho_\phi c_{p\phi} \left( \frac{St_s}{c_{p_s}} + \frac{St_l}{c_{p_l}} \right)}{\rho_s} \quad (3.22)$$

For melting, one can use Eqs. (3.14a) and (3.12a), while for solidification process, one can use Eqs. (3.12b) and (3.14b) to obtain the solid-liquid interface position.

This is expressed as:

$$\frac{dx'_{sl}}{dF_0} = \gamma_s P'_{ms} (x'_{sl}) - \gamma_l \alpha'_l \left( \frac{(\theta_p^{k-1} - \theta_m)}{(x'_{al}{}^{k-1} - x'_{sl}{}^{k-1})} + P'_{ml} (x'_{sl}) \right) \quad \text{for melting} \quad (3.23a)$$

$$\frac{dx'_{sl}}{dF_0} = \gamma_s \alpha'_s \left( \frac{(\theta_p^{k-1} - \theta_m)}{(x'_{as}{}^{k-1} - x'_{sl}{}^{k-1})} + P'_{ss} (x'_{sl}) \right) - \gamma_l P'_{sl} (x'_{sl}) \quad \text{for solidification} \quad (3.23b)$$

where

$$P_{ms} (x') = \sum_{m=1}^{\infty} C_m^{k-1} \sin \left( \frac{\pi(2n-1)(x' - x'_{sl}{}^k)}{2(1-x'_{sl}{}^k)} \right) e^{(-\beta_m'^2 F_0^k)} \quad (3.24a)$$

$$P_{ml}(x') = \sum_{m=1}^{\infty} E_m^{k-1} \sin\left(\frac{n\pi(x' - x_{sl}'^k)}{(x_{sl}'^k - x_{al}'^k)}\right) e^{(-\alpha_l' \beta_m'^2 F_0^k)} \quad (3.24b)$$

$$P_{ss}(x') = \sum_{m=1}^{\infty} D_m^{k-1} \sin\left(\frac{n\pi(x' - x_{sl}'^k)}{(x_{sl}'^k - x_{as}'^k)}\right) e^{(-\alpha_s' \beta_m'^2 F_0^k)} \quad (3.24c)$$

$$P_{sl}(x') = \sum_{m=1}^{\infty} F_m^{k-1} \sin\left(\frac{\pi(2n-1)(x' - x_{sl}'^k)}{2(1 - x_{sl}'^k)}\right) e^{(-\beta_m'^2 F_0^k)} \quad (3.24d)$$

The value of solid-liquid interface at any time instant during melting and solidification of PCM can be calculated by using Euler method [79] as:

$$x_{sl}'^k = x_{sl}'^{k-1} + \Delta F_0 (\delta^{k-1}) \quad (3.25)$$

where  $\delta^{k-1}$  is given by right hand sides of Eqs. (3.23a) and (3.23b) for melting and solidification, respectively. Initial values of  $x_{sl}'^{k-1}$  and  $x_{al}'^{k-1}$  are taken as 2.01 mm and 2.0 mm for melting process; the initial values of  $x_{sl}'^{k-1}$  and  $x_{as}'^{k-1}$  are taken as 0.501 mm and 0.5 mm for solidification process. In order to obtain the air-liquid interface position during melting and air-solid interface position during solidification process, one can assume the mass balance equation at the respective interfaces and the expression for  $x_{al}'^k$  and  $x_{as}'^k$  are given as:

$$x_y'^k = x_y'^{k-1} + (1 - \rho_n)(x_{sl}'^k - x_{sl}'^{k-1}) \quad (3.26)$$

where

$$\rho_n = \begin{cases} \frac{\rho_l}{\rho_s}, & \text{solidification} \\ \frac{\rho_s}{\rho_l}, & \text{melting} \end{cases} \quad (3.27)$$

After solving Eqs. 3.7a, 3.7b, 3.12a, 3.12b, 3.14a, 3.14b, 3.17a, 3.17b, and 3.25 the values of  $\theta_a^k$ ,  $\theta_s^k$ ,  $\theta_l^k$ ,  $\theta_p^k$ ,  $x_{as}'^k$ ,  $x_{al}'^k$  and  $x_{sl}'^k$  at the present time step is obtained. Present model yields mathematical expressions to evaluate temperature distribution in different regimes (air, solid and liquid) and interface positions (air-

solid, air-liquid, and solid-liquid) with pure PCM and PCM-MF composite. With the help of known values of thermo-physical properties of pure PCM and MF, one can calculate the temperature distribution and interface position for three different domains.

In addition to this, to analyze the effect of shrinkage/expansion on the heat transfer performance of TES system, one needs to evaluate various parameters such as total energy stored, and total energy extracted at any time instant. This has been estimated as [120]:

$$Q_{stored/extracted} = \frac{1}{A} \iiint_{V_y} \rho_y C_{py} \Delta T dV_y + \iiint_{V_T} \rho_y f_y L dV_T \quad (3.28a)$$

where

$$y = \begin{cases} l, & \text{for melting} \\ s, & \text{for solidification} \end{cases} \quad (3.28b)$$

$$\Delta T = \begin{cases} T_l - T_m, & \text{for melting} \\ T_m - T_s, & \text{for solidification} \end{cases} \quad (3.28c)$$

### 3.4 Validation of the present analytical model

Here, results obtained from present analysis are compared with the test data of Zhou et al. [121] for both melting and solidification with pure PCM and PCM-MF composite. The authors analyzed the heat transfer during melting and solidification in the rectangular TES system with pure PCM, PCM-graphite composite, and PCM-MF composite. In their experiments, other wall is maintained at adiabatic condition while one wall is maintained at constant wall heat flux and convective heat transfer boundary condition for melting and solidification, respectively. The test set up consist of a rectangular container (80×50×30 mm<sup>3</sup>) with copper plate at the bottom and synthetic glass cover at both side and top surfaces. Rubber heater, with same dimension of the copper plate, is tightly attached to the bottom surface of copper plate to provide constant heat flux at the wall. Paraffin RT27 (melting point of 25°C-28°C) is considered as a PCM material and copper foam with 30 PPI and 18.5% relative density is used for the analysis; the properties are summarized in Table 3.1. The authors used  $q'' = 3750$

W/m<sup>2</sup> during melting process; while the heater is switched off and the insulation of one of the walls is removed to keep the surface open to the ambient during solidification process. All other boundaries are remained insulated during solidification.

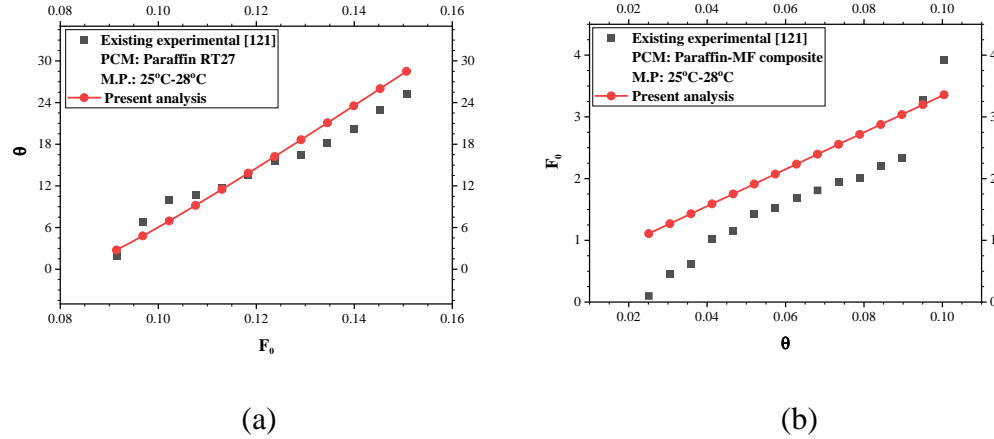


Fig. 3.2 Comparison of temperature of melting process obtained from present predictions with the test data of Zhou et al. [121] at  $x=10$  mm ( $x' = 0.33$ ) for (a) pure PCM, (b) PCM-MF Composite

Figs. (3.2a) and (3.2b) show the comparison of temperature distribution of pure PCM for melting and solidification process, respectively at 10 mm ( $x' = 0.33$ ) from the upper surface of copper plate during melting process. Present prediction exhibits good agreement with the test data of Zhou et al. [121] within the maximum error of 8.68% and 4.19% for pure PCM and PCM-MF composite, respectively. In addition to this, the comparison of results obtained from the present model with Zhou et al. [121] during melting and solidification process is shown in Figs. (3.3a-b). The temperature distribution is obtained at 10 mm ( $x' = 0.33$ ) from the surface open to ambient during solidification of PCM. Present prediction exhibits excellent agreement with test data of Zhou et al. [121] and the maximum error was found to be 0.59% and 0.51% for pure PCM and PCM-MF composite, respectively.

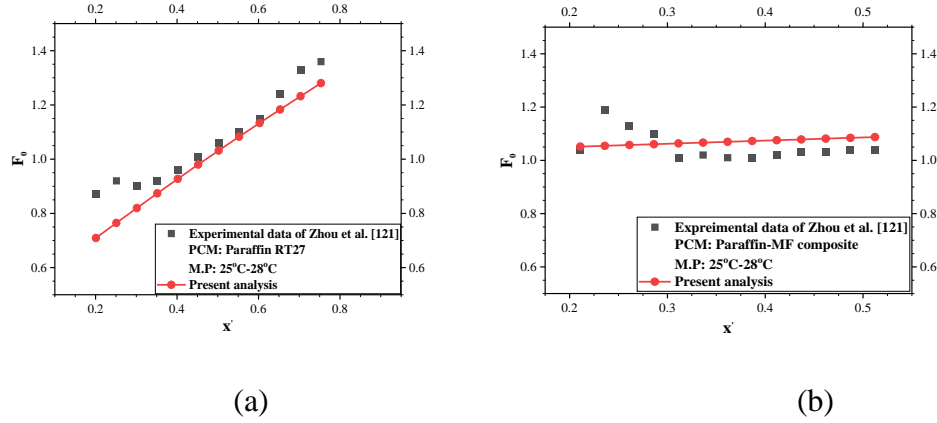


Fig. 3.3 Comparison of temperature of solidification process obtained from present predictions with the test data of Zhou et al. [121] at  $x=10$  mm ( $x' = 0.33$ ) for (a) pure PCM, (b) PCM-MF Composite

### 3.5 Result and Discussions

In this study, the thermal performance of pure PCM and PCM-MF composite based systems with steady and transient heat loads incorporating the effect of air void in the analysis is investigated. Separation of variable method with Bessel function is used to obtain the solution; the energy balance in terms of Stefan condition and mass balance equation are used to obtain the interface positions. Effect of various parameters such as heat flux values, convective heat transfer coefficients, and density ratios on the heat transfer performance, melting/solidification rate and the movement of solid-liquid, air-solid/air-liquid interfaces, melting time, and energy extracted/stored are reported for pure PCM and PCM-MF composite. The details are elaborated below.

#### 3.5.1 Melting and solidification analysis of pure PCM for steady heat load with air gap

Initially, air gap of 2 mm and solid-liquid interface at 2.01 mm from the left wall is considered to accommodate the volume expansion of PCM during melting process. Steady heat flux of  $250 \text{ W/m}^2$  is applied at the left boundary, while initial temperature of PCM is considered as 336 K ( $\theta_o = 0$ ) to ensure solid state of the entire PCM. In case of solidification process, an initial air gap of 0.5 mm and

solid-liquid interface at 0.501 mm from the left convective wall is considered. For solidification analysis, ambient temperature, and initial temperature of PCM are considered as 298 K ( $\theta_\infty = 40$ ) and 338 K ( $\theta_o = 0$ ), respectively. Initial PCM temperature indicates that PCM is liquid state before starting of the solidification process. Natural convection boundary condition is provided at the left wall, where ambient temperature is considered and convective heat transfer coefficient ( $h$ ) is taken as 8 W/m<sup>2</sup>-K. Effect of various parameters expansion/shrinkage, heat flux values, convective heat transfer coefficients, and density ratios on the heat transfer performance, melting/solidification rate and the movement of solid-liquid, air-solid/air-liquid interfaces are detailed below.

#### *Effect of expansion/shrinkage*

Fig. (3.4a) shows temperature distribution at various locations from the left boundary for three domains namely, air, solid, and liquid during melting process. Spatial variation of temperature is obtained at three different time step 200 s ( $F_o = 0.043$ ), 1200 s ( $F_o = 2.56$ ), and 2400 s ( $F_o = 5.12$ ). The position of air-liquid and solid-liquid interface can be obtained from the figure with the change in slope (Fig. 3.4a). Initially, air-solid, and solid-liquid interfaces are kept at 2 mm and 2.01 mm, respectively from the left wall. It can be seen from the figure that position of air-liquid interface are 2 mm ( $x'_{al} = 0.2$ ), 1.8 mm ( $x'_{al} = 0.18$ ), and 1.6 mm ( $x'_{al} = 0.16$ ) at 200 s, 1200 s, and 2400 s, respectively. While the position of solid-liquid interfaces are 2.2 mm ( $x'_{sl} = 0.22$ ), 3.4 mm ( $x'_{sl} = 0.34$ ), and 4.8 mm ( $x'_{sl} = 0.48$ ) at 200 s, 1200 s, and 2400 s, respectively. Solid-liquid interface moves towards the adiabatic wall (right boundary) and the movement of solid-liquid interface is found to be 1.39 mm and 1.4 mm for 0-1200 s and 1200-2400 s, respectively. It is observed that air-liquid interface moves towards the left boundary that indicates the expansion of the PCM in the rectangular container due to difference in density ratio. It can be concluded that with the progress of melting process expansion of PCM occurs that results in decrease in volume of void and the solid-liquid interface movement increases with the progress of time. This may

be due to decrease in void space which results in increase in heat transfer rate to PCM. Also, it may be noted that after 2400 s, 35% of melting process is completed and volume of void is decreased by 20% with density ratio  $\sim 1.16$  and heat flux  $250 \text{ W/m}^2$ .

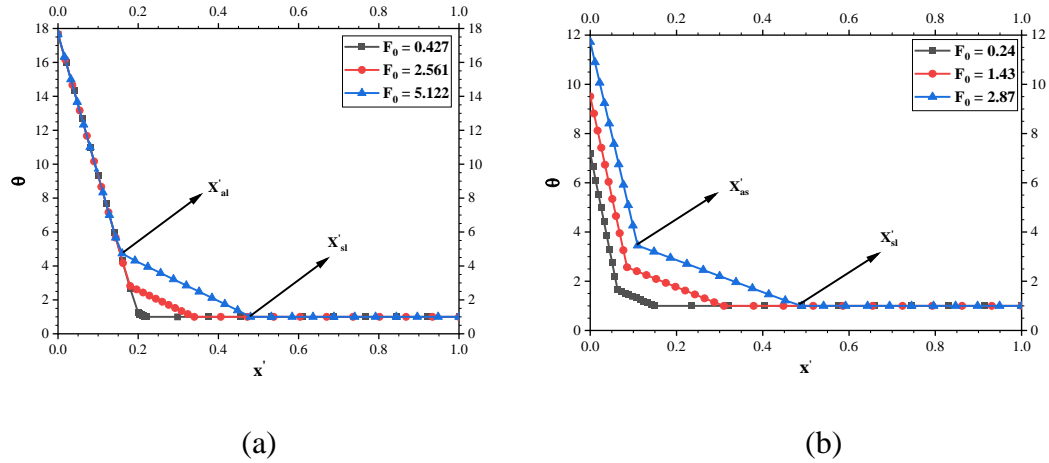


Fig. 3.4 Spatial variation of non-dimensional temperature at different time duration (a) melting, (b) solidification process

Fig (3.4b) shows the spatial variation of temperature for three different domains at various locations from the left wall at three time instants 200 s ( $F_0 = 0.24$ ), 1200 s ( $F_0 = 1.43$ ), and 2400 s ( $F_0 = 2.87$ ). One can observe from Fig (3.4b) that the slope is changed at two positions indicating the position of air-solid and solid-liquid interfaces. Initially air-solid and solid-liquid interface is considered at 0.5 mm and 0.501 mm, respectively from the left boundary. It can be seen from the figure that position of air-solid interface are 0.635 mm ( $x'_{as} = 0.064$ ), 0.854 mm ( $x'_{as} = 0.085$ ), and 1.1 mm ( $x'_{as} = 0.11$ ) at 200 s, 1200 s, and 2400 s, respectively. Also, the position of solid-liquid interface is found at 1.5 mm ( $x'_{sl} = 0.15$ ), 3.5 mm ( $x'_{sl} = 0.35$ ), and 4.9 mm ( $x'_{sl} = 0.49$ ) at 200 s, 1200 s, and 2400 s, respectively. It can be noted that air-solid and solid-liquid interfaces move towards the adiabatic wall indicating the progress of phase change process. During solidification process PCM shrinks and shrinkage of PCM increases with the progress of time due to higher density of solid phase compared to liquid phase of PCM. Shrinkage of PCM increases the void space between the left wall

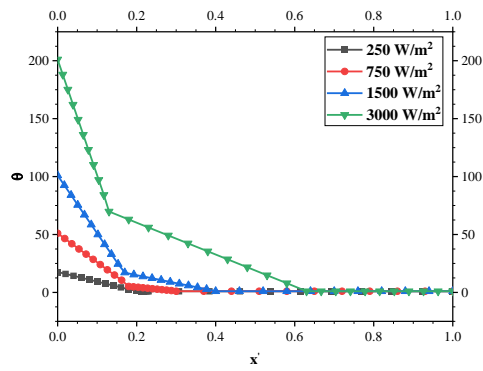
(convective wall) and first layer of solid PCM that in turn affects the heat transfer process because of low thermal conductivity of air. Solid-liquid interface moves towards the adiabatic wall (right boundary) and the movement of solid-liquid interface is found to be 3 mm and 1.4 mm for 0-1200 s and 1200-2400 s, respectively. It can be concluded that the solid-liquid interface movement decreases with the progress of time. This may be due to increase in void space which results in decrease in heat transfer rate to PCM. Also, it may be noted that after 2400 s, 49% of solidification process is completed and volume of void is increased by 120% for PCM density ratio  $\sim 1.16$  and heat transfer coefficient of  $8 \text{ W/m}^2\text{-K}$ .

#### *Effect of heat flux and heat transfer coefficient values*

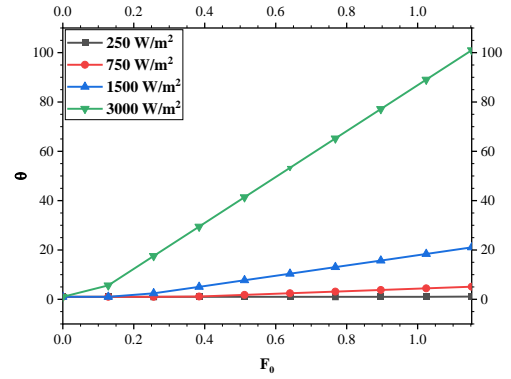
Fig. (3.5a) shows spatial variation of temperature for four different heat flux values such as  $250 \text{ W/m}^2$ ,  $750 \text{ W/m}^2$ ,  $1500 \text{ W/m}^2$ , and  $3000 \text{ W/m}^2$  at  $t = 300 \text{ s}$  ( $F_0 = 0.64$ ). The position of air-liquid interface is found to be 2 mm ( $x'_{al} = 0.2$ ), 1.8 mm ( $x'_{al} = 0.18$ ), 1.7 mm ( $x'_{al} = 0.17$ ), and 1.3 mm ( $x'_{al} = 0.13$ ) and solid-liquid interface is obtained at 2.3 mm ( $x'_{sl} = 0.23$ ), 3 mm ( $x'_{sl} = 0.3$ ), 4 mm ( $x'_{sl} = 0.4$ ), and 6.3 mm ( $x'_{sl} = 0.63$ ) from the left boundary for the heat flux 250, 750, 1500  $\text{W/m}^2$ , and 3000  $\text{W/m}^2$  respectively. Air-liquid interface temperatures for different heat fluxes are calculated as 337.4 K ( $\theta_p = 1.4$ ), 341.1 K ( $\theta_p = 5.1$ ), 353.2 K ( $\theta_p = 17.2$ ), and 405.82 K ( $\theta_p = 69.2$ ). With increase in input heat flux value, air-liquid interface position moves at faster rate towards the left boundary for a given time instant. This also indicates with the increase in heat flux values the expansion rate of PCM and solid-liquid interface movement increases that results in increase in melting rate of PCM. Fig. (3.5b) shows the temperature transients at a distance of 2.5 mm from the left boundary for various heat flux ( $250\text{-}3000 \text{ W/m}^2$ ) at the time instant  $t = 540 \text{ s}$ . Temperature of PCM is found to be 337.17 K ( $\theta_l = 1.17$ ), 341.78 K ( $\theta_l = 5.78$ ), 359.73 K ( $\theta_l = 23.73$ ), and 436.99 K ( $\theta_l = 100.99$ ) at 2.5 mm for 250, 750, 1500  $\text{W/m}^2$ , and 3000  $\text{W/m}^2$  respectively. Maximum increase in

temperature at an axial distance of 2.5 mm is found to be 99.82 K ( $\Delta\theta_l = 99.82$ ) with increase in heat flux from 250 W/m<sup>2</sup> to 3000 W/m<sup>2</sup>. It can be concluded that with increase in heat flux values the temperature in PCM increases due to the absorption of higher amount of energy.

In this analysis, three values of  $h$  are considered such as 5, 8, and 10 W/m<sup>2</sup>-K. Ambient and initial PCM temperature is considered as 298 K and 338 K, respectively. Fig. (3.6a) shows the position of air-solid and solid-liquid interfaces at a given time instant of  $t = 2000$  s ( $F_0 = 2.39$ ). Air-solid interface is found to be 0.885 mm ( $x'_{as} = 0.0885$ ), 1 mm ( $x'_{as} = 0.1$ ), and 1.1 mm ( $x'_{as} = 0.11$ ) for  $h = 5, 8, 10$  W/m<sup>2</sup>-K, respectively. This indicates that shrinkage (volume of void) increases with the increase in value of convective heat transfer coefficient. Also, position of solid-liquid interface is obtained at 3.3 mm ( $x'_{sl} = 0.33$ ), 4.3 mm ( $x'_{sl} = 0.43$ ), and 4.8 mm ( $x'_{sl} = 0.48$ ) for  $h = 5, 8, 10$  W/m<sup>2</sup>-K, respectively. It indicates that solidification rate increases with the increase in value of  $h$ . Figure shows that air-solid interface temperature is 335.85 K ( $\theta_p = 2.15$ ), 334.82 K ( $\theta_p = 3.18$ ), and 334.16 K ( $\theta_p = 3.84$ ) at  $t = 2000$  s for  $h = 5, 8, 10$  W/m<sup>2</sup>-K, respectively; i.e. air-solid interface temperature decreases by 1.69 K with the increase in  $h$  from 5 to 10 W/m<sup>2</sup>-K. Temperature history at 1.5 mm from the left boundary for the time duration 2000 s and for  $h = 5, 8, 10$  W/m<sup>2</sup>-K is shown in Fig. (3.6b). Temperature values at 1.5 mm are obtained as 336.14 K ( $\theta = 1.86$ ), 335.14 K ( $\theta = 2.86$ ), and 334.46 K ( $\theta = 3.54$ ) for the respective  $h$  values. It may be noted that due to increase in value of  $h$  from 5 to 10 W/m<sup>2</sup>-K temperature at 1.5 mm is decreased by 1.68 K ( $\Delta\theta = 1.68$ ) that is with temperature drop and solidification rate increases with the increase in value of  $h$ .

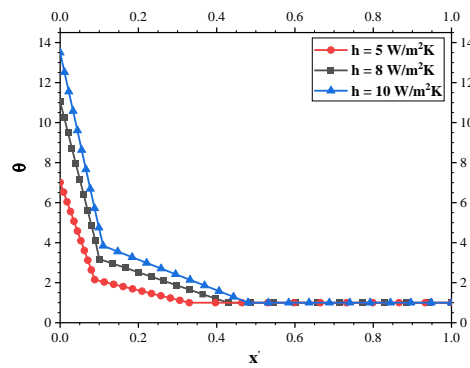


(a)

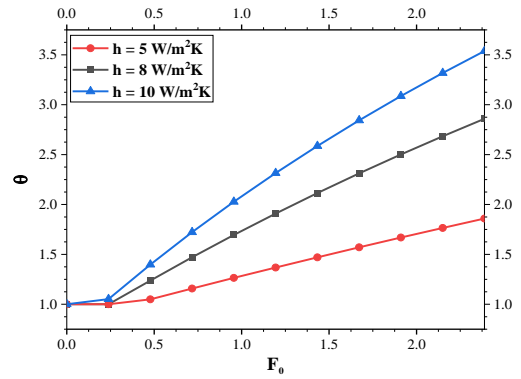


(b)

Fig. 3.5 Temperature variation for different wall heat fluxes at (a)  $t = 300$  s ( $F_0 = 0.64$ ) for different axial distance, (b)  $x = 2.5$  mm ( $x' = 0.25$ ) for different time duration



(a)



(b)

Fig. 3.6 Temperature variation for different convective heat transfer coefficient ( $h$ ) values at (a)  $t = 2000$  s ( $F_0 = 2.39$ ) for different axial distance, (b)  $x = 1.5$  mm ( $x' = 0.15$ ) for different time duration

### Effect of density ratio

Density ratio is defined as the ratio of density of solid PCM to the density of liquid PCM. Density ratios of  $\sim 1.16$ ,  $\sim 1.07$ , and  $\sim 1.03$  are considered for the

present analysis. Fig. (3.7a) shows the spatial variation of temperature for different axial distance from the left wall. Position of air-liquid interface at 1400 s ( $F_0 = 2.98$ ) are 1.7 mm ( $x'_{al} = 0.17$ ), 1.9 mm ( $x'_{al} = 0.19$ ), and 2 mm and the position of solid-liquid interface is found to be 3.6 mm ( $x'_{sl} = 0.36$ ), 2.9 mm ( $x'_{sl} = 0.29$ ), and 2.4 mm ( $x'_{sl} = 0.24$ ) for density ratio 1.16, 1.07, and 1.03, respectively from the left wall. Also, air-liquid interface temperature is found to be 339.14 K ( $\theta_p = 3.14$ ), 337.497 K ( $\theta_p = 1.497$ ), and 337.11 K ( $\theta_p = 1.11$ ). It may be noted that air-liquid moves at a faster rate towards the left wall with increase in density ratio while movement of solid-liquid interface increases towards the adiabatic wall with increase in density ratio at the given time instant. This indicates that rate of expansion of PCM and melting rate increases with increase in the density ratio. Therefore, volume of void decreases that result in increase in the heat transfer and melting rates. The percentage increase in melting rate due to increase in density ratio from 1.03 to 1.16 is found to be 15%, while volume of void decreases by 15% due to expansion of the melt PCM.

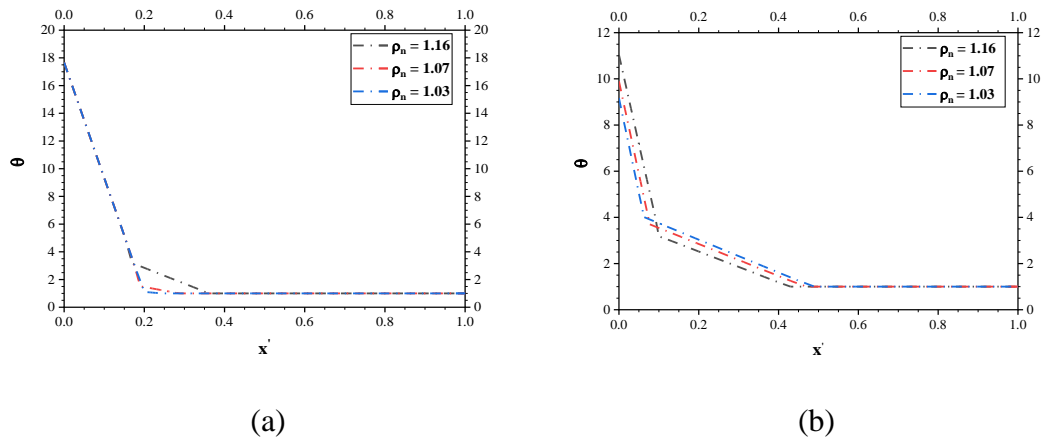


Fig. 3.7 Temperature variation with axial distance for different density ratio values, (a) melting, (b) solidification process

Effect of density ratio on temperature distribution, air-solid, and solid-liquid interface position are also analyzed during solidification of PCM. Results are reported in Fig. (3.7b) for density ratios of  $\sim 1.16$ ,  $\sim 1.07$ , and  $\sim 1.03$  at  $t = 2000$  s.

Location of air-solid interface is obtained as 1 mm ( $x'_{as} = 0.1$ ), 0.772 mm ( $x'_{as} = 0.0772$ ), and 0.63 mm ( $x'_{as} = 0.063$ ) while solid-liquid interface is located at 4.3 mm ( $x'_{sl} = 0.43$ ), 4.7 mm ( $x'_{sl} = 0.47$ ), and 4.9 mm ( $x'_{sl} = 0.49$ ) for the density ratio 1.16, 1.07, and 1.03, respectively. It can be concluded that shrinkage increases with the increase in the density ratio. Increase in shrinkage increases the void space that acts as an insulating material to the heat transfer through PCM. Therefore, the growth of solid-liquid interface decreases due to hindrance in the heat transfer. Also, air-solid interface temperature is observed as 334.82 K ( $\theta_p = 3.18$ ), 334.3 K ( $\theta_p = 3.7$ ), and 333.99 K ( $\theta_p = 4.01$ ) for the density ratio 1.16, 1.07, and 1.03, respectively. That is air-solid interface temperature is increased by 0.83 K ( $\Delta\theta_p = 0.83$ ). It can be reported that with the increase in density ratio from 1.03 to 1.16 volume of void is increased by 3.7% while solidification rate is decreased by 7.5%.

### 3.5.2 Melting/solidification analysis in PCM-MF composite with void for

#### *Steady heat load*

Fig. 3.8a depict the comparison of air-liquid and solid-liquid interfaces for pure PCM and PCM-MF composite with 97% ( $\xi = 0.97$ ) porosity of MF. The propagation of air-liquid and solid-liquid interface is faster for PCM-MF composite compared to pure PCM. During melting process  $t = 0$  to 2400 s, the air-solid interface moves from 2 mm to 1.6 mm, and 2 mm to 1.5 mm for pure PCM and PCM-MF composite system, respectively (Fig. 8a); the solid-liquid interface propagates from 2.01 mm to 4.8 mm, and 2.01 mm to 5.9 mm for pure PCM and PCM-MF composite, respectively. For the duration of 2400 s, the melting process is found to be completed by 35% and 48.75% for PCM and PCM-MF composite, respectively; the volume of void is decreased by 20% and 25% for pure PCM and

PCM-MF composite, respectively. The study shows that in case of PCM-MF, melting and expansion rate increases and results in the decrease in the volume of void at a faster rate.

Fig. 3.8b shows spatial variation of temperature at different axial distance for PCM-MF composite with different porosity values ( $\xi = 0.97, 0.94$  and  $0.9$ ). At  $t = 1400$  s ( $F_0 = 2.99$ ), the air-liquid interface moves by 1.7 mm ( $x'_{al} = 0.17$ ), 1.5 mm ( $x'_{al} = 0.15$ ), and 1.4 mm ( $x'_{al} = 0.14$ ) and solid-liquid interface moves by 4.9 mm ( $x'_{sl} = 0.49$ ), 6.1 mm ( $x'_{sl} = 0.61$ ), and 7.4 mm ( $x'_{sl} = 0.74$ ) for  $\xi = 0.97, 0.94$  and  $0.9$ , respectively. Also, the air-liquid interface temperatures for the respective porosity are 337.12 K ( $\theta_p = 1.12$ ), 337.12 K ( $\theta_p = 1.12$ ), and 337.11 K ( $\theta_p = 1.11$ ) for  $\xi = 0.97, 0.94$  and  $0.9$ , respectively. The study shows that for the duration of 1400 s, the melting rate increases by 31.25 % and expansion rate increases by 7% with the decrease in porosity from 0.97 to 0.90.

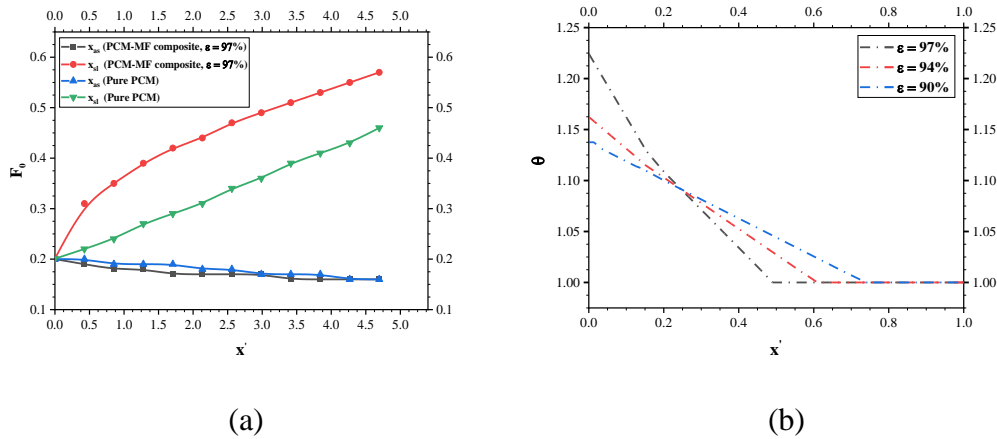


Fig. 3.8 (a) Comparison of interface movement in TES system with pure PCM and PCM-MF composite (97% porosity) for 2400 s ( $F_0 = 5.12$ ) duration, and (b) Spatial variation of temperature with different axial distance at  $t = 1400$  s ( $F_0 = 2.99$ ) for different porosity, during melting process

Similar observations have been noticed during solidification process. Fig. 3.9a depict the comparison of air-solid and solid-liquid interfaces for pure PCM

and PCM-MF composite with  $\xi = 0.97$ . The PCM-MF composite increases the solidification and shrinkage rates compared to the pure PCM system. The propagation of air-solid and solid-liquid interface is faster for PCM-MF composite compared to pure PCM. It is found that during solidification process from  $t = 0$  to 2400 s air-solid moves 0.5 mm to 1.1 mm, and 0.5 mm to 1.3 mm for pure PCM and PCM-MF composite, respectively (Fig. 9a). While solid-liquid interface moves from 0.501 mm to 4.9 mm ( $x'_{sl} = 0.49$ ) and 6.3 mm ( $x'_{sl} = 0.63$ ) for pure PCM and PCM-MF composite, respectively. For the 2400 s duration the solidification process is found to be completed by 49% and 63% for PCM and PCM-MF composite, respectively; the volume of void is increased by 11% and 13% for pure PCM and PCM-MF composite, respectively. The study shows that in case of PCM-MF, solidification and shrinkage rate increases and results in the increase in the volume of void at a faster rate.

Fig. (3.9b) shows spatial variation of temperature at different axial distance for PCM-MF with different porosity values porosity ( $\xi = 0.99, 0.97$  and  $0.94$ ). At  $t = 2000$  s ( $F_0 = 2.39$ ), the air-solid interfaces are 0.98 mm ( $x'_{as} = 0.098$ ), 1.2 mm ( $x'_{as} = 0.12$ ), and 1.6 mm ( $x'_{as} = 0.16$ ) and solid-liquid interfaces are obtained at 4 mm ( $x'_{sl} = 0.4$ ), 5.8 mm ( $x'_{sl} = 0.58$ ), and 8.3 mm ( $x'_{sl} = 0.83$ ) for  $\xi = 0.99, 0.97$  and  $0.94$ , respectively. Also, air-solid interface temperature is obtained as 336.65 K ( $\theta_p = 1.35$ ), 336.79 K ( $\theta_p = 1.21$ ), and 336.84 K ( $\theta_p = 1.16$ ) for  $\xi = 0.99, 0.97$  and  $0.94$ , respectively. The study shows that for the duration of 2000 s, the solidification rate increases by 107.5% and shrinkage rate increases by 63.26% with the decrease in porosity from 0.99 to 0.94.

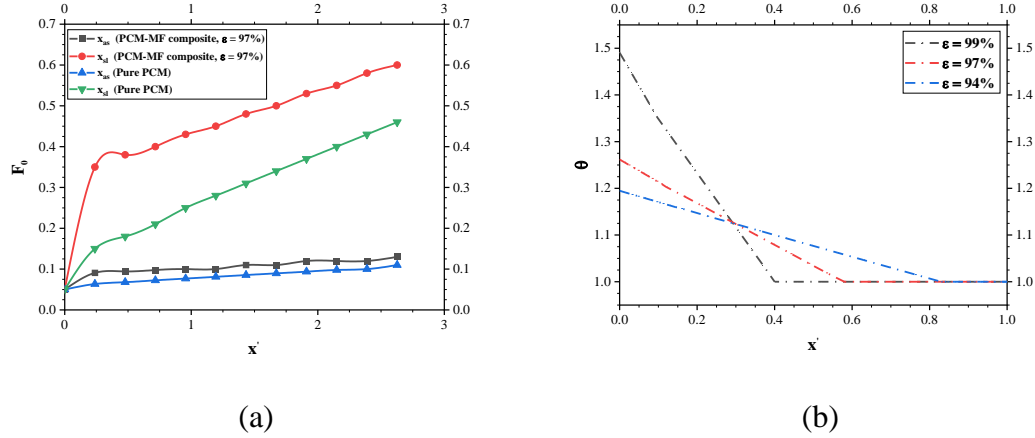


Fig. 3.9 (a) Comparison of interface movement in TES system with pure PCM and PCM-MF composite (97% porosity) for 2400 s ( $F_0 = 2.87$ ) duration, and (b) Spatial variation of temperature with different axial distance at  $t = 2000$  s ( $F_0 = 2.39$ ) for different porosity, during solidification process

### 3.5.3 Melting analysis of pure PCM with void for transient heat load

In order to analyze transient heat load condition, initially the constant value of wall heat flux ( $q'' = 100 \text{ W/m}^2$ ) is provided at the left boundary up to 500 s ( $F_0 = 1.07$ ). After 500 s, the load is fluctuated by employing the transient boundary condition  $q''_w = q''_{w_0} (1 + \gamma)$ ;  $\gamma = 1, 2, 3$  up to 1400 s ( $F_0 = 1.92$ ). One can observe from Fig. (3.10a) that for the first 500 s air-liquid and solid-liquid interfaces are at 1.9 mm ( $x'_{al} = 0.19$ ) and 2.8 mm ( $x'_{sl} = 0.28$ ). For 500 s  $< t < 1400$  s, the air-liquid interface moves to 1.7 mm ( $x'_{al} = 0.17$ ), 1.7 mm ( $x'_{al} = 0.17$ ), and 1.6 mm ( $x'_{al} = 0.16$ ) from 1.9 mm, while the solid-liquid interface moves to 3.6 mm ( $x'_{sl} = 0.36$ ), 3.9 mm ( $x'_{sl} = 0.39$ ), and 4.2 mm ( $x'_{sl} = 0.42$ ) from 2.8 mm for  $\gamma = 1, 2$ , and 3, respectively.

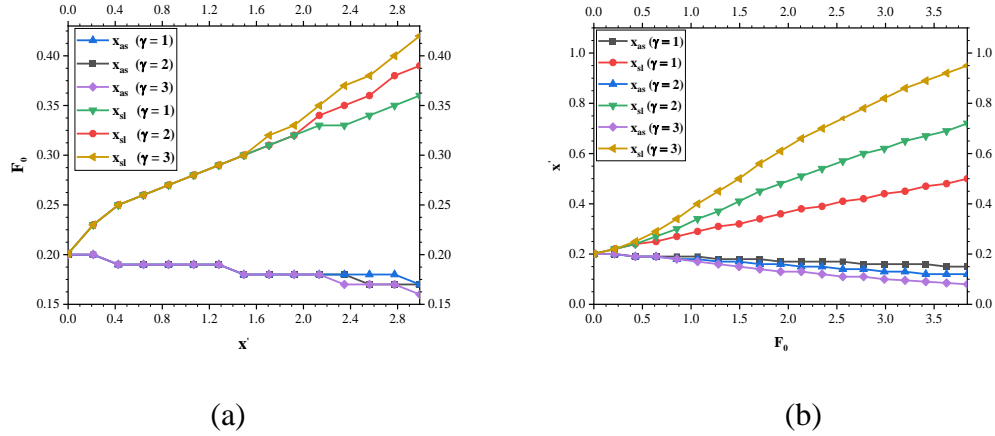


Fig. 3.10 Movement of air-liquid and solid-liquid interface (a) Initiation of various pulse heat load  $200 \text{ W/m}^2$  ( $\gamma = 1$ ),  $300 \text{ W/m}^2$  ( $\gamma = 2$ ), and  $400 \text{ W/m}^2$  ( $\gamma = 3$ ) during  $500 \text{ s} < t < 1400 \text{ s}$  ( $1.07 < F_0 < 2.99$ ) (b) Initiation of various pulse heat load  $400 \text{ W/m}^2$  ( $\gamma = 1$ ),  $600 \text{ W/m}^2$  ( $\gamma = 2$ ), and  $800 \text{ W/m}^2$ , ( $\gamma = 3$ ) during  $100 \text{ s} < t < 800 \text{ s}$  ( $0.213 < F_0 < 1.7$ ) and shut-off for  $1800 \text{ s}$  ( $F_0 = 3.84$ )

It is interesting to analyze the effect of pulse heat load on thermal performance by altering the magnitude of heat flux values and imposition of pulse load duration. Initially ( $0 < t < 100\text{s}$ ), the constant heat load ( $q'' = 200 \text{ W/m}^2$ ) is applied followed by a sudden fluctuation in heat load of  $400 \text{ W/m}^2$  ( $\gamma = 1$ ),  $600 \text{ W/m}^2$  ( $\gamma = 2$ ), and  $800 \text{ W/m}^2$  ( $\gamma = 3$ ) during ( $100 < t < 800\text{s}$ ) in different cases. Later on, the pulse heat load is switched off after  $800 \text{ s}$  and the initial heat load of  $200 \text{ W/m}^2$  is provided during ( $800 < t < 1800\text{s}$ ). Fig. 3.10b shows the movement of air-liquid and solid-liquid interface positions from  $0$  to  $1800 \text{ s}$ . The air-liquid interface moves to  $1.5 \text{ mm}$ ,  $1.1 \text{ mm}$ , and  $0.7 \text{ mm}$  from  $2 \text{ mm}$ , whereas solid-liquid interface moves to  $5.2 \text{ mm}$ ,  $7.6 \text{ mm}$ , and  $9.9 \text{ mm}$  for  $\gamma = 1, 2$ , and  $3$ , respectively. At  $t = 800 \text{ s}$ , the pulse heat loads ( $400, 600$  and  $800 \text{ W/m}^2$ ) supplied in different cases are switched off; the solid-liquid interface is found to move at the same rate as during pulse heat load up to  $t = 1400 \text{ s}$ . Afterwards the rate of movement of solid-liquid interface decreases. This may be due to conversion of sensible heat of liquid PCM into the latent heat of PCM at the interface [122]. Also, it may be

noted that due to increase in fluctuating load melting rate and expansion in the PCM increases.

### **3.5.4 Total melting time and solidification time for steady and transient heat loads**

Fig. 3.11a shows the comparison of total melting time of pure PCM considering air gap near the left wall for different density ratio such as 1.16, 1.07, and 1.03. For  $q'' = 250 \text{ W/m}^2$ , the total melting time for density ratios 1.16, 1.07, and 1.03 are found to be 6336 s, 12771 s, and 26460 s, respectively; while, for  $q'' = 750 \text{ W/m}^2$ , the total melting time are found to be 2172 s, 4482 s and 9714 s, respectively. Also, for  $q'' = 1500 \text{ W/m}^2$ , total melting time are found to be 1108 s, 2280 s, and 5013 s for density ratio of 1.16, 1.07, and 1.03, respectively. With the increase in density ratio from 1.03 to 1.16, the total melting time reduces by 76%, 77.6%, and 77.8% for  $q'' = 250, 750$  and  $1500 \text{ W/m}^2$ , respectively. This indicates that total melting time decreases with the increase in heat flux values and increase in density ratio.

Fig. 3.11b shows the comparison of total melting time for different cases such as pure PCM without void, pure PCM with void, and PCM-MF composite with void for a density ratio of 1.16. The total melting time for pure PCM without void are found to be 797 s, 1593 s and 4779 s for  $q'' = 1500 \text{ W/m}^2, 750 \text{ W/m}^2$ , and  $250 \text{ W/m}^2$ , respectively. While, in case of pure PCM with void, the total melting time is 1108 s, 2172 s, and 6336 s for  $q'' = 1500, 750$ , and  $250 \text{ W/m}^2$ , respectively. Total melting time decreases by 28%, 26.7%, and 24.6% for pure PCM without void compared to pure PCM with void for  $q'' = 1500, 750$ , and  $250 \text{ W/m}^2$ , respectively. Present study shows that because of void at the left wall, the melting rate tends to slower, because the air affects the heat transfer performance. Comparison of total melting time of pure PCM and PCM-MF composite with void at the left wall for constant density ratio 1.16 can be seen from Fig. 3.11b. Total melting time of PCM-MF composite is found to be 796, 1592 and 4628 s for 1500, 750, and  $250 \text{ W/m}^2$ , respectively. This indicates that the total melting time for PCM-MF composite with void is decreased by 28.15%, 26.7%, and 26.95%,

respectively compared to pure PCM with void for  $q'' = 1500, 750, \text{ and } 250 \text{ W/m}^2$ , respectively. This indicates that addition of MF as TCE increases the heat transfer during melting process.

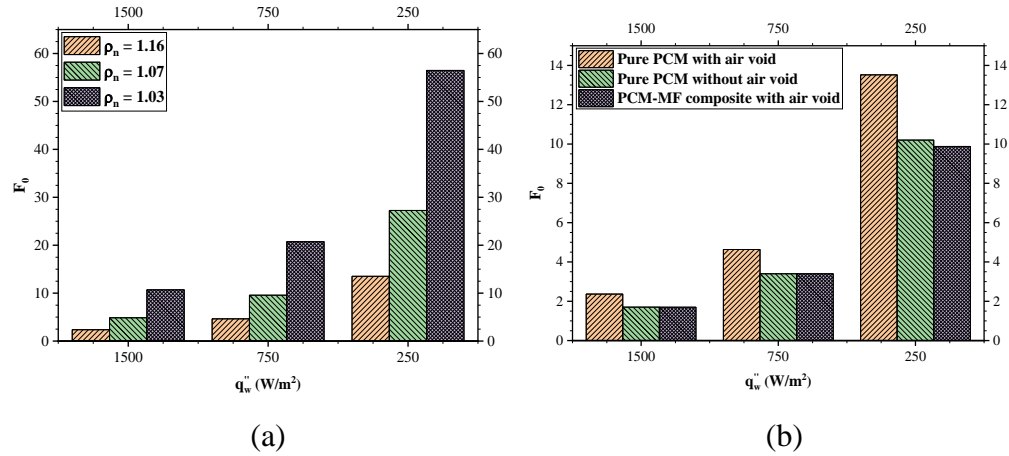


Fig. 3.11 Comparison of total melting time for (a) different density ratio of pure PCM (b) pure PCM with and without air void and PCM-MF with air void

Total solidification time for different density ratio and different values of heat transfer coefficient ( $h = 5, 8, \text{ and } 10 \text{ W/m}^2\text{K}$ ) are shown in Fig. 3.12a. For  $h = 5, 8, 10 \text{ W/m}^2\text{K}$  and  $\rho_n = 1.16$ , the total solidification time are found to be 8652 s, 6096 s, and 5004 s, respectively. For  $h = 5, 8, 10 \text{ W/m}^2\text{K}$  and  $\rho_n = 1.07$ , the solidification time are found to be 8592 s, 5955 s and 5049 s, respectively. At the same time for  $h = 5, 8, 10 \text{ W/m}^2\text{K}$  and  $\rho_n = 1.03$ , the corresponding values are found to be 7090 s, 5853 s, and 4938 s, respectively. With the increase in density ratio from 1.03 to 1.16 total solidification time is increased by 22.03%, 4.1%, and 1.3% at  $h = 5, 8, \text{ and } 10 \text{ W/m}^2\text{K}$ , respectively. For a given value of  $\rho_n$ , the total solidification time decreases with the increase in  $h$ ; the value increases with density ratio for a given value of  $h$ . This may be due to increase in volume of void that acts as an insulating medium and decreases the solidification rate.

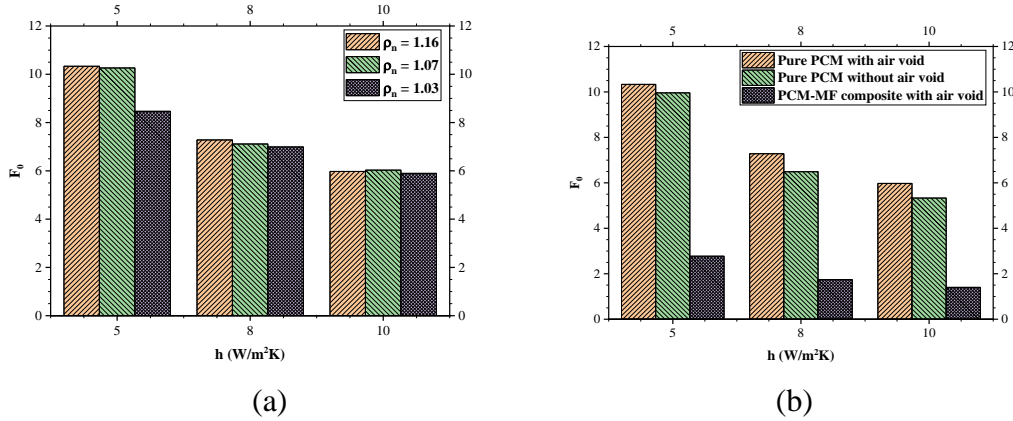


Fig. 3.12 Comparison of total solidification time for (a) Different density ratio of pure PCM (b) Pure PCM with and without air gap and PCM-MF with air gap

Fig. 3.12b shows the comparison of total solidification time for different cases such as pure PCM without void, pure PCM with void, and PCM-MF composite with void for  $\rho_n = 1.16$ . The total solidification time for pure PCM without void are found to be 8340 s, 5435 s and 4465 s for  $h = 5, 8,$  and  $10 W/m^2K$ , respectively. While, in case of pure PCM with void, the total solidification time is 8652 s, 6096 s, and 5004 s, for 5, 8, and 10  $W/m^2K$ , respectively. The total solidification time is decreased by 3.7%, 12.1%, and 12.07% for pure PCM without void compared to pure PCM with void at 5, 8, and 10  $W/m^2K$ , respectively. The study shows presence of void at the left wall, lowers the solidification rate, this may be due to lower heat transfer rate. The total solidification time of MF-PCM composite is found to be 2322 s, 1461s, and 1173 s, respectively for  $h = 5, 8,$  and  $10 W/m^2K$ , respectively. This shows that the total solidification time of PCM in PCM-MF composite with void decreases by 272%, 317%, and 326%, respectively compared to pure PCM with void for the  $h = 5, 8,$  and  $10 W/m^2K$ , respectively. The study shows that addition of MF as TCE improves the heat transfer rate and significantly reduces the solidification time.

### 3.5.5 Energy stored/extracted during melting and solidification for steady and transient heat load.

Here, the energy stored during melting process and energy extracted during solidification process can be calculated by using Eq. (3.28a). Fig. 3.13a shows the comparison of latent heat, and total heat stored in the pure PCM with and without void at  $\rho_n = 1.16$  and  $q'' = 750 \text{ W/m}^2$ . At  $t = 1000 \text{ s}$ , total latent heat stored in PCM storage system with and without void are found to be  $506.9 \text{ kJ/m}^2$  and  $644.2 \text{ kJ/m}^2$  and total energy stored are found to be  $551.3 \text{ kJ/m}^2$  and  $714 \text{ kJ/m}^2$ , respectively. This indicates that energy stored in the PCM with void is lower compared to case that does not include void in the model. The comparison of total energy and latent heat stored with pure PCM involving void and PCM-MF composite including void is shown in Fig. 3.13b. At  $t = 1000 \text{ s}$  ( $F_0 = 2.13$ ), for PCM-MF composite system with void, the latent heat and total heat stored are found to be  $675.5 \text{ kJ/m}^2$  and  $679.4 \text{ kJ/m}^2$ , respectively. Energy stored in PCM-MF composite is greater compared to pure PCM due to enhancement in heat transfer with the addition of MF.

Fig. 3.13c shows the variation of total energy stored with time during melting process with transient heat load for different  $\gamma$  values. Initially ( $0 < t < 100\text{s}$ ), the constant heat load ( $q'' = 200 \text{ W/m}^2$ ) is applied followed by a sudden fluctuation in heat load of  $400 \text{ W/m}^2$  ( $\gamma = 1$ ),  $600 \text{ W/m}^2$  ( $\gamma = 2$ ), and  $800 \text{ W/m}^2$  ( $\gamma = 3$ ) during ( $100 < t < 800\text{s}$ ) in different cases. Later on, the pulse heat load is switched off after  $800 \text{ s}$  and the initial heat load of  $200 \text{ W/m}^2$  is provided during ( $800 \text{ s} < t < 1800 \text{ s}$ ). At  $t = 1800 \text{ s}$  and  $\rho_n = 1.16$ , the latent heat storage are found to be  $407.8 \text{ kJ/m}^2$ ,  $723.7 \text{ kJ/m}^2$ , and  $1097.5 \text{ kJ/m}^2$ ; while, the total energy stored are found to be  $418.7 \text{ W/m}^2$ ,  $777.3 \text{ W/m}^2$ , and  $1257.5 \text{ W/m}^2$  for  $\gamma = 1, 2, \text{ and } 3$ , respectively. The study shows that energy stored in the PCM increases by 208.23% with increase in pulse heat load from  $400 \text{ W/m}^2$  ( $\gamma = 1$ ) to  $800 \text{ W/m}^2$  ( $\gamma = 3$ ).

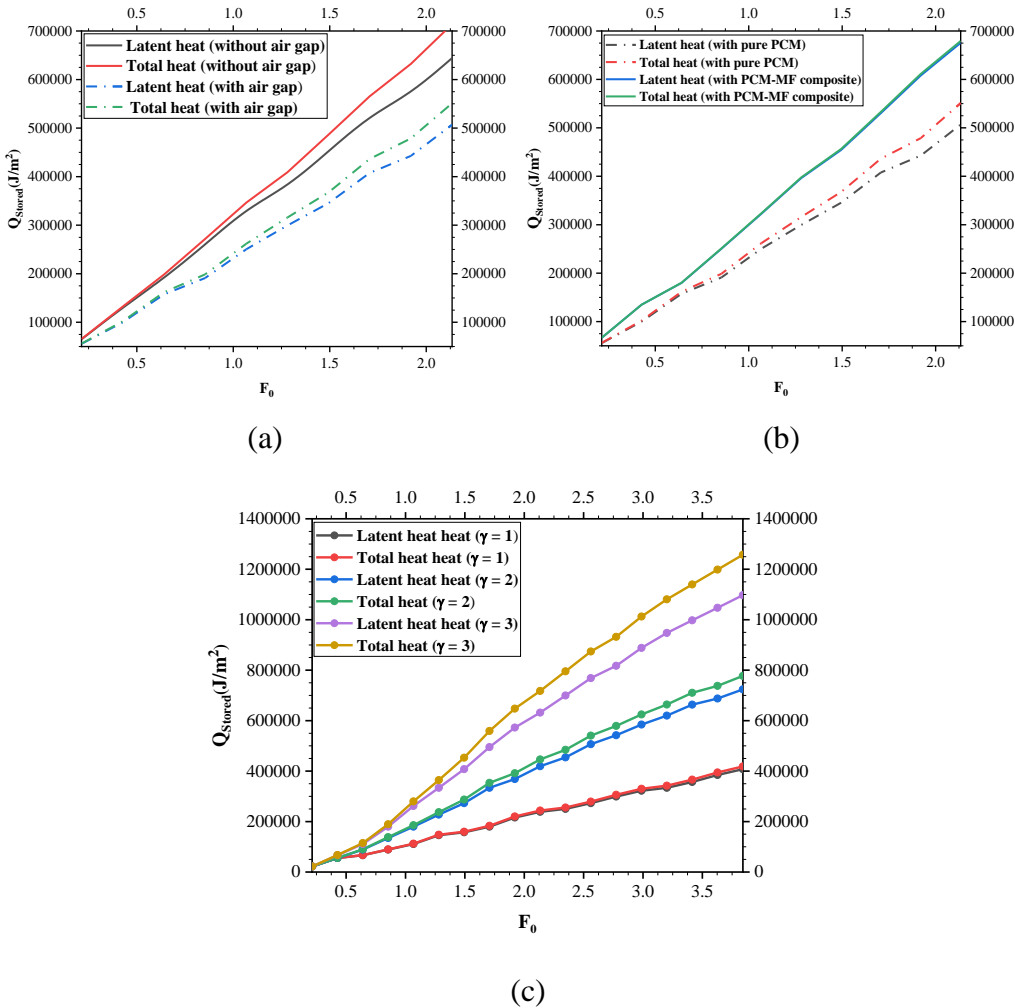


Fig. 3.13 Comparison of total energy stored (a) pure PCM considering with and without air gap (b) pure PCM and PCM-MF composite considering void for (c) transient heat load condition for different  $\gamma$  value

Latent heat and total energy extracted during solidification for a density ratio of 1.16 and convective heat transfer coefficient ( $h$ ) of  $8 \text{ W/m}^2\text{K}$  is shown in Fig. 14. Comparison of latent heat and total energy extracted in case of pure PCM with and without air gap consideration is shown in Fig. 3.14(a). Total latent heat extracted with and without air gap consideration are found to be  $266.14 \text{ kJ/m}^2$  and  $381.42 \text{ kJ/m}^2$  and total energy extracted are found to be  $267.9 \text{ kJ/m}^2$  and  $385.4 \text{ kJ/m}^2$  at  $t = 1000 \text{ s}$  ( $S=1.19$ ). This indicates that energy extracted from the PCM with void is lower compared to case that does not include void in the model. The comparison of total energy and latent heat extracted from pure PCM involving

void and PCM-MF composite including void is shown in Fig. 3.14b. At  $t = 1000$  s ( $F_0 = 1.19$ ), for PCM-MF composite system with void, the latent heat and total heat extracted are found to be  $573.4 \text{ kJ/m}^2$  and  $574.41 \text{ kJ/m}^2$ , respectively. Energy extracted from PCM-MF composite is greater compared to pure PCM due to enhancement in heat transfer with the addition of MF.

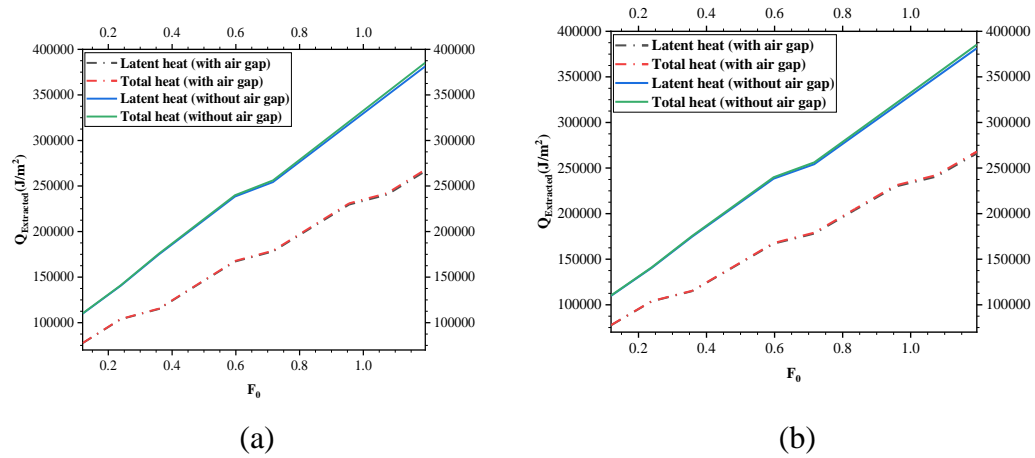


Fig. 3.14 Comparison of total energy extracted (a) pure PCM considering with and without air gap, (b) pure PCM and PCM-MF composite considering void

### 3.6 Concluding remarks

A one dimensional analytical model is developed to study heat transfer process in a rectangular container with pure PCM and PCM-MF composite incorporating the effect of volumetric change. Here, expansion/ shrinkage are considered during melting/solidification. Also, both transient and steady heat load is considered during phase change process. Separation of variable method is considered to obtain the solution for temperature distribution and interface position with constant wall and natural convection boundary condition. Effect of various parameters such as density ratio, wall heat flux, convective heat transfer coefficient, porosity, pulse heat load on the thermal performance is analyzed. Results obtained from this analysis are found to be in good agreement with the test data. The effect of shrinkage/expansion is more prominent for different cases

such as higher value of wall heat flux ( $q_w''$ ), convective heat transfer coefficient ( $h$ ), density ratio, and lower value of porosity. This study can be useful in designing thermal energy storage and thermal management system with the consideration of void on heat transfer performance.

## Chapter 4

### Conclusions and Scope of Future Work

The present dissertation reports the analytical study pertaining to the phase change process of PCM based systems in two different geometries (rectangular and annulus) incorporating volumetric shrinkage/expansion void. The first problem considers the pure PCM based system in an annulus for the analysis. While, the second problem considers pure PCM and PCM-MF in the rectangular system for the analysis. Both the analysis incorporates expansion/shrinkage void during melting/solidification process. Paraffin wax is considered as PCM and air is considered inside the void. Separation of Variable method involving Bessel's function is employed to obtain the temperature distribution for air, solid and liquid domains and to locate interface positions. Stefan condition and mass conservation equation are used at the interfaces. Results obtained from the present model are found to be in good agreement with the existing test results. Effect of various parameters such as density ratio, end wall temperature, wall heat flux, convective heat transfer coefficient, porosity, and radius ratio on the solidification/melting of PCM have been investigated. The significant findings obtained from the present study are elaborated below:

#### **4.1 Solidification and melting model of phase change material with volumetric shrinkage/expansion void in an annulus**

Here, a one dimensional analytical model has been proposed to analyze the solidification and melting of PCM in an annulus incorporating the shrinkage and expansion during solidification and melting, respectively. The model involves three different regions such as air, solid and liquid. Separation of Variable method using Bessel function has been employed for all domains, namely, air, solid and liquid domains to solve the conduction equation. The key findings obtained from the present analysis are elaborated below.

1. Present model yields expressions for temperature distribution in PCM, location of air-solid/air-liquid and solid-liquid interface during solidification and melting of PCM in an annulus.
2. Solidification rate decreases with the increase in density ratio, while melting rate increases with the increase in density ratio. Also, the solidification and melting rate is found to increase with the increase in radius ratio.
3. For a time, duration of 1400 s, the solid-liquid interface moves by 76.53% and 70.88% during solidification and 34.26% and 35.32% during melting for density ratio of 1 and 1.16, respectively.
4. Shrinkage (solidification rate) increases with the decrease in cold wall temperature and increase in Stefan number, while expansion (melting rate) increases with the increase in hot wall temperature and increase in Stefan number.
5. The energy extracted is found to be lower in case of higher density ratio (1.16) compared to the unit density ratio, while energy stored is higher with higher density ratio (1.16) compared to the unit density ratio.

It may be summarized that with lower value of cold wall temperature ( $T_c$ ), higher value of hot wall temperature ( $T_h$ ) and higher density ratio, higher value of radius ratio, the effect of shrinkage and expansion is more prominent. This study can be useful in solar heating or cooling, thermal management of electrical vehicle and electronic devices.

## **4.2 Solidification and melting analysis of phase change material-metal foam composite with expansion/shrinkage void in rectangular system**

Here, a one dimensional analytical model is proposed to investigate the thermal performance of PCM/PCM-metal foam (MF) composite based rectangular energy storage system incorporating the volumetric change and void in PCM with steady and transient heat loads. Separation of variable method with Bessel function has been employed to solve the conduction equation associated

with different thermal boundary conditions. The Stefan condition and mass balance equation are used to locate the interface position during both solidification and melting process. Paraffin wax and copper is considered as PCM and MF material, respectively.

1. Present model yields expressions for temperature distribution in PCM, location of air-liquid/air-solid and solid-liquid interfaces during melting and solidification of PCM.
2. For the time duration of 2400 s, the volume of void decreases by 20% and increases by 120% during melting and solidification, respectively. Decrease in void space results in increase in heat transfer rate to PCM, while increase in void decreases the heat transfer rate to the PCM.
3. With the increase in input heat flux value from 250 to 3000 W/m<sup>2</sup>, the expansion rate of PCM and solid-liquid interface movement increases leading to the increase in melting rate of PCM. During solidification, shrinkage (volume of void) increases with the increase in the value of convective heat transfer coefficient from 5 to 10 W/m<sup>2</sup>-K.
4. With the increase in density ratio from 1.03 to 1.16, the melting rate increase by 15% for time duration of 1400 s and solidification rate decreases by 7.5% for time duration of 2000 s. With the increase in fluctuating load melting rate and expansion in the PCM increases.
5. Thermal system with PCM-MF composite exhibits faster movement of interfaces, greater capacity in energy storage and extraction. The melting and solidification rate increases by 31.25% and 107.5% for lower porosity value of the MF.
6. Total melting time of PCM in PCM-MF composite with void decreases by 28.15%, 26.7%, and 26.95%, respectively compared to pure PCM with void for 1500, 750 and 250 W/m<sup>2</sup>, respectively. While total solidification time of PCM in PCM-MF composite with void decreases by 272%, 317%, and 326%, respectively compared to pure PCM with void for  $h = 5, 8, \text{ and } 10$  W/m<sup>2</sup>K, respectively.

The effect of shrinkage and expansion is more prominent for different cases such as higher value of wall heat flux ( $q_w''$ ), convective heat transfer coefficient ( $h$ ), density ratio, and lower value of porosity. This study can be useful in designing thermal energy storage and thermal management system with the consideration of void on heat transfer performance.

### **4.3 Scope of future work**

Phase change material based thermal energy storage system or thermal management system is widely used in numerous industrial and applications including solar energy storage, electronic cooling and buildings. The present dissertation reports the analytical study pertaining to the phase change process of PCM based systems in two different geometries (rectangular and annulus) incorporating volumetric shrinkage/expansion void. Effect of various parameters such as density ratio, end wall temperature, wall heat flux, convective heat transfer coefficient, porosity, and radius ratio on the solidification/melting of PCM have been investigated here. The Analysis carried out in this dissertation may provide some useful information for further study in this area. In addition to this, the work can be extended to explore further advancement in this problem and summarized below.

1. Experiments need to be conducted to analyze the effect of void on the thermal performance with and without thermal conductivity enhancers.
2. The effect of void on the thermal performance for various systems such as in nano enhanced PCM and fin based PCM system.
3. Numerical investigation can be made to consider the effect of wide range of operating parameters on the thermal performance.
4. Optimization study can be made to evaluate the best range of thermal and design parameters for the thermal performance.

## References

- [1] Heriot-Watt University, Bp statistical review of world energy june 2017. Technical report, BP at <https://www.bp.com/content/dam/bp/en/corporate/pdf/energyeconomics/statistical-review/bp-stats-review-2018-full-report.pdf>, 2017.
- [2] EIA, International energy outlook, in U.S. Energy Information Administration. 2017.
- [3] Statista.com, "Share of population that owned and used tablet computers in 2012, by country " Retrieved January 15, 2016, from <http://www.statista.com/statistics/256277/ownership-and-personal-use-of-tablet-computers-by-country/>.
- [4] Statista.com, "Shipment forecast of tablets, laptops and desktop PCs worldwide from 2010 to 2019 (in million units)." Retrieved January 15, 2016, from <http://www.statista.com/statistics/272595/global-shipments-forecast-for-tablets-laptops-and-desktop-pcs/>.
- [5] Courtney T, "How Much Power Do Common Devices Consume?" Retrieved April 4, 2016, from <https://www.gozolt.com/blog/power-devices-consume/>.
- [6] Greenspan JD, Roy EA, Caldwell PA, Farooq NS, Thermosensory intensity and affect throughout the perceptible range, Somatosensory & motor research, 20, pp. 19-26.
- [7] Patapoutian, A, Peier AM, Story GM, Viswanath V, Thermo TRP channels and beyond: mechanisms of temperature sensation, Nature Reviews Neuroscience, 4, pp. 529-539.
- [8] Story GM, The emerging role of TRP channels in mechanisms of temperature and pain sensation, Current neuropharmacology, 4, pp. 183.
- [9] Cheng W, Liu N, Wu W, Studies on thermal properties and thermal control effectiveness of a new shape-stabilized phase change material with high thermal conductivity, Applied Thermal Engineering, 36, pp. 345-352.

- [10] Mithal P, Design of experimental based evaluation of thermal performance of a flichip electronic assembly, ASME EEP Proceedings. New York: ASME, 18, pp. 109-115.
- [11] Dincer I, Rosen MA, Thermal Energy Storage: System and Applications. 2nd ed. Chichester: John Wiley & Sons; 2003.
- [12] Zalba B, Marin JM, Cabeza LF, Mehling LF, Review on thermal energy storage with phase change materials, heat transfer analysis and applications. Appl Therm Eng. 2003;23:251-283.
- [13] Farid MM, Khudhair AM, Cabeza LF, Mehling H, A review on phase change energy storage: materials and applications. Energ Conver Manage. 2004;45:1597-1615.
- [14] Sharma SD, Sagara K, Latent heat storage materials and systems: a review. Int J Green Energ. 2005;2:1-56.
- [15] Baljit SSS, Chan H, Sopian K, Review of building integrated applications of photovoltaic and solar thermal systems. J Clean Prod. 2016;137:677-689.
- [16] ISarbu I, Dorca A, Review on heat transfer analysis in thermal energy storage using latent heat storage systems and phase change materials. Int J Energ Res. 2018;43:1-36.
- [17] Jaguemont J, Omar N, Van den Bossche P, Mierlo J, Phase-change materials (PCM) for automotive applications: a review. Appl. Therm. Eng. 2018;132:308–320.
- [18] Narayanan SS, Kardam A, Kumar V, Bhardwaj N, Madhwal D, Shukla P, Kumar A, Verma A, Jain VK, Development of sunlight-driven eutectic phase change material nanocomposite for applications in solar water heating. Resour Technol. 2017;3:272-279.
- [19] Murat MK, High-temperature phase change materials for thermal energy storage. Renew. Sustainable Energ Rev. 2010;14:955-970.
- [20] Huang X, Alva G, Jia YT, Fang GY, Morphological characterization and applications of phase change materials in thermal energy storage: a review. Renew Sustain Energ Rev. 2017;72:128–45.

- [21] Socaciu L, Giurgiu O, Banyai D, Simion M, PCM selection using AHP method to maintain thermal comfort of the vehicle occupants. *Energ Proced.* 2016;85:489–97.
- [22] Zhou ZH, Zhang ZM, Zuo J, Huang K, Zhang LY, Phase change materials for solar thermal energy storage in residential buildings in cold climate. *Renew Sustain Energ Rev.* 2015;48:692–703.
- [23] Alva G, Liu LK, Huang X, Fang GY, Thermal energy storage materials and systems for solar energy applications. *Renew Sustain Energy Rev.* 2017;68:693–706.
- [24] Lane GA, Heat of fusion systems for solar energy storage. in *Proc. Workshop on Solar Energy Storage Subsystems for the Heating and Cooling of Buildings.* 1975.
- [25] Herrick C, Golibersuch D, Qualitative behavior of a new latent heat storage device for solar heating/cooling systems. 1977: General Electric Company Corporate Research and Development.
- [26] Sharma SD, Kitano H, Sagara K, Phase change materials for low temperature solar thermal applications. *Res. Rep. Fac. Eng. Mie Univ,* 2004. 29(1).
- [27] Lane G, Macro-encapsulation of PCM. Report No. oro/5117-8, Dow Chemical Company, Midland, Michigan, 1978. 152.
- [28] Khudhair AM, Farid MM, A review on energy conservation in building applications with thermal storage by latent heat using phase change materials. *Energy conversion and management,* 2004. 45(2): p. 263-275.
- [29] Oró E, Gracia AD, Castell A, Farid MM, Cabeza LF, Review on phase change materials (PCMs) for cold thermal energy storage applications. *Applied Energy,* 2012. 99: p. 513-533.
- [30] Safari A, Saidur R, Sulaiman FA, Xu Y, Dong J, A review on supercooling of Phase Change Materials in thermal energy storage systems. *Renewable and Sustainable Energy Reviews,* 2017. 70: p. 905-919.

- [31] Sharma, A, Tyagi VV, Chen CR, Buddhi D, Review on thermal energy storage with phase change materials and applications. *Renewable and Sustainable Energy Reviews*, 2007. 13(2): p. 318-345.
- [32] Zalba B, Marin JM, Cabeza JM, Mehling H, Review on thermal energy storage with phase change: materials, heat transfer analysis and applications. *Applied thermal engineering*, 2003. 23(3): p. 251-283.
- [33] Mehling H, Cabeza LF, *Heat and cold storage with PCM*. 2008: Springer.
- [34] Baran G, Sari A, Phase change and heat transfer characteristics of a eutectic mixture of palmitic and stearic acids as PCM in a latent heat storage system. *Energy Conversion and Management*, 2003. 44(20): p. 3227-3246.
- [35] Mehling H, Cabeza LF, *Heat and cold storage with PCM*. 2008: Springer.
- [36] Baran G, Sari A, Phase change and heat transfer characteristics of a eutectic mixture of palmitic and stearic acids as PCM in a latent heat storage system. *Energy Conversion and Management*, 2003. 44(20): p. 3227-3246.
- [37] Abhat A, Low temperature latent heat thermal energy storage: heat storage materials. *Solar energy*, 1983. 30(4): p. 313-332.
- [38] Jegadheeswaran S, Pohekar SD, Performance enhancement in latent heat thermal storage system: A review. *Renewable and Sustainable Energy Reviews*, 2009. 13(9): p. 2225-2244.
- [39] Nanofluid. (2016, April 9). In Wikipedia, The Free Encyclopedia. Retrieved 17:18, May 6, 2016, from <https://en.wikipedia.org/w/index.php?title=Nanofluid&oldid=714344322>
- [40] Shin D, Banerjee D, "Enhanced thermal properties of SiO<sub>2</sub> nanocomposite for solar thermal energy storage applications. " *International Journal of Heat and Mass Transfer* 84 (2015): 898-902.
- [41] Wang J, Xie H, Xin Z, Li Y, Chen L, "Enhancing thermal conductivity of palmitic acid based phase change materials with carbon nanotubes as fillers." *Solar Energy* 84.2 (2010): 339-344.

- [42] Alexiades V, Solomon AD, *Mathematical Modelling of Melting and Freezing Processes*. Washington DC: Hemisphere Publishing Corporation; 1993.
- [43] Ozisik MN, *Heat Conduction*, John Wiley Sons, 1993.
- [44] Weiner JH, Transient heat conduction in multiphase media, *Br J Appl Phys*. 1955;6:361–363.
- [45] Dantzig JA, Rappaz M, *Solidificatoin*, EPFL Press, 2009.
- [46] Mazzeo D, Oliveti G, Thermal field and heat storage in a cyclic phase change process caused by several moving melting and solidification interfaces in the layer. *Int J Therm Sci*. 2018;129:462–488.
- [47] Mazzeo D, Oliveti G, Simone DM, Arcuri N, Analytical model for solidification and melting in a finite PCM in steady periodic regime. *Int J Heat Mass Transf*. 2015;88:844–861,
- [48] Singh AK, Kumar A, Rajeev A, Stefan problem with variable thermal coefficients and moving phase change material. *J King Saud Univ. – Sci*. 2019;31:1064-1069.
- [49] Mosaffa AH, Talati F, Basirat TH, Rosen MA, Analytical modeling of PCM solidification in a shell and tube finned thermal storage for air conditioning systems. *Energ. and Build*. 2012;49:356-361.
- [50] Bansal NK, Buddhi D, An analytical study of a latent heat storage system in a cylinder. *Energ Conv and Manage*. 1992;33:235-242.
- [51] Kothari R, Sahu SK, Kundalwal SI, Comprehensive analysis of melting and solidification of a phase change material in an annulus. *Heat Mass Transfer*. 2019;55:769–790.
- [52] Mosaffa AH, Talati F, Rosen MA, Tabirizi HB, Approximate analytical model for PCM solidification in a rectangular finned container with convective cooling boundaries. *Int Comm Heat Mass Trans*. 2012;39:318–324.
- [53] Kothari R, Das S, Sahu SK, Kundalwal SI, Analysis of solidification in a finite PCM storage with internal fins by employing heat balance integral method. *Int J Energ Res*. 2019;43:6366-6388.

- [54] Talati F, Mosaffa AH, Rosen MA, Analytical approximation for solidification processes in PCM storage with internal fins: imposed heat flux. *Heat Mass Transf.* 2011;47:369–376.
- [55] Lamberg P, Approximate analytical model for two-phase solidification problem in a finned phase-change material storage. *Appl Energ.* 2004;77:131–152.
- [56] Sandip KS, Pradip D, Performance Analysis of Heat Sinks with Phase Change Materials subjected to Transient and Cyclic Heating. *Heat Trans Engg.* 2015;36: 1349-1359.
- [57] Bechiri M, Mansouri K, Analytical study of heat generation effects on melting and solidification of nano-enhanced PCM inside a horizontal cylindrical enclosure. *Appl Therm Engg.* 2016;104:779-790.
- [58] Voller VR, Prakash C, A fixed grid numerical modelling methodology for convection-diffusion mushy region phase-change problems. *Int. J Heat Mass Transf.* 1987;30:1709–1719.
- [59] Voller VR, Cross M, Markatos NC, An enthalpy method for convection/diffusion phase change. *Int J Numer Methods Eng.* 1987;24:271–284.
- [60] Voller VR, Brent AD, Prakash C, The modelling of heat, mass and solute transport in solidification systems. *Int. J. Heat Mass Transf.* 1989;32:1719–1731.
- [61] Voller VR, Swaminathan CR, General source-based method for solidification phase change, *Numer Heat Transf Part B Fundam.* 1991;19:175–189.
- [62] Voller VR, An overview of numerical methods for solving phase change problems. *Advance Numerical Heat Transfer*, 1997.
- [63] Bennon WD, Incropera FP, A continuum model for momentum, heat and species transport in binary solid-liquid phase change systems-I. Model formulation, *Int J Heat Mass Transf.* 1987;30:2161–2170.
- [64] Shamsundar N, Sparrow E, Effect of density change on multidimensional conduction phase change. *J. Heat Transfer.* 1976;4:550–557.

- [65] Xu D, Li Q, Gravity- and solidification-shrinkage-induced liquid flow in a horizontally solidified alloy ingot. *Numer Heat Transf Part A Appl.* 1991;20:203–221.
- [66] Gudibande N, Iyer K, Thermal shrinkage-based model for predicting the voids during solidification of lead. *Nucl Technol.* 2016;196:674–683.
- [67] Chiang KC, Tsai HL, Shrinkage-induced fluid flow and domain change in two dimensional alloy solidification. *Int. J Heat Mass Transf.* 1992;35:1763–1770.
- [68] Kim CJ, Ro ST, Shrinkage formation during the solidification process in an open rectangular cavity. *ASME J Heat Transf.* 199;115:1078–1081.
- [69] Trovant M, Argyropoulos SA, Mathematical modeling and experimental measurements of shrinkage in the casting of metals. *Can Metall Q.* 1996;35:75–84.
- [70] McBride E, Heinrich JC, Poirier DR, Numerical simulation of incompressible flow driven by density variation during phase change. *Int. J Numer Meth Fluids.* 1999;31:787–800.
- [71] Ehlen G, Schweizer A, Ludwig A, Sahm PR, Free surface model to predict the influence of shrinkage cavities on the solute redistribution in castings. *Proc Ninth Int Conf Model Cast Weld Adv Solidif Process.* 2000, p. 632.
- [72] Raessi M, Mostaghimi J, Three-dimensional modeling of density variation due to phase change in complex free surface flows. *Numer Heat Transf Part B Fundam.* 2005;47:507–531.
- [73] Sun D, Garimella SV, Numerical and experimental investigation of solidification shrinkage. *Numer Heat Transf Part A Appl.* 2007;52:145–162.
- [74] Monde AD, Chakraborty PR, 1-D diffusion based solidification model with volumetric expansion and shrinkage effect: a semi-analytical approach. *Phys Lett Sect A Gen At Solid State Phys.* 2017;381:3349–3354.

- [75] Santiago RD, Hernández EM, Otero JA, Constant mass model for the liquid-solid phase transition on a one-dimensional Stefan problem: Transient and steady state regimes. *Int J Therm Sci.* 2017;118:40–52.
- [76] Solomon L, Elmozughi AF, OztekinA, Neti S, Effect of internal void placement on the heat transfer performance – encapsulated phase change material for energy storage. *Renew Energ.* 2015;78:438–447.
- [77] Hassab MA, Sorour MM, Mansour MK, Zaytoun MM, Effect of volume expansion on the melting process’s thermal behavior. *Appl Therm Eng.* 2017;115:350–362.
- [78] Chiew J, Chin CS, Toh WD, Gao Z, Jia J, Low-temperature macro-encapsulated phase change material based thermal energy storage system without air void space design. *Appl Therm Eng.* 2018;141:928–938.
- [79] Janghel D, Saha SK, Karagadde S, Effect of shrinkage void on thermal performance of pure and binary phase change materials based thermal energy storage system: A semi-analytical approach. *Appl Therm Eng.* 2020;167:1359-4311.
- [80] Lamberg P, Siren K, Approximate analytical model for solidification in a finite PCM storage with internal fins. *Appl Math Model.* 2003;27:491-513.
- [81] Lamberg P, Siren K, Analytical model for melting in a semi-infinite PCM storage with an internal fin. *Heat and mass Transf.* 2003;39:167-176.
- [82] Yang Z, Garimella SV, Melting of Phase Change Materials With Volume Change in MFs. *J Heat Transf.* 2010;132: 062301.
- [83] Nazir H, Batool M, Osorio FJB, Isaza-Ruiz M, Xu X, Vignarooban K, Phelan P, Kannan AM, Recent developments in phase change materials for energy storage applications: A review. *Int J Heat Mass Transf.* 2019;129:491-523.
- [84] Du K, Calautit J, Wang Z, Wu Y, Liu H, A review of the applications of phase change materials in cooling, heating and power generation in different temperature ranges. *Appl Energ.* 2018;220:242-273.

- [85] Lin Y, Jia Y, Alva G, Fang G, Review on thermal conductivity enhancement, thermal properties and applications of phase change materials in thermal energy storage. *Renew Sustain Energ Rev*, 2018;82:2730-2742.
- [86] Bondareva NS, Buonomo B, Manca O, Sheremet MA, Heat transfer performance of the finned nano-enhanced phase change material system under the inclination influence. *Int. J Heat Mass Transf.*, 2019;135:1063-1072.
- [87] Bondareva NS, Buonomo B, Manca O, Sheremet MA, Heat transfer inside cooling system based on phase change material with alumina nanoparticles. *Appl Therm Engg.* 2018;144:972-981.
- [88] Ghalambaz M, Doostani A, Chamkha AJ, Ismael MA, Melting of nanoparticles enhanced phase-change materials in an enclosure: effect of hybrid nanoparticles. *Int J Mech Sci.* 2017;134:85-97.
- [89] M. Ghalambaz M, Doostani A, Izadpanahi E, Chamkha A, Phase-change heat transfer in a cavity heated from below: the effect of utilizing single or hybrid nanoparticles as additives. *J Taiwan Inst of Chem. Engg.* 2017;72:104-115.
- [90] Sheikholeslami M, Haq RU, Shafee A, Li Z, Heat transfer behavior of nanoparticle enhanced PCM solidification through an enclosure with V shaped fins. *Int J Heat Mass Transf.* 2019;130:1322-1342.
- [91] Sheikholeslami M, Ghasemi A, Li Z, Shafee A, Saleem S, Influence of CuO nanoparticles on heat transfer behavior of PCM in solidification process considering radiative source term. *Int J Heat and Mass Transf.* 2018;126:1252- 1264.
- [92] Sheikholeslami M, Jafaryar M, Shafee A, Li Z, Simulation of nanoparticles application for expediting melting of PCM inside a finned enclosure. *Phy A: Stat. Mech and its Appl.* 2019;523:544-556.
- [93] Alizadeh M, Hosseinzadeh K, Ganji D, Investigating the effects of hybrid nanoparticles on solid-liquid phase change process in a Y-shaped fin-assisted LHTESS by means of FEM. *J Mol Liq.* 2019;287:110931.

- [94] Hosseinzadeh K, Alizadeh M, Ganji D, Solidification process of hybrid nano-enhanced phase change material in a LHTESS with tree-like branching fin in the presence of thermal radiation. *J Mol Liq.* 2019;275:909-925.
- [95] Alizadeh M, Hosseinzadeh K, Mehrzadi H, Ganji D, Investigation of LHTESS filled by Hybrid nano-enhanced PCM with Koch snowflake fractal cross section in the presence of thermal radiation. *J Mol Liq.* 2019;273:414-424.
- [96] Doostani A, Ghalambaz M, Chamkha AJ, MHD natural convection phase-change heat transfer in a cavity: analysis of the magnetic field effect. *Journ of the Braz Society of Mech Sci and Engg.* 2017;39:2831-2846.
- [97] Ghalambaz M, Doostanidezfuli A, Zargartalebi H, Chamkha AJ, MHD phase change heat transfer in an inclined enclosure: Effect of a magnetic field and cavity inclination. *Num. Heat Transf. Part A: Appl.* 2017;71:91-109.
- [98] Pop I, Roşca NC, Roşca AV, MHD stagnation-point flow and heat transfer of a nanofluid over a stretching/shrinking sheet with melting, convective heat transfer and second-order slip. *Int. J Num Method Heat Fluid Flow.* 2018;28:2089-2110.
- [99] Chamkha AJ, Selimefendigil F, MHD mixed convection of nanofluid due to an inner rotating cylinder in a 3D enclosure with a phase change material. *Int J Num Method Heat Fluid Flow.* 2018;29: 0961-5539.
- [100] Bechiri M, Mansouri K, Analytical study of heat generation effects on melting and solidification of nano-enhanced PCM inside a horizontal cylindrical enclosure. *Appl Therm Engg.* 2016;104:779-790.
- [101] Kalaiselvama S, Parameshwarana R, Harikrishnan S, Analytical and experimental investigations of nanoparticles embedded phase change materials for cooling application in modern buildings. *Renew Energ.* 2012;39:375-387.
- [102] Sivasankaran S, Alsabery A, Hashim I, Internal heat generation effect on transient natural convection in a nanofluid-saturated local thermal non-

- equilibrium porous inclined cavity. *Phys A: Stat Mech and its Appl.* 2018;509:275-293.
- [103] Sardari PT, Mahani RB, Giddings D, Yasseri S, Ardekani MM, Bahai H, Energy recovery from domestic radiators using a compact composite MF/PCM latent heat storage. *J Clean Prod.* 2020;257:120504.
- [104] Paknezhad M, Rashidi A, Yousefi T, Saghir Z, Effect of aluminum-foam heat sink on inclined hot surface temperature in the case of free convection heat transfer, *Case studies in thermal engineering.* 2017;10:199-206.
- [105] Xiao X, Zhang P, Li M, Preparation and thermal characterization of paraffin/MF composite phase change material. *Appl Energ.* 2013;112:1357-1366.
- [106] Zheng H, Wang C, Liu Q, Tian Z, Fan X, Thermal performance of copper foam/paraffin composite phase change material. *Energ Conv and manag* 2018;157:372-381.
- [107] Hossain R, Mahmud S, Dutta A, Pop I, Energy storage system based on nanoparticle enhanced phase change material inside porous medium. *Int. Journ of Therm Sci.* 2015;91:49-58.
- [108] Li Z, Sheikholeslami M, Samandari M, Shafee A, Nanofluid unsteady heat transfer in a porous energy storage enclosure in existence of Lorentz forces. *Int J Heat Mass Transf.* 2018;127:914-926.
- [109] Al-Jethelah MS, Tasnim SH, Mahmud S, Dutta A, Melting of nano-phase change material inside a porous enclosure. *Int J Heat Mass Transf.* 2016;102:773-787.
- [110] Zhu ZQ, Huang YK, N. Hu, Zeng Y, Fan LW, Transient performance of a PCM based heat sink with a partially filled MF: Effects of the filling height ratio. *Appl Therm Engg.* 2018;128:966-972.
- [111] Chakraborty S, Dutta P, Analytical Solutions for Heat Transfer During Cyclic Melting and Freezing of a Phase Change Material Used in Electronic or Electrical Packaging. *ASME J Electr Pack.* 2003;125:126-133.

- [112] Ghalambaz M, Zhang J, Conjugate solid-liquid phase change heat transfer in heatsink filled with phase change material-MF. *Int J Heat and Mass Transf.* 2020;146:118832.
- [113] Abdulateef AM, Mat S, Abdulateef J, Sopian K, Al-Abidi AA, Geometric and design parameters of fins employed for enhancing thermal energy storage systems: a review. 2018;82: 1620-1635.
- [114] Sari A, Kaygusuz K, Thermal energy storage system using stearic acid as a phase change material. 2001;61:365-376.
- [115] Sari A, Kaygusuz K, Thermal performance of a eutectic mixture of lauric and stearic acids as PCM encapsulated in the annulus of two concentric pipes. 2002;72:493-504.
- [116] Sari A, Kaygusuz K, Thermal and heat transfer characteristics in a latent heat storage system using lauric acid. *Energ Conv and Manage.* 2002;43:2493-2507.
- [117] Mithat A, Orhan A, Kamil K, Experimental study on melting/solidification characteristics of a paraffin as PCM. *Energ Conv and Manage.* 2007;48:669-678.
- [118] Krishna J, Kishore PS, Solomon AB, Heat pipe with nano enhanced-PCM for electronic cooling application. *Exp Therm Fluid Sci.* 2017;81:84–92.
- [119] Sahoo S, Das M, Rath P, Application of TCE-PCM based heat sinks for cooling of electronic components: a review. *Renew Sust Energ Rev.* 59:550–582.
- [120] Janghel D, Karagadde S, Saha SK, Thermal performance analysis of phase change material based thermal storage system using a generalized numerical model with volumetric expansion and shrinkage. *Appl Therm Engg.* 2020;180:115826.
- [121] Zhou D, Zhao CY, Experimental investigations on heat transfer in phase change materials (PCMs) embedded in porous materials. *Appl Therm Engg.* 2011;31: 970-977.

- [122] Chamkha A, Veismoradi A, Ghalambaz M, Talebizadehsardari P, Phase change heat transfer in an L-Shape heatsink occupied with paraffin copper MF. *Appl. Therm. Engg.* 2020;177: 115493.
- [123] Bhattacharya A, Calmidi VV, Mahajan RL, Thermophysical properties of high porosity MFs. *Int J Heat and Mass Transf.* 2002;45:1017-1031.



# Resume

## JAYANTA SUTRADHAR

Address 

Phone 

Email 

[jayanta-sutradhar](#) 

### OBJECTIVE

---

A dedicated, hard-working, and motivated graduate with proven communication, understanding and numeracy skills seeking an apt position in your highly esteemed organization. Passionate to learn and wishing to associate with an organization which progresses dynamically and gives me a chance to hone my knowledge and skills in the field of technology.

#### ➤ EDUCATION

- ❖ M.S (Research)
  - Indian Institute of Technology, Indore
  - Period: 2019-2021
  - CGPA: 8.93
- ❖ B.Tech
  - National Institute of Technology, Agartala
  - Period: 2013-2017
  - CGPA: 8.43
- ❖ Higher Secondary

#### ➤ Achievements

- Participated in 8th International and 47th National Conference on Fluid Mechanics and Fluid Power (FMFP) , IIT Guwahati.
- Completed my B.Tech degree in Mechanical Engineering Department with a “First class with distinction” from NIT, Agartala. (Batch:2013-2017)
- Student member of ISRAE KOLKATA Chapters for the period

- Netaji Subhash Vidyaniketan
- Period: 2013
- Percentage: 78.2

❖ **Secondary**

- Netaji Subhash Vidyaniketan
- Period: 2011
- Percentage: 88

➤ **AREA OF INTEREST**

- Fluid Mechanics
- Microfluids
- Heat transfer
- Multi-phase flow
- Thermodynamics

from March 2016- March 2017.

- Organized the annual fest of NIT Agartala ‘Advaitam’ in February 2016.
- Participated in the 30th National Convention of Production Engineers and National Seminar on “Sustainable Manufacturing”.
- Organizing member of a gaming event and robotics event in college Fest.
- Active member of a College Robotics club. And completed basic Robotics Course.
- 5th position holder in Regional Mathematical Olympiad.
- 10th position holder in Chemistry Aptitude Test.
- Awarded in Mathematical Olympiad.

➤ **Language**

- English
- Hindi
- Bengali

➤ **Software**

- MATLAB
- Ansys
- OpenFOAM

➤ **Training**

- Industrial Training in Rashtriya Ispat Nigam Limited, Visakhapatnam from 14-12-2016 to 02-01-2016.

➤ **B. Tech final year project**

- Design and Fabrication of Bael Slicing Machine.

➤ **hobbies**

- Football
- Cricket
- Chess

➤ **MS (R) project Details**

- Thermal performance analysis of phase change material based systems with volumetric expansion and shrinkage.
- Investigated the effect of thermal conductivity enhancer such as porous matrix, nano-particle, and transient boundary condition.
- Analysis for heat sink application as well as waste heat recovery application.